Technical Report

537

Millstone Hill Thomson Scatter Results for 1973

J. V. Evans
R. R. Babcock, Jr.
J. M. Holt

22 October 1979

Prepared for the National Science Foundation
under NSF Grants No. ATM75-22193 and ATM79-09189

Lincoln Laboratory
MASSACHUSETTS INSTITUTE OF TECHNOLOGY
LEXINGTON, MASSACHUSETTS

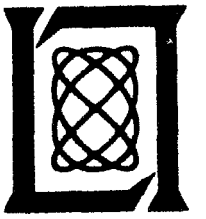

ABSTRACT

During 1973, the vertically-directed incoherent scatter radar at Millstone Hill (42.6°N, 71.5°W) was employed to measure electron density, electron and ion temperature and vertical ion velocity in the F-region over periods of 24 hours one or two times per month. The observations spanned the height interval 200-900 km approximately, and achieved a time resolution of about 30 minutes. This report presents the results of these measurements in a set of contour diagrams.

For a number of the days, the results have been used to derive the diurnal variation of the temperature of the neutral atmosphere above 300 km (the exospheric temperature) as well as the speed of the neutral wind in the magnetic meridian plane at this altitude. These results were used to define a model for the pressure variation in the thermosphere over Millstone whose E-W variation is set by the observed temperature variation, and whose N-S variation was adjusted to reproduce the observed winds calculated by solving momemtum equations for the neutral air. These results, together with similar results obtained using data gathered over the six-year period 1970-1975 have been used in a study of the seasonal and sunspot cycle variation of the mean meridional and zonal winds. Also reported are the results of a study of the effect of magnetic storms on the thermospheric winds observed over Millstone Hill.

Table of Contents

MILLSTONE HILL THOMSON SCATTER RESULTS FOR 1973

I. INTRODUCTION.

Since 1963, incoherent (Thomson) scatter radar measurements of F-region electron densities, and electron and ion temperatures have been conducted at Millstone Hill, Westford, Massachusetts (42.6°N, 71.5°W) (Refs. 1 to 10). This paper is the eleventh in a series of annual reports, and presents the results gathered in this program during the calendar year 1973. The observations reported were made for periods of 24 hours, approximately once a month. The results obtained in earlier years have been published and discussed in the articles listed in Table I, and have been transmitted to the World Data Center A, Boulder, Colorado.

The results reported in this paper are of F-region electron density N_e, electron and ion temperature T_e, T_i, and vertical velocity V_z and span the altitude interval 200-900 km, approximately. The measurements were made by transmitting single long pulses on each sweep of the radar time base and integrating the returns in a digital computer. Spectral information (from which T_e and T_i are determined) was obtained by examining the outputs from a bank of filters matched to the length of the pulse (0.5 or 1.0 msec)[20]. Additional measurements were made of the E- and F-regions by transmitting pairs of pulses, whose spacing could be varied allowing the echo autocorrelation function to be determined in the computer. This approach also allowed for the digital subtraction of unwanted returns from distant hills[21], and has been described in detail elsewhere[22]. Results gathered for E-region ion temperature using this pulse-pair method in 1972 have been employed in the study of tides in the lower thermosphere and reported in a number of papers (e.g., Ref. 23).

Other observations conducted in 1973 that are not reported here include short observing periods chosen to coincide with the overhead pass of two satellites (ISIS II and Atmospheric Explorer) or with the launch of a rocket from Wallops Island.

TABLE I

PUBLICATIONS CONCERNING THE MILLSTONE HILL UHF (68-cm Wavelength) THOMSON SCATTER RESULTS

Year	Months Covered	Publication
1963	February 1963 to January 1964 March, July, August, September April, July, November	Ref. 1 Ref. 11 Ref. 12
1964	January through December April, July, November	Ref. 2 Ref. 13
1965	January through December January, April, August June June, August, September	Ref. 3 Ref. 14 Ref. 15 Ref. 16
1966	January through December January, March, July, September	Ref. 4 Ref. 17
1967	January through December February, June, October, December	Ref. 5 Ref. 17
1968	January through December October	Ref. 6 Ref. 18
1969	January through December February, April, July September, October	Ref. 7 Ref. 19
1970	January through December	Ref. 8
1971	January through December	Ref. 9
1972	January through December	Ref. 10

Section II describes the equipment, data gathering and reduction procedures. During 1973, these were changed little from those employed the previous year and described in Ref. 9. Results for electron density, electron and ion temperature and vertical velocity are presented in Section III. In Section IV, we report results obtained from the data gathered in the years 1970 through 1975 for the mean meridional and zonal winds in the thermosphere and relate these to present understanding of thermospheric circulation. This work represents a continuation of an effort begun by Barbara A. Emery and reported in Refs. 9 and 24. Section V presents results of separate study of the effect of magnetic storms on the thermospheric winds over Millstone. The work presented in Sections IV and V represent the principal results obtained by R. R. Babcock[25], a graduate student at the M.I.T. Meteorology Department.

II. EQUIPMENT, OBSERVING AND DATA-ANALYSIS PROCEDURES.

A. Equipment.

a. General.

The UHF (68 cm wavelength) incoherent scatter radar equipment has been described[1]. This system employs a fixed vertically-directed 220-foot diameter antenna and hence can measure only the vertical component of the ion drift. Extensive modifications to the data-taking procedures were made in 1968 (Ref. 6) which allowed the echo power spectra to be measured for many heights simultaneously. This scheme made use of banks of matched filters for each of the pulse lengths (0.5, 1.0 or 2.0 msec) employed, and has been described in detail in Ref. 20. Owing to an imperfect match between the filters and the spectra of the pulses (especially for the 0.5 msec pulses), some systemmatic errors were introduced in the measurements of T_e and T_i over some altitudes and empirical correction procedures were developed in an effort to remedy these[7,9]. In 1976, the filter bank system was replaced by a digital correlator which obviated this problem.

During 1972, some incoherent scatter observations were conducted using the smaller 84 ft. diameter steerable antenna and associated L-band (23 cm

wavelength) radar. This system is described in Ref. 26. When used for incoherent scatter studies, control of the radar timing was assumed by the incoherent scatter timing unit (located in the Ionosphere Laboratory) and the 30 MHz IF output of the L-band receiver was connected to the 30 MHz IF input to the UHF receiver, so that the data taking and sampling procedure remained unchanged. (Actually, it was necessary to rearrange the elements of the filter bank to span a wider frequency range as described in Ref. 20.)

b. New Timer.

The only significant change made to the apparatus in 1973 was the introduction of a new timer system for the radar. This controls all of the timing functions such as pulse repetition frequency, transmitter pulse length, receiver suppression length, noise calibration pulse length and position, sample spacing and position, etc.

The previous timer was constructed using a commercial line of digital function boards (counters, gates, clock pulse generators, etc.) that used printed wire construction and discrete transistors. It had undergone almost continuous modification during 1970 and 1971 as the two-pulse modes were developed and brought into use[22]. When, in 1972, it became evident that further changes were unlikely, it was decided to rebuild the timer to improve its reliability and reduce the space it occupied. TTL logic was selected for this purpose.

The new timer follows the design of the old which was described in Ref. 22. It employs essentially two separate time-base generators (adjustable counters) driven by the same 1 MHz site frequency standard. The two are synched together, then progressively stepped apart in two pulse experiments. Essentially, only one is employed for single pulse experiments. Triggers are developed through the detection of coincidences between the counters and an array of preset numbers via diode "and" gates. In the old counter, these were hard-wired, but in the new one, a matrix plug-board was included that allows up to sixteen different modes to be established by inserting diode pins at the appropriate locations. Selection of which mode shall operate the radar can be made from the front panel via push buttons, or by the computer which can call modes through relays.

The new timer operates at a clock frequency (1 MHz) that is ten times that of the old one and provides 1 μsec adjustments in all of the pulse times.

B. Observing Procedures.

During 1972, we attempted to make observations using the single long pulse method and the newer pulse pair scheme at least once per month for 24 hours. Table II lists the operating modes employed for the single long pulse measurements and the altitudes over which these provided data. In normal or 'regular' operations, the cycle A, B, C was repeated every 30 minutes with 8 minutes of data being collected in each mode.

As described in Ref. 9, provision was made in 1971 to switch rapidly between the L-band and UHF radar transmitters and reload the computer with a new data-taking program which established automatically the proper condition for the interface equipment that transfers data from the radar to the computer[26]. During 1973, advantage was taken of this capability to switch rapidly between operation of the vertical and the L-band radars. Since the UHF radar measures only the vertical (V_z) component of the drift of the ions in the F-region, it is possible to recover from the measurements information only about the meridional winds in the thermosphere. To determine F-region electric fields and/or winds at E-region heights, it is necessary to measure the horizontal components of the ion drift. By employing the steerable L-band radar to measure the drift in the magnetic N-S and E-W directions, two additional components of the drift velocity could be measured. This allows for a solution for three orthogonal components. Measurements were conducted in 1973 that attempted to secure three drift components and were termed '3-D' (Table III). The L-band observations (D-mode) were conducted at 345° Az, 18° El, and 255° Az, 45° El. The sequence then was A-mode 4 mins., B-mode 4 mins., C-mode 8 mins., D-mode 16 mins., D-mode 16 mins (Table II). A shortened version of this sequence in which only the L-band observations in the magnetic meridian plane were included (termed 2-D) was used several times in 1972 (Ref. 10) and once in 1973 (Table III).

TABLE II
THE NORMAL "ONE-PULSE" EXPERIMENT MODE SEQUENCE

Mode	Pulse Length (μsec)	Height Resolution (km)	Sample Spacing (km)	Altitude Coverage (km)	Measured Parameters	
					Direct	Deduced
A	100	15	7.5	100-1000	Power	Ne
B	500	75	30	150-1500	Power	N_e
			75	225- 675	Power spectrum	T_e, T_i, V_z
C	1000	150	30	300-2000	Power	N_e
			75	450-1125	Power spectrum	T_i, T_i, V_z
D*	1000	50	30	150- 500	Power	—
			75	150- 350	Power Spectrum	V_d

*Employed with the L-band steerable radar during 2-D and 3-D experiments.

TABLE III
INCOHERENT SCATTER OBSERVATIONS – 1973

Begin			End			Mean Kp	Obs+	Comment
Date	C*	EST	Date	C*	EST			
2 Jan	QQ	1020	3 Jan	QQ	1230	0+	2-D	Az = 345°, El = 15°
16 Jan	Q	1500	17 Jan	QQ	1440	2-	Reg.	
13 Feb	QQ	0920	14 Feb	QQ	1140	2-	Reg.	
19 Mar	D	1450	20 Mar	D	2350	6+	Reg.	Magnetic Storm.
24 Apr		1820	25 Apr	Q	1830	3-	Reg.	
22 May		0830	23 May		1040	3_o	Reg.	
18 Jul	Q	1100	19 Jul		1530	2_o	3-D	Az = 345°, El = 18° Az = 255°, El = 45°
7 Aug		1120	8 Aug		1430	2_o	3-D	As Above.
14 Aug		1100	15 Aug	QQ	0940	1+	Reg.	
19 Sep	QQ	0930	20 Sep		1500	2_o	Reg.	
16 Oct	D	0800	17 Oct		1050	4+	Reg.	Disturbed
13 Nov		0900	14 Nov		1530	2+	Reg.	

* Condition

QQ One of the five quietest days in the month.
Q One of the ten quietest days in the month.
D One of the five most disturbed days in the month.

\+ Observations

Reg = Regular.
2-D, 3-D = L-band and UHF radar measurements.

C. Data Reduction.

As described previously[20], no attempt is made to analyse the data in real time (i.e., as it is gathered) as this would be too time consuming. Instead, the samples of echo power collected as functions of range and frequency are stored on magnetic tape at the end of each integration period along with other pertinent information such as the mode type, start time and duration of the run. A profile of echo power vs. height (i.e., corrected for the R^{-2} dependence where R is the range) is computed and printed out by a high speed printer. Together with a printout of the signal-to-noise ratio at each point within each frequency spectrum, this allows the data quality to be monitored while it is being gathered.

The first step in analysing the data is to construct a plot of the F-region critical frequency f_oF2 vs. time for the days of observation. For this, the values are scaled from the Millstone ionograms. Also included in the plots are values obtained at Ottawa (45°N) and Wallops Island (38°N), which are the two stations in routine operation closest to Millstone. Including values from these stations usually reveals any errors in scaling the local ionograms, and can serve to guide the interpolation that is necessary if any half-hourly values from Millstone are missing for any reason. Examples of these plots have been included in a number of previous reports[4,5].

Values for f_oF2 are scaled from the smooth curves drawn through the points on the plots at half-hour intervals and entered into the computer via punched cards. These are stored and used to obtain the value of f_oF2 at the mid-point of each A-mode run by linear interpolation*. The program combines measurements of echo power made with the all A-, B- and C-mode runs in each cycle of observation into a single "power profile". This is converted to an absolute profile of electron density vs. altitude by allowing for the effects on the backscatter power of altitude variations in the ratio T_e/T_i and normalising the resultant curve to have the correct value of electron density (N_{max})† at the peak of the layer.

---

*Actually, the time chosen = start time + 4 minutes.

†$N_{max} = 1.24 \times 10^4 (f_oF_2)^2$ el/cm^3 when f_oF2 is expressed in MHz.

Values for electron and ion temperature are recovered from the spectra assuming that O^+ is the only ion present. This assumption is a good one except at night near sunspot minimum when sufficient H^+ ions may be present at altitudes below 900 km to render the temperature estimates unreliable. More accurate values can be obtained using a program due to J. L. Massa (private communication, 1976) which attempts to recover T_e, T_i and the H^+/N_e ratio at each altitude (Section III). Unfortunately this program consumes a considerable amount of computer time and hence is not run routinely.

It has been found[20] that estimates of T_e/T_i obtained from the B- and C-mode data tend to differ at night in summer when $T_e/T_i \to 1.0$. This leads to differences in the etimates for T_i. It is believed that the discrepancy stems from the large amount of smearing of the frequency spectra of the signals introduced using 0.5 msec pulses (B-mode) particularly at night when the spectra are narrow. In principle, attempts are made to compensate for this by the method employed in the data analysis[20], but the measurement accuracy must suffer at such times. Since it also was evident that the filters employed in the receiver spectrum analyser in the B-mode are less perfectly matched to the transmitter pulse than those in the C-mode, it is believed that the systemmatic errors are primarily in the B-mode estimates. Assuming that C-mode is correct, J. E. Salah derived an empirical correction scheme by comparing the data in the two modes gathered at 525 km nominal height on four days[7], and this was employed to correct the B-mode temperatures gathered in 1969 and 1970[7,8]. Subsequently, B. A. Emery performed a more detailed comparison employing several heights, (to allow for differences in the effective center height of the pulse for the two modes) using two years' data[9]. Emery found that the corrections to be applied to the T_i and T_e/T_i values obtained in the B-mode depend not only on the prevailing value of T_e/T_i (taken to be that observed in the C-mode) but to a lesser extent also on T_i (again assumed to be the C-mode value). A smooth continuous correction scheme was derived from this comparison and employed to correct the results reported for 1971[9] and 1972[10]. The same scheme was employed for the results reported here. Finally, the values for electron temperature were corrected for the effect of the changing Debye length with altitude[8].

Beginning in 1976, the analog filter bank spectrum analyser was replaced by a digital correlator that is believed to be less likely to introduce systemmatic error. The data gathered with this device cannot be analysed with the ANALYSIS program and a new program (INSCAL) has been written which attempts to recover N_e, T_e, T_i as functions of height, allowing for the influence on the N_e profile of height variations of T_e/T_i and on the T_e profile of variations in N_e (via the Debye length correction), in a truly self-consistent fashion. That employed in ANALYSIS[20] represents only a first-order correction, but in view of the possible bias errors in the B-mode results at some times, a more elaborate approach seems unwarranted.

The next part of the analysis involves smoothing the electron density, electron and ion temperature and vertical velocity estimates as functions of height and time. This operation is performed by fitting, in a least-mean-squares sense, a two-dimensional polynomial surface that best represents the data. The program that performs this is known as INSCON, and has been described in Ref. 8. The INSCON program can compensate for distortion in the profiles of T_e and T_i vs. altitude introduced by the fact that the effective center height for the pulse is not given simply by the time at which the echoes are sampled (i.e., the so-called "nominal" height), but is shifted owing to the variation of echo power with delay within the pulse. This effect automatically is taken into account in constructing the electron density profiles, but was not included routinely for the plots of T_e, T_i prior to 1970.

A subroutine of the INSCON program produces a plotting tape to drive a Calcomp plotter which is used to obtain contour diagrams of N_e, T_e, T_i and V_z. These are given in the next section. In addition, INSCON provides the coefficients of the polynomial fit from which the variation of any parameter as a function of height or time (within the period fitted) can be recovered. The sets of coefficients for each day are combined on a single tape which is transmitted to the World Data Center (in Boulder) together with a listing given here as Appendix A. These, together with a simple FORTRAN recovery program (RCVR) allow numerical values to be obtained in machine-readable form by other users[8].

III. RESULTS FOR ELECTRON DENSITY, ELECTRON AND ION TEMPERATURES AND VERTICAL VELOCITY.

A. General.

Computer drawn contour plots of N_e, T_e, T_i and V_z as functions of altitude and time have been generated in the manner outlined above (and described in detail in Ref. 8); these are presented for the days listed in Table III in Figures 1 through 12. Contours of N_e are labeled in units of $\log_{10}N_e$ (el/cm^3) and are drawn in steps of $\log_{10} N_e = 0.2$ wherever $\log_{10}N_e \geq 3.0$. Regions well above h_{max} F2 sometimes are encountered where, owing to experimental error, the density appears to be increasing with altitude. These usually have been edited from the plots, but in any case are not considered real. The accuracy of these plots is greatest in the vicinity of h_{max} F2 (shown as a broken line) where the experimental uncertainty is set chiefly by the uncertainty in determining f_0F2 (typically ±0.2 MHz). At higher altitudes, however, the uncertainty in the incoherent scatter measurements contributes to the overall uncertainty – especially at night when the echoes are weakest.

It is believed that the 30 minute time resolution provided by the "regular" measurement scheme allows the normal diurnal variations to be followed adequately, but fluctuations caused, for example, by Traveling Ionospheric Disturbances (TIDs) with periods of less than about 2 hours, are effectively smoothed out.

The results for the electron and ion temperatures are presented as isotherms at 200°K and 100°K, respectively. The contours of vertical velocity V_z are plotted at intervals of 5 m/sec and have been corrected for the frequency "chirp" introduced by the transmitter[7]. Since the beam is directed at an elevation of 88° due south, the drift component of the plasma that is measured is not precisely vertical, but for most purposes the distinction is unimportant.

Values of the drift observed with the L-band radar usually were very scattered at night and quite unreliable. Accordingly, these measurements

have not been included in this report. These data have, however, been employed by Kirchhoff and Carpenter in a study of the diurnal variation of the ionospheric polarization electric field over Millstone and its dependence on magnetic activity[27].

The signal spectra of the reflections over the altitude interval 450 to 1125 km, approximately, are measured at intervals of 75 km using a pulse that yields a height resolution of 150 km. Normally, these spectra are analysed to yield estimates of T_e and T_i assuming that O^+ is the only ion present. It also is possible to reanalyse these spectra to yield estimates of the H^+ percentage as well as T_e and T_i. The computer program employed for this was written by J. L. Massa[28] and modified subsequently by R. Julian. Unfortunately, the program is slow, owing to the large search that must be undertaken, and thus far this has limited the number of days that could be examined.

Early attempts to use this program were for data gathered in 1969, i.e., close to sunspot maximum[19,29]. Subsequently, the program was used to reduce data gathered in 1972 and 1973, i.e., nearer sunspot minimum[10,30]. We believe that the results are of great interest since they allow conclusions to be drawn concerning the proton fluxes between the ionosphere and magnetosphere over Millstone. The results obtained for the H^+ percentage at either 725 or 800 km altitude by the method outlined in Ref. 10 for some days in 1973 are given in Figure 13a-h.

B. *Quiet Winter Behavior.*

There is a characteristic quiet-time winter and summer behavior of the ionosphere over Millstone that has been discussed in many previous reports[5-9]. In winter, the electron density exhibits a pronounced diurnal variation with the daytime densities near $h_{max}F2$ exceeding the nighttime densities by a factor of 10 and exceeding the midday density in summer also. As sunspot minimum is approached, this seasonal variation becomes less pronounced. In addition, the F-layer is formed lower in altitude as the neutral atmosphere density at all levels of the thermosphere is reduced. Both of these trends can be detected in the results presented here.

One interesting feature, discussed in a number of previous papers[3,6,31] and reviewed in Ref. 7, is the increase in N_{max} that occurs over Millstone during many quiet winter nights. This feature is evident in Figures 7a and 26a. Typically, N_{max} declines during the evening and reaches a minimum a little after midnight. The density then may remain constant for many hours (as on 2-4 February – Figure 3a) or may increase and reach a peak after 0200 L.T. and before sunrise (as on 13-14 November – Figure 12a). Accompanying this increase is invariably a decrease in electron temperature indicating that precipitation of energetic particles is not the responsible agent. We argued earlier[31] that a downward flux of H^+ ions from the protonosphere which charge exchange via the reaction

$$H^+ + O \rightleftharpoons H + O^+ \qquad (1)$$

is responsible for the increase. The results of Figure 13, which show periods when a downward H^+ flux can be identified by the large H^+/N_e percentages seen at 725 or 800 km altitude, support this view[10,30]. In addition, the scale height of the layer at altitudes $h > 600$ km is seen to increase at these times and this also provides evidence for a lowering of the O^+/H^+ transitional altitude associated with the downward flux.

We now believe that the timing of the event can be explained quite simply as a consequence of the diurnal variation of the exospheric temperature. This reaches its minimum at about 0300 L.T. with the result that the abundance of atomic oxygen in the thermosphere is at a minimum, while that of neutral hydrogen is at a maximum. This is just the condition necessary to cause the charge exchange reaction from H^+ to O to proceed most rapidly (i.e., to the right in Eq. 1), thereby ensuring that the protonospheric flux is downward and large[10,30].

C. Quiet Equinox Behavior.

There seems no very obvious separation of the behavior over Millstone into three separate seasonal dependencies. Rather, there is a rapid transition around Equinox from Summer to Winter. This transition is not clearly evident in the results obtained in 1973, in large part, because the days obtained near

Equinox tended to be disturbed. (*This is partly a consequence of the fact* that magnetic disturbances tend to maximize near Equinox.)

To the extent that there can be said to be a typical quiet equinox pattern, it is represented in these results by the behavior observed on 19-20 September (Figure 10). The daytime variation tends to follow the winter pattern with N_{max} reaching a maximum shortly after noon. At night, however, *significant increases in* N_{max} (*as on* 13-14 Nov.) seem absent. The length of the night is of course quite short.

On some equinoctal nights, it is possible to observe a predawn increase in electron temperature associated with the onset of photoelectron production at the time of ionospheric sunrise ($\chi = 105°$) at the conjugate point[32,33]. As we have shown[32], the magnitude of this effect is controlled by the local electron density. When this is sufficiently large (as apparently was the case on 19-20 September), no significant T_e increase is detectable near the layer peak.

D. Quiet Summer Behavior.

In summer time, the electron density at levels near h_{max} F2 is lower than in winter during the daytime by an amount that increases at sunspot maximum. It now is recognized that this reflects a change in the composition of the neutral air at these levels introduced by horizontal transport of atomic oxygen from the summer-to-winter hemisphere[7,9].

The diurnal variation differs also in that the largest electron density is encountered near sunset and not near midday. The electron temperature exhibits a much larger diurnal variation at Millstone in summer than winter, as then conjugate heating is absent at night. Examples of this characteristic pattern can be seen on 22-23 May, 18-19 July, 7-8 August and 14-15 August (Figures 6-9).

The cause of the evening increase was reviewed in Ref. 10; it appears to be produced by the reversal of the meridional component of the thermospheric wind from equatorwards (i.e., tending to drive the layer into regions of

higher recombination rate) to polewards (tending to lift it to where the losses are lower). The cooling of the layer associated with sunspot causes a contraction of the layer which also may contribute.

Although the summer night is (at ionospheric heights) very much shorter than in winter, the variation of the electron temperature between day and night is then largest. This is because in summer $T_e/T_i \rightarrow 1.0$ at night while in winter T_e is maintained above T_i by heat conducted from the protonosphere. The heating of the protonosphere in winter is caused by escape of photoelectrons from the conjugate point which remains sunlit.

E. Disturbed Behavior.

Two days of observation, namely, 19-20 March (Figure 4) and 16-17 October (Figure 11) were quite active magnetically. In addition, the results for 24-25 April (Figure 5) exhibit some of the characteristics that commonly are seen during disturbed periods.

On 19 March, there was a large evening increase around sunset, associated with upward vertical velocities. Based upon a prior study[18], we attribute this behavior to the lifting of the layer while it still is sunlit and production is taking place. We believe that the lifting is caused by an eastward electric field which drives the plasma (in an $\vec{E} \times \vec{B}$ direction) northwards and upwards. The field is presumably caused by the penetration of substorm electric fields to midlatitudes[18].

Following this increase, the density dropped to extremely low values suggesting that the main trough now was over Millstone. During the second day, the electron density was below normal until late afternoon when a second evening increase occurred.

Both evening increases appear to have caused large decreases in electron temperature which reached a minimum somewhat before the density maximum. As the density decayed, T_e rose again to its daytime values before decreasing again during the hours of darkness. While few reliable results appear to have been obtained at night, the electron temperature does not

appear to have been abnormally high, suggesting that Millstone lay some distance from the trough minimum[34,35].

The depressed value of the electron density on the second day of the storm which persisted until midafternoon is a common feature of summertime storms at Millstone that has been attributed to a change in the chemical composition of the neutral atmosphere that results from the transport of atomic oxygen towards the equator by larger than normal thermospheric winds (Section V).

The 24 hour period of 19-20 March 1973 appears to have been one of the most disturbed intervals ever encountered during operations of the incoherent scatter radar at Millstone Hill. The storm was in progress when observations began and continued throughout the following day. By contrast, the observation of 16-17 October were taken during a less intense period of disturbance that had begun only about 6 hours previous. There was no pronounced evening increase in electron density nor a fall to very low nocturnal values. The most obviously anomalous feature of this day was the increase in electron temperature commencing around 19 EST that persisted until about 01 EST (Figure 11b).

Nocturnal increases of T_e have been seen previously at Millstone during disturbed periods. They are most readily detectable in winter when the hours of darkness are long. There appear to be two separate causes, viz.: heat conducted from the magnetosphere, where it may be deposited by interaction between the ambient plasma and the ring current particles, and heat caused by precipitation of low energy particles. In the latter case, we usually find abnormally high electron densities in the E-region. This signature appears to be missing in the case of 16-17 October, suggesting that magnetospheric heat conduction is the responsible mechanism.

A similar instance of nocturnal heating appears to have occurred on 24-25 April. During this night, T_e began to increase at about 22 EST and began to decrease at little after 01 EST as the electron density began to increase. The nocturnal increase in density commencing near 02 EST has all the characteristics of the winter night increases described above, i.e., it is associated with a decrease in T_e and an increase in the downward flux. It

may, therefore, have the same explanation though increases due to a protonospheric flux normally are not seen this late in the year. A more complete study of this night utilizing estimates of the H^+ abundance (Section III-F) appears warranted.

F. H^+ Estimates.

Figure 13a-h presents plots of the H^+ percentage (of the total ion abundance) at either 725 or 800 km altitude. Based upon previous studies[10], we believe that we can identify periods when the flux is downwards by noting when the H^+ percentage at 800 km exceeds 20% (at 725 km > 10%). Such intervals are indicated in Figure 13a-h. As can be seen, periods of downward flux usually begin around midnight and end a little after ionospheric sunrise. In summer, there may be no time when the flux is not escaping (e.g., Figure 13c), though this becomes less frequent as sunspot minimum is approached[10,30].

IV. SEASONAL AND SOLAR CYCLE VARIATIONS IN THE THERMOSPHERIC WINDS.

A. Introduction.

A summer-to-winter circulation of the mid-latitude thermosphere has been inferred from seasonal differences in the structure of the ionosphere[3,36] and neutral thermospheric composition[37]. Support for this notion has been provided by estimates of the diurnal variation of the neutral winds in the thermosphere in different seasons derived from observations made at Millstone Hill[9,24,38-41], by nighttime measurements of thermospheric winds from 6300 Å airglow observations[42], and by theoretical models such as the zonally averaged model of Dickinson et al[43-45]. All available results indicate that the diurnally averaged values of the zonal and meridional winds are strongly equatorward and eastward in summer with weak poleward and strong westward winds in the winter. Near equinox, there is a short-lived transition period (3-4 weeks) in which the global circulation is relatively symmetric. The meridional mass flow patterns shown in Figure 14 from the model of Roble et al[45] depict the symmetric equinox pattern and the rapid transition to the

asymmetric solstice pattern. The net equatorward winds at equinox arise from the inclusion of high latitude heating. At solstice, the auroral zone heating in the summer hemisphere combines with solar EUV to drive a Hadley cell in which air is transported across the equator from the summer to the winter hemisphere. This flow is resisted by an oppositely directed flow in the winter hemisphere driven by the auroral heat deposited in that hemisphere. This flow is resisted by an oppositely directed flow in the winter hemisphere driven by the auroral heat deposited in that hemisphere. It has been found necessary to include these high latitude heat sources as well as the in situ EUV and UV absorption in self-consistent models in order to reproduce the observed wind and temperature patterns[43,46]. The reverse cell acts to decrease the winter hemisphere poleward winds driven by the solar heating centered in the summer hemisphere, and results in an asymmetric behavior of the mean meridional winds at mid-latitudes.

To date, the largest sample of thermospheric wind measurements used to examine this wind pattern has been presented by Emery[9,26,41]. Using neutral winds and temperature data derived from ionospheric measurements made at Millstone over the two-year period 1970-1971 as input to a semi-empirical dynamic model, Emery confirmed the persistence of this pattern over the two year period 1970-1971.

Roble et al[45] have varied the solar and high latitude heating rates in their model to simulate changes with the solar cycle. Using wind and temperature observations made by Hernandez and Roble[47] near solar minimum, as a guide to set the heating rates, they found that the high latitude heating was too small to drive a reverse cell in the winter hemisphere (Figure 15) at solar minimum. In addition, the mid-latitude zonally averaged meridional winds are more strongly poleward in winter than at solar maximum. To test these conditions, an additional four years of data from Millstone Hill (42°N) taken from 1972 through 1975 have been added to the two years analyzed by Emery[9,24,41]; this period covers the declining portion of the last sunspot cycle. The results are presented in this Section.

B. Data Analysis Procedures.

Measurements of electron density, electron and ion temperature and vertical ion drift have been made at Millstone over periods of $\sim$ 24 hours approximately once per month since 1963 (Section I). After smoothing with respect to height and time, these have been used to derive the exospheric temperature, T_∞, and a measure of the horizontal neutral wind at 300 km in the magnetic meridian, V_{Hn}. (For Millstone, $V_{Hn} = .97V - .24U$, where V and U are the meridional and zonal winds, positive northward and eastward, respectively.) These neutral parameters then were employed as input to a dynamic semi-empirical model of the local thermosphere[24,40].

This model assumes that the neutral constituents are in hydrostatic equilbrium distribution above a lower boundary (120 km) so that the E-W pressure variation is set by the observed local time variation of the exospheric temperature T_∞. The N-S pressure variation in the model is adjusted until the winds U and V at 300 km computed from solving the momentum equations give the observed diurnal variation of V_{Hn} in a least squares sense. A detailed description of the model will not be presented here.

Emery analyzed 37 days from December 1969 through December 1971. To these, we have added another 48 days from 1972 through 1975. Of the total of 85 days, 21 were considered disturbed days (daily average of auroral index AE > 300γ), and their behavior is discussed in Section V. Neutral densities needed in the calculations were taken from the Mass Spectrometer/Incoherent Scatter (MSIS) model[48].

C. Results.

Figure 16 presents results for the diurnally averaged meridional wind at 300 km obtained from the analysis. The solid line is a least squares fit to the data of an analytical function with 12, 6 and 4 month harmonics, whose amplitudes are linear functions of the 10 cm solar radio flux $F_{10.7}$. The fit is given by

$$\bar{V} = [18.2 \pm 11.7 - (27.1 \pm 5.6)\bar{F}] + [52.2 \pm 19.3 + (4.2 \pm 14.9)\bar{F}]*$$
$$\cos [2\pi/365 \ (day + 5 \pm 4)] + [-31.9 \pm 7.8 + (17.4 \pm 10.5)\bar{F}]*$$
$$\cos [4\pi/365 \ (day + 15 \pm 12)] + [5.3 \pm 7.8 - (3.7 \pm 8.4)\bar{F}]*$$
$$\cos [6\pi/365 \ (day - 11 \pm 5)] \qquad (2)$$

with $\bar{F} = \bar{F}_{10.7}/100$, where $\bar{F}_{10.7}$ is an 81 day average of $\bar{F}_{10.7}$ centered on the day being analyzed. The rms error between the points and the fitted curve (Eq. 2) is ±31 m/sec and the linear correlation coefficient is $r = 0.84$ The mean, annual and semiannual terms all are statistically significant but the only one having a significant variation with $\bar{F}$ is that of the mean wind. For solar maximum ($\bar{F}_{10.7} = 160$), the fit gives an annual mean velocity of 25.2 m/sec. The summer wind is about 75 m/sec equatorward and the winter wind is about 30 m/sec poleward, with a seasonal variation of about ±50 m/sec. At solar minimum ($\bar{F}_{10.7} = 70$), the mean annual wind is 0.7 m/sec (i.e., approximately zero). The average winter wind has increased to about 40 m/sec poleward. Near solstice, the average summer wind still is about 70 m/sec equatorward; however, duration of the period of equatorward winds appears to be reduced compared to solar maximum. At solar maximum, the winds tend to be equatorward at equinox, while at minimum, they tend to be poleward.

Figure 17 shows the diurnally averaged zonal winds at 300 km, with a least squares fit to the data of the same form as in Eq. 2, given by

$$U = [-0.8 \pm 23.9 - (1.7 \pm 18.8)\bar{F}] + [27.9 \pm 31.0 + (1.6 \pm 24.2)\bar{F}]*$$
$$\cos [2\pi/365 \ (day + 29 \pm 74)] + [-14.7 \pm 32.9 + (12.3 \pm 25)\bar{F}]*$$
$$\cos [4\pi/365 \ (day + 36 \pm 78)] + [2.7 \pm 30.7 - (4.3 \pm 24.5)\bar{F}]*$$
$$\cos [6\pi/365 \ (day + 8 \pm 48)] \qquad (3)$$

There is a great deal of scatter in the points, and the fit is not statistically significant, since $r = 0.60$ and the standard deviation in the amplitudes generally is the same order of magnitude as the coefficients. Nevertheless, there seems to be a recognizable seasonal pattern with a westward wind in summer and an eastward wind in winter and no obvious solar cycle variation.

D. Discussion.

From the results presented here, it appears that the seasonal pattern in the winds seen by Emery[24,41] persists through the solar cycle with only minor variations. The magnitudes of the diurnally averaged winds and of the seasonal variation remain about the same, suggesting that the decrease in the day-night temperature (pressure) gradient which accompanies the decrease in solar EUV and UV flux is balanced by an equivalent decrease in the ion drag force as the electron density decreases.

In their zonally averaged model, Roble et al[45] reduced the globally averaged EUV flux by a factor of two to simulate the decline in solar activity at sunspot minimum. In order to reproduce the winds and temperatures observed by Hernandez and Roble[47], the high latitude heating had to be reduced by a factor of 4.5. With the reduced high latitude heating, the reverse cell in the winter hemisphere was not present and with the result that, in the winter, hemisphere winds at mid-latitudes tended to become more poleward. The present analysis also shows the winds becoming more poleward in winter.

The change in the equinox meridional wind from equatorward at solar maximum to poleward at minimum also can be explained in terms of a decrease in high latitude heating relative to the solar EUV flux. Because the thermosphere is so optically thin, the latitudinal variation in the solar heating rate at equinox is very small. The high latitude heating, which is concentrated in a narrow latitudinal region and also tends to maximize near the equinoxes, then can be quite effective in driving a reverse circulation. Figure 14(a) shows the zonally averaged equinox circulation for an average level of geomagnetic activity at solar maximum. The high latitude heating then drives an equatorward flow between 150 and 400 km at all latitudes. As the magnitude of the high latitude heating decreases relative to the solar heating at minimum, the extent of the region controlled by the reverse cell shrinks, and the region dominated by an equator-to-pole circulation pattern driven by the solar heating will expand. The generally equatorward equinox winds found in this analysis for 1974 and 1975 support the view, advanced by Roble et al[45], that there is a larger decrease in the high latitude heating relative to solar EUV in going from sunspot maximum to minimum.

The net flow from summer to winter hemisphere at mid-thermospheric levels plays a major role in the "wind diffusion" explanation of the seasonal oxygen anomaly[37,49] and the anomalous seasonal behavior of the F-region at midlatitudes. The almost complete disappearance of the anomalous seasonal variation in the ionospheric f_0F2 at sunspot minimum might be taken to imply that the seasonal variation in the thermospheric winds also decreases. However, the present analysis, and also that of Hernandez and Roble[47], does not support such a conclusion. A three-dimensional global model for thermospheric oxygen transport by Straus and Christopher[46] also suggests that the magnitude of the oxygen bulge in the lower thermosphere does not decrease significantly with reduced $F_{10.7}$. Furthermore, satellite observations near solar minimum ($F_{10.7} \cong 90$) by Maurersberger et al[50] and by von Zahn and Fricke[51] both showed a definite seasonal variation in the O/N_2 ratio. The height and magnitude of the peak electron density is dependent not only on the photochemical balance, but also on dynamical processes such as diffusive transport and neutral winds. At solar minimum, when the scale height of the atmosphere in the lower thermosphere is reduced, the ionosphere is formed at lower altitudes. Presumably the winter oxygen enrichment at the level where production, loss and diffusion balance (i.e., the F-region peak) then is less pronounced.

The winds calculated by the model are constrained to reproduce the observed V_{Hn}, (where $V_{Hn} = .97V - .24U$). As a result, the calculated meridional winds closely represent observed values of V_{Hn}. By contrast, the zonal winds are computed from the linearized momentum equations using the observed temperature (pressure) gradient, and accordingly, these results are more sensitive to assumptions made in the analysis, especially the neglect of the non-linear terms and electric fields. This may explain partly the large scatter in the zonal wind values.

E. Conclusions.

Analysis of results for the diurnal variation of the meridional and zonal winds computed using the dynamic model of Emery[24,40] adjusted to match Millstone Hill incoherent scatter data gathered over 1970-75 shows:

1. The seasonal variation in the mean meridional winds of about ±50 m/sec seen by Emery[24,41] in 1970-71 persists through the solar cycle to solar minimum. This result is consistent with observations by Hernandez and Roble[47] and the results of the diurnally averaged circulation model of Roble et al[45].

2. The equinox period winds changed from generally equatorward at solar maximum to poleward at solar minimum. The annual mean meridional wind, which was about 25 m/sec equatorward at solar maximum, became about 0 m/sec at solar minimum, causing the winds in winter to be more strongly poleward. Both effects are consistent with the conclusions reached by Roble et al[45], namely, that the magnitude of the high latitude heating decreases by a larger factor than the solar EUV and UV heating between maximum and minimum.

3. The scatter in the zonal data is too large to permit any detailed analysis, but a general pattern of eastward average winds in the winter and westward winds in the summer is found that persisted through the solar cycle.

V. EFFECT OF GEOMAGNETIC DISTURBANCES ON THERMOSPHERIC NEUTRAL WINDS.

A. Intoduction.

The marked depression of the ionospheric peak electron density, N_mF2, at mid-latitudes during geomagnetic disturbances (e.g., in Section III-E) has been attributed (e.g., by Duncan[36]) to changes in the global neutral density structure caused by the strong equatorward winds forced by high latitude heating (for review, see Rishbeth[52]) Mayr and Volland[53,54] have shown that the transport could be explained as the same "wind diffusion" effect that causes the seasonal oxygen anomaly. Averaged over the globe, the increased equatorward winds result in a net transport of atomic oxygen (and other light constituents) equatorward from high and mid-latitudes, thus decreasing the

O/N_2 ratio. A lower O/N_2 ratio results in a higher recombination rate for atomic oxygen ions at all levels and so, lower ionization density values.

There have been several efforts to observe thermospheric winds during disturbed periods. For example, Roper and Baxter[55] conducted barium release measurements which suggested strong equatorward winds are present and are induced in part through momentum forcing by the increased speed of the anti-solar convection over the polar cap. Winds derived from ion drift measurements made at the Chatanika incoherent scatter radar also suggest strong momentum forcing at high latitudes[56]. Most of the published mid-latitude observations have been obtained by means of 630 nm airglow measurements. Hays and Roble[57] reported equatorward winds of $\sim$ 400 m/sec associated with an aurora, while Sipler and Biondi[58] found enhanced neutral temperature and winds estimated at 600 m/sec during a substorm. These very strong equatorward winds persisted throughout the night, and were observed to be faster when looking to the north than when looking to the south. Hernandez and Roble[59] reported 630 nm airglow observations made during a series of four disturbed nights. All disturbed cases showed stronger equatorward winds, enhanced neutral temperatures and, in some cases, the zonal winds became westward near dusk and remained westward throughout the night. They also detected a difference in meridional wind speed when looking north compared to looking south, implying that the air is diverging from a source of limited E-W extend.

In this Section, the thermospheric neutral winds and temperatures derived from Millstone Hill incoherent scatter radar observations (Section I) have been examined to determine the effect of geomagnetic disturbances. Over the six-year period 1970 through 1975, there were 21 days of data for which auroral activity was high (daily average of AE > 300γ). Since the measurements were made over twenty-four hour periods, the effect of the high latitude heating could be examined for all time sectors.

B. Data Analysis Procedures.

We outlined in Section IV-B the method of deriving estimates of the meridional and zonal winds (V and U) over Millstone Hill from our incoherent scatter

observations. Three variations to the analysis procedures employed previously for quiet days (Section IV) were included for the analysis of these disturbed days. Since the derived neutral winds were found to be significantly larger than during quiet times, the contribution of frictional heating, caused by ion-neutral collisions to the heat balance equation was included in the derivation of T_∞; this tended to reduce the derived values of T_∞. The derived values of V_{Hn} are highly sensitive to the ion-neutral collision frequency used in computing the ambipolar diffusion velocity. In turn, the collision frequency is dependent on the neutral density assumed[40]. For the analysis of the winds on quiet days, the required neutral densities were derived from the Mass Spectrometer/Incoherent Scatter (MSIS) model[48]. For this analysis, the densities used were derived using the lower boundary density values contained in the MSIS model and integrating to 300 km, assuming diffusive equilibrium and the observed neutral temperature profile. This procedure tended to decrease the winds derived at night, since the higher temperatures led to higher density estimates and collision frequencies, thereby lowering the ambipolar diffusion velocity calculated.

A major source of uncertainty in the neutral parameters derived during disturbed periods is the possible effect of large magnetospheric electric fields appearing over Millstone. Large electric-field-induced drifts not only affect the derivation of V_{Hn} (through the interpretation of the observed vertical drifts and the ion drag term in the momentum equations), but also will affect the calculation of the relative ion-neutral velocity which determines the frictional heating term in the ion heat balance equation. There were no coincident electric field measurements available for the days analyzed, so an "averaged" disturbed period field was constructed from a number of disturbed period observations made by Wand[60]. The averaged east-west field does not differ significantly from the quiet time field, except for being slightly larger. The averaged north-south field is about twice as large as the quiet time field and exhibits a strong northward field near dusk, consistent with earlier reported measurements[27,61]. Only two of the ten days which went into this disturbed electric field model included a full twenty-four hours of data. Examining individual days, it appears that the mid-latitude electric field reflects the rapidly varying substorm activity, so that an average model can at best remove only the general trend of the effects introduced by electric fields.

C. Results.

To illustrate the behavior observed during disturbed periods, we present results for a sample of winter and equinox days. All the effects to be discussed were seen in each of the disturbed days, although their magnitude varied considerably. Figure 18 shows the diurnal variation of the exospheric temperature seen on a seven of the disturbed days. Unlike the generally unstructured sinusoidal variation typically seen on quiet days, large irregular increases in the temperature are evident after sunset on each of the disturbed days. During the night of 12-13 February 1974, the nighttime temperature actually rose above the daytime maximum.

Figure 19 shows the smoothed meridional and zonal winds derived for a typical quiet winter day. The meridional wind, V, is poleward during the day at about 75-100 m/sec. During the night, the wind turns equatorward for 3-4 hours either side of midnight, with a magnitude of about 50 m/sec. Since the poleward meridional winds during the day are stronger and persist longer than the nighttime equatorward wind, the diurnally averaged meridional wind V is poleward. The zonal wind, U, changes direction in the afternoon at the pressure maximum and remains eastward through the night, reversing again to westward just before dawn. The morning reversal is found to occur earlier during equinox and is encountered near local midnight in summer.

Figure 20 depicts the smoothed meridional wind derived for the seven disturbed days shown in Figure 18. The length of the period during the night when the winds are equatorward is not significantly longer than on quiet days; however, the magnitude is found to be much larger, approaching 200 m/sec in many instances. One characteristic freqently encountered is the strong surge in the winds near local midnight, or one to two hours after midnight.

The smoothed zonal winds derived from the model for the same seven days are shown in Figure 21. The derived zonal winds are much stronger than the quiet time winds, with the westward winds in the morning sector occasionally exceeding 350 m/sec. For most disturbed days, the time of reversal between eastward and westward winds at night has been shifted into the pre-midnight

sector. For 12-13 February 1974, the derived winds actually are reversed from the normal pattern, with westward winds between noon and 2000 L.T. and eastward through the night and morning.

The dynamic model of Emery[40] uses a third order harmonic fit to the data in deriving the forcing functions for the winds, so that short period fluctuations, such as gravity wave pulses, tend to be smoothed out. The effect of the smoothing employed to secure the results shown in Figures 20 and 21 is to cause the midnight surge and any gravity wave pulse occurring within a couple of hours of each other to be merged into a single pulse. Thus, the midnight surge may appear shifted in time and extend over a longer period than really is the case. To differentiate the different forcing effects, the experimentally derived wind, V_{Hn}, for the disturbed day 17-18 August 1970 has been compared with the hourly average of the AE index in Figure 22. The equatorward pulses at 2200 L.T., 0500 L.T. and 1200 L.T. seem to be related to individual substorms, and their effects also were evident in raising the electron and ion temperatures and h_mF2. The surge at midnight does not appear to be related to any particular substorm nor to increased auroral activity. (The pulse at 1700 L.T. may be associated with a substorm, but could be a result from increased eastward electric field in the dusk sector, which the disturbed electric field does not properly represent. The resulting lifting of the ionization then would be interpreted as an equatorward wind.)

D. Discussion.

The observed meridional winds clearly show the effect of the strong forcing which occurs during auroral disturbances. The largest effect is the surge in the wind near local midnight, which probably is an extension of the midnight surge observed at Chatanika[56]. Joule heating occurring along the nightside auroral oval and possibly at the cleft creates a horseshoe shaped heated region[62,63] The easiest method of escape for the expanded atmosphere in the polar cap is through the midnight region near the Harang discontinuity, where the heating is small. Momentum forcing by the ion convection flow over the polar cap also can assist in generating large equatorward winds near midnight[64]. Detailed analyses of the experimental results, such as those

shown in Figure 22, indicate that this surge is a distinct feature separable from the gravity wave pulses associated with substorm onsets[65].

The computed values of the diurnally averaged meridional wind do not entirely support a picture of an increase global equatorward flow on disturbed days, which is the basis of the "wind diffusion"[54] used to explain the transport of oxygen and the negative phase of an ionospheric storm. Some disturbed days do exhibit weaker poleward winds on the dayside than normal, but this is not a consistent feature. The diurnally averaged meridional winds tend to be more equatorward on very disturbed days, but again the pattern is not consistent. In analyzing 64 quiet days (daily average of AE < 300γ) over a six-year period (Section IV), there is a small but not statistically significant correlation between diurnally averaged meridional wind and AE as may be seen in Figure 23. The present analysis suggests that the transport of heat and mass associated with geomagnetic activity may result from short-lived pulses and surges rather than overall changes in the global circulation, and that these short-lived events are either not fully resolved in our measurements and/or supressed by the 3 harmonic smoothing employed in the data analysis.

The meridional winds computed by the model are tied to the experimental observations, so they are a fairly good representation of the neutral wind, given the uncertainties in neutral densities and electric fields which affect the calculations. However, the zonal winds are derived theoretically from the observed temperature (pressure) field, and are less reliable. Roper and Baxter[55] have found that equatorward transport of zonal momentum forced by the ion convection pattern, can be important at subauroral latitudes ($\Lambda < 63°$). The use in our analysis of linearized momentum equations neglects such transport. Moreover, during disturbed periods, the local temperature gradient probably does not represent the forcing of the global circulation. Thus, the very unusual zonal wind pattern of 12-13 February 1974 may be a result of neglecting the non-linear transport terms. By the beginning of the observation period for this particular day, there had been over 24 hours of intense auroral activity. The transport of the auroral heating to lower latitudes had reversed the normal diurnal temperature gradient at Millstone, but it is not clear that the global circulation had reversed, as the derived zonal winds suggest.

ACKNOWLEDGEMENTS

We are grateful to R. H. Wand, W. A. Reid, L. B. Hanson, S. Sawicki and others at the Millstone Hill Observatory who assisted in gathering the data reported here, as well as Mrs. Alice Freeman who helped with the data reduction. During 1973, the incoherent scatter work at Millstone was supported by the U.S. Army as part of a program of radar propagation study. Preparation of this report was supported by the National Science Foundation under Grants ATM75-22193 and ATM79-09189.

REFERENCES

1. J. V. Evans, "Ionospheric Backscatter Observations at Millstone Hill", Technical Report 374, Lincoln Laboratory, M.I.T. (22 January 1965), DDC AD-616607.

2. _____, "Millstone Hill Thomson Scatter Results for 1964", Technical Report 430, Lincoln Laboratory, M.I.T. (15 November 1967), DDC AD-668436.

3. _____, "Millstone Hill Thomson Scatter Results for 1965", Technical Report 474, Lincoln Laboratory, M.I.T. (18 December 1969), DDC AD-707501.

4. _____, "Millstone Hill Thomson Scatter Results for 1966", Technical Report 481, Lincoln Laboratory, M.I.T. (15 December 1970), DDC AD-725742.

5. _____, "Millstone Hill Thomson Scatter Results for 1967", Technical Report 482, Lincoln Laboratory, M.I.T. (22 July 1971), DDC AD-735727.

6. _____, "Millstone Hill Thomson Scatter Results for 1968", Technical Report 499, Lincoln Laboratory, M.I.T. (23 January 1973), DDC AD-767251/2.

7. _____, "Millstone Hill Thomson Scatter Results for 1969", Technical Report 513, Lincoln Laboratory, M.I.T. (23 July 1974), DDC AD-A008505/0.

8. J. V. Evans and J. M. Holt, "Millstone Hill Thomson Scatter Results for 1970", Technical Report 522, Lincoln Laboratory, M.I.T. (11 May 1976).

9. J. V. Evans, Barbara A. Emery and J. M. Holt, "Millstone Hill Thomson Scatter Results for 1971", Technical Report 528, Lincoln Laboratory, M.I.T. (24 March 1978).

10. J. V. Evans and J. M. Holt, "Millstone Hill Thomson Scatter Results for 1972", Technical Report 530, Lincoln Laboratory, M.I.T. (18 September 1978).

11. J. V. Evans, Planet. Space Sci. 13, 1031 (1965), DDC AD-616607.

12. _____, J. Geophys. Res. 70, 1175 (1965), DDC AD-614310.

13. _____, Planet. Space Sci. 15, 1387 (1967).

14. _____, Planet. Space Sci. 18, 1225 (1970), DDC AD-716056.

15. _____, J. Atmos. Terr. Phys. 32, 1629 (1970), DDC AD-716057.

16. _____, J. Geophys. Res. 75, 4803 and 4815 (1970), DDC AD-714447 and DDC AD-714446, respectively.

17. _____, Planet. Space Sci. 21, 763 (1973), DDC AD-772137/6.

18. _____, J. Atmos. Terr. Phys. 35, 593 (1973), DDC AD-771877/8.

19. _____, Planet. Space Sci. 23, 1461 (1975).

20. J. V. Evans, R. Julian and W. A. Reid, "Incoherent Scatter Measurements of F-region Density Temperatures and Vertical Velocity at Millstone Hill", Technical Report 477, Lincoln Laboratory, M.I.T. (6 February 1970).

21. G. W. Armistead, J. V. Evans and W. A. Reid, Radio Sci. 7, 153 (1972).

22. W. L. Oliver, J. E. Salah, R. H. Wand and J. V. Evans, "Incoherent Scatter Measurements of E- and F-region Density, Temperatures, and Collision Frequency at Millstone Hill", Technical Report , Lincoln Laboratory, M.I.T. (in press).

23. J. E. Salah, R. H. Wand and J. V. Evans, Radio Sci. 10, 347 (1975).

24. B. A. Emery, "Seasonal Wind Variations in the Mid-Latitude Neutral Thermosphere", Ph.D. Thesis, M.I.T. Department of Meteorology, Cambridge, Massachusetts (May 1977).

25. R. R. Babcock, "The Dependence of the Circulation of the Thermosphere on Solar Activity", Ph.D. Thesis, M.I.T. Department of Meteorology, Cambridge, Massachusetts (September 1978).

26. J. C. Ghiloni, "Millstone Hill Radar Propagation Study: Instrumentation", Technical Report 507, Lincoln Laboratory, M.I.T. (20 September 1973).

27. V. W. J. H. Kirchhoff and L. A. Carpenter, J. Geophys. Res. 81, 2737 (1976).

28. J. L. Massa, "Theoretical and Experimental Studies of Ionization Exchange between the Ionosphere and Plasmasphere", Ph.D Thesis, The University of Michigan, Ann Arbor, Michigan (1974).

29. J. V. Evans, Planet. Space Sci. 23, 1611 (1975).

30. J. V. Evans and J. M. Holt, Planet. Space Sci. 26, 727 (1978).

31. J. V. Evans, J. Geophys. Res. 70, 4331 (1965).

32. _____, ibid. 73, 3489 (1968).

33. J. V. Evans and I. J. Gastman, J. Geophys. Res. 75, 807 (1970).

34. L. H. Brace and R. F. Theis, J. Geophys. Res. 79, 1871 (1974).

35. L. H. Brace, E. J. Maier, J. H. Hoffman, J. Whitteker and G. G. Shepherd, J. Geophys. Res. 79, 5211 (1974).

36. R. A. Duncan, J. Atmos. Terr. Phys. 31, 59 (1969).

37. H. G. Mayr and H. Volland, J. Geophys. Res. 77, 6774 (1972).

38. D. A. Antoniadis, J. Atmos. Terr. Phys. 38, 187 (1976).

39. R. G. Roble, J. E. Salah and B. A. Emery, J. Atmos. Terr. Phys. 39, 503 (1977).

40. B. A. Emery, J. Geophys. Res. 83, 5691 (1978).

41. _____, ibid. 83, 5704 (1978).

42. G. Hernandez and R. G. Roble, J. Geophys. Res. 81, 2065 (1976).

43. R. E. Dickinson, E. C. Ridley and R. G. Roble, J. Atmos. Sci. 32, 1737 (1975).

44. _____, ibid. 34, 178 (1977).

45. R. G. Roble, R. E. Dickinson and E. C. Ridley, J. Geophys. Res. 82, 5493 (1977).

46. J. M. Straus and L. A. Christopher, "Dynamical Effects on the Global Distribution of Thermospheric Oxygen", Aerospace Corporation Report ATR-78(8203)-3, 53 pp. (1978).

47. G. Hernandez and R. G. Roble, J. Geophys. Res. 82, 5505 (1977).

48. A. E. Hedin, C. A. Reber, G. P. Newton, N. W. Spencer, H. C. Brinton, H. G. Mayr and W. E. Potter, J. Geophys. Res. 82, 2148 (1977).

49. H. G. Mayr, A. E. Hedin, C. A. Reber and G. R. Carignan, J. Geophys. Res. 79, 619 (1974).

50. K. Mauersberger, D. C. Kayser, W. E. Potter and A. O. Neir, J. Geophys. Res. 81, 7 (1976).

51. U. von Zahn and K. H. Fricke, Rev. Geophys. Space Phys. 16, 169 (1978).

52. H. Rishbeth, J. Atmos.Terr. Phys. 37, 1055 (1975).

53. H. G. Mayr and H. Volland, Planet. Space Sci. 20, 379 (1972).

54. _____, J. Geophys. Res. 78, 2251 (1973).

55. D. W. Roper and A. J. Baxter, J. Atmos. Terr. Phys. 40, 585 (1978).

56. H. F. Bates and T. D. Roberts, J. Atmos. Terr. Phys. 39, 87 (1977).

57. P. B. Hays and R. G. Roble, J. Geophys. Res. 76, 5316 (1971).

58. D. W. Sipler and M. A. Biondi, J. Geophys. Res. 84, 37 (1979).

59. G. Hernandez and R. G. Roble, J. Geophys. Res. 81, 5173 (1976).

60. R. H. Wand, private communication (1978).

61. J. V. Evans, J. Geophys. Res. 77, 2341 (1972).

62. P. M. Banks, J. Atmos. Terr. Phys. 39, 179 (1977).

63. J. S. Nisbet, M. J. Miller and L. A. Carpenter, J. Geophys. Res. 83, 2647 (1978).

64. J. M Straus and M. Schulz, J. Geophys. Res. 81, 5822, (1976).

65. A. D. Richmond, J. Geophys. Res. 83, 4131, (1978).

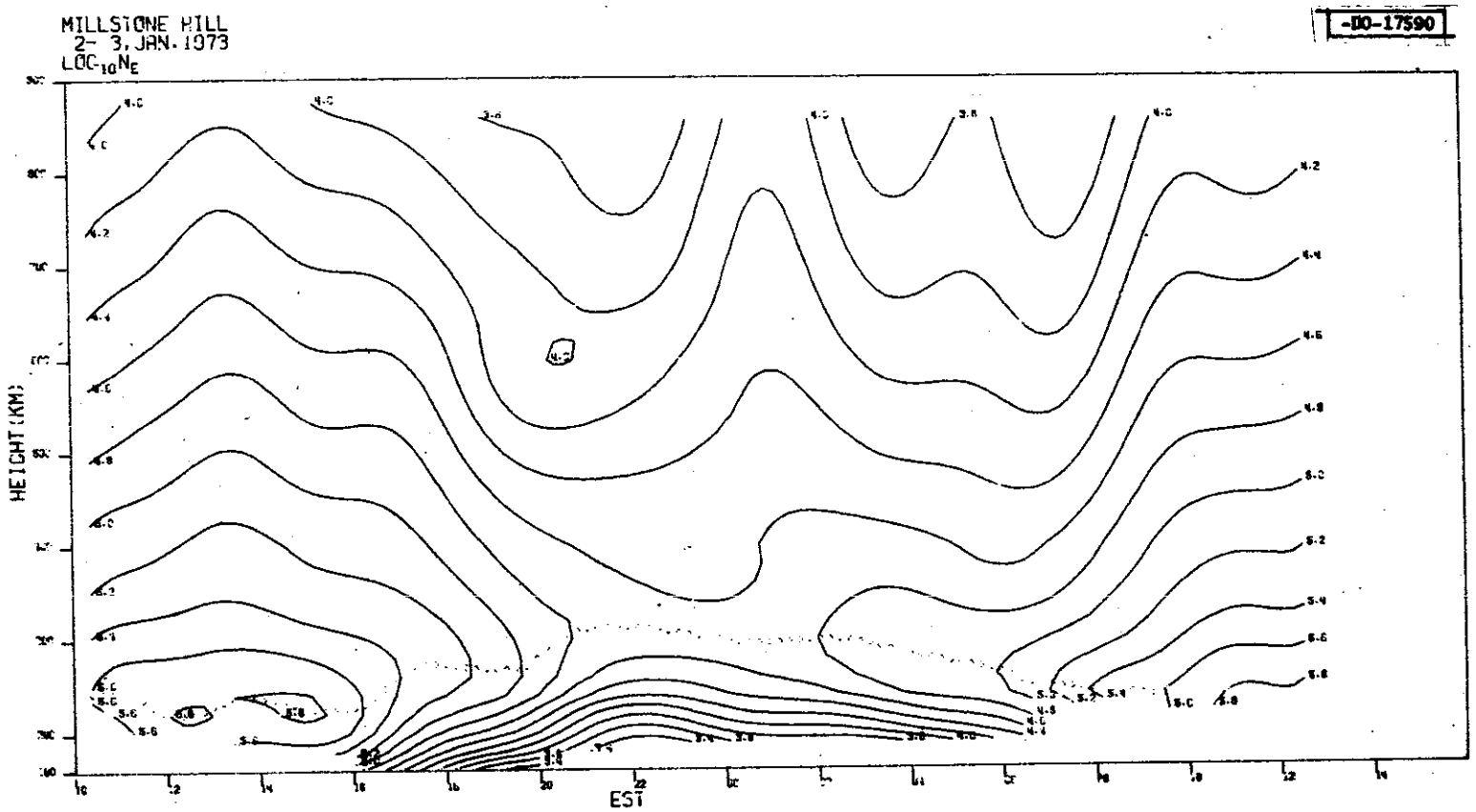

(a) Contours of Log_{10} Ne.

Fig. 1(a-d). Results for 2-3 January.

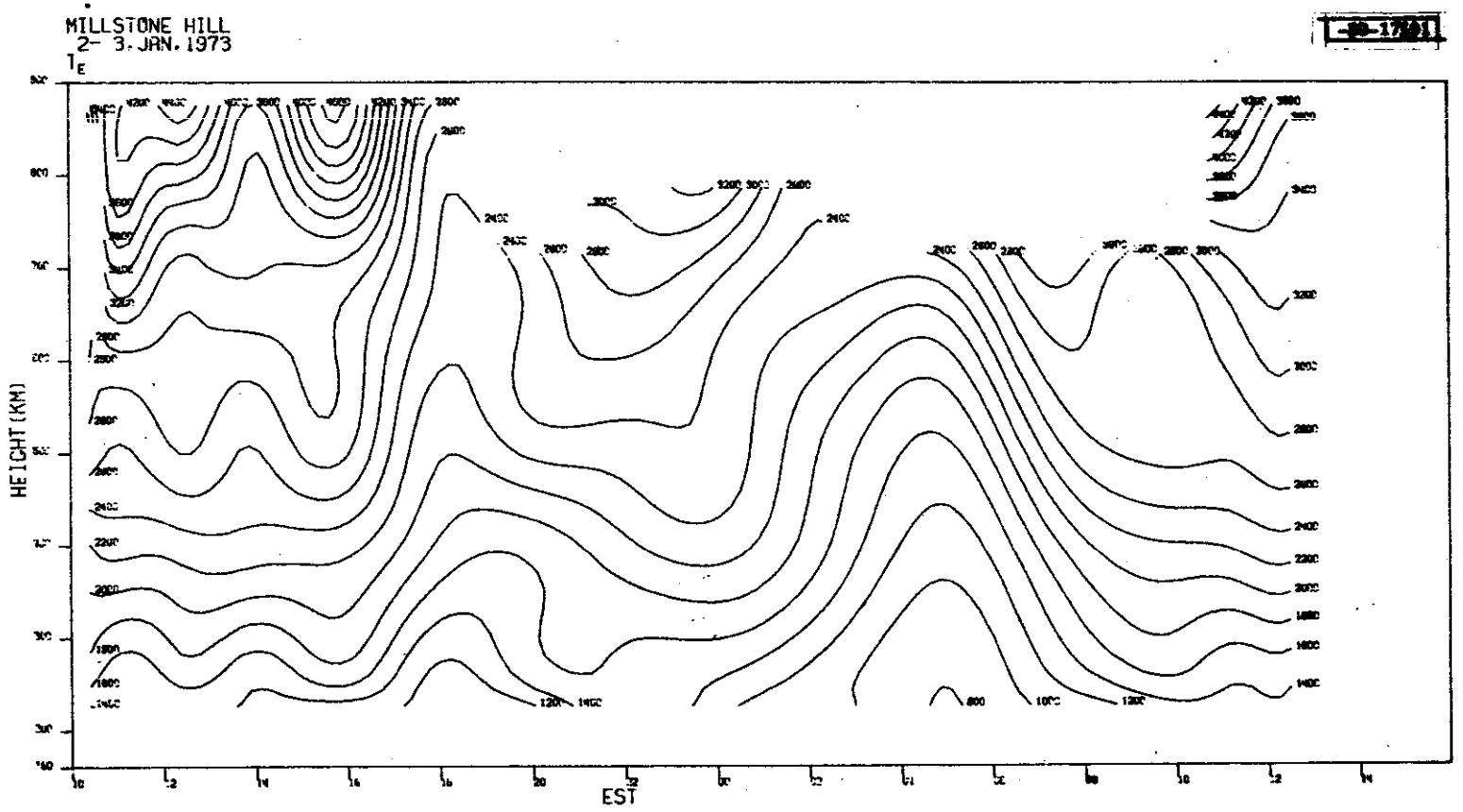

(b) Contours of T_e.

Fig. 1(a-d). Continued.

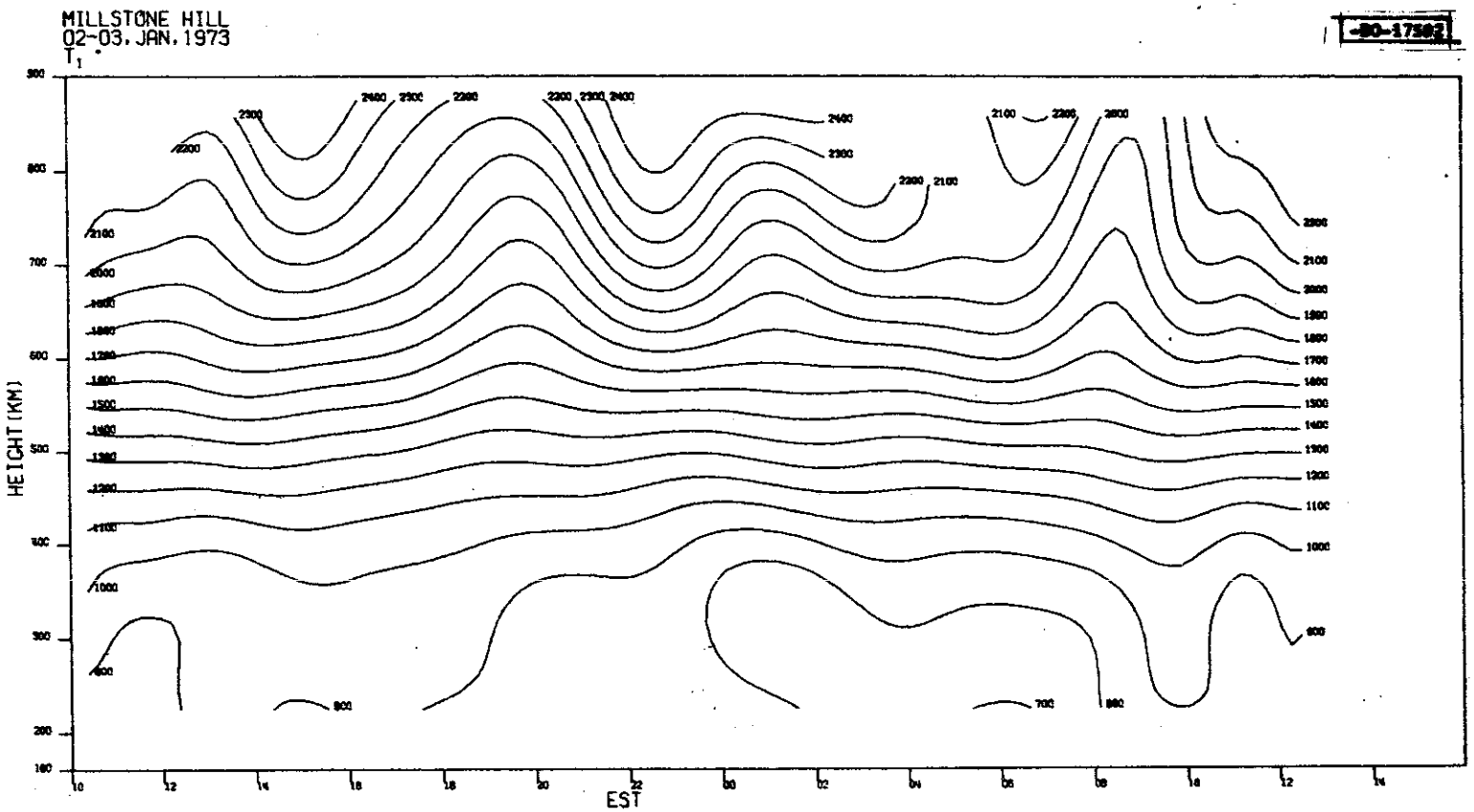

(c) Contours of T_i.

Fig. 1(a-d). Continued.

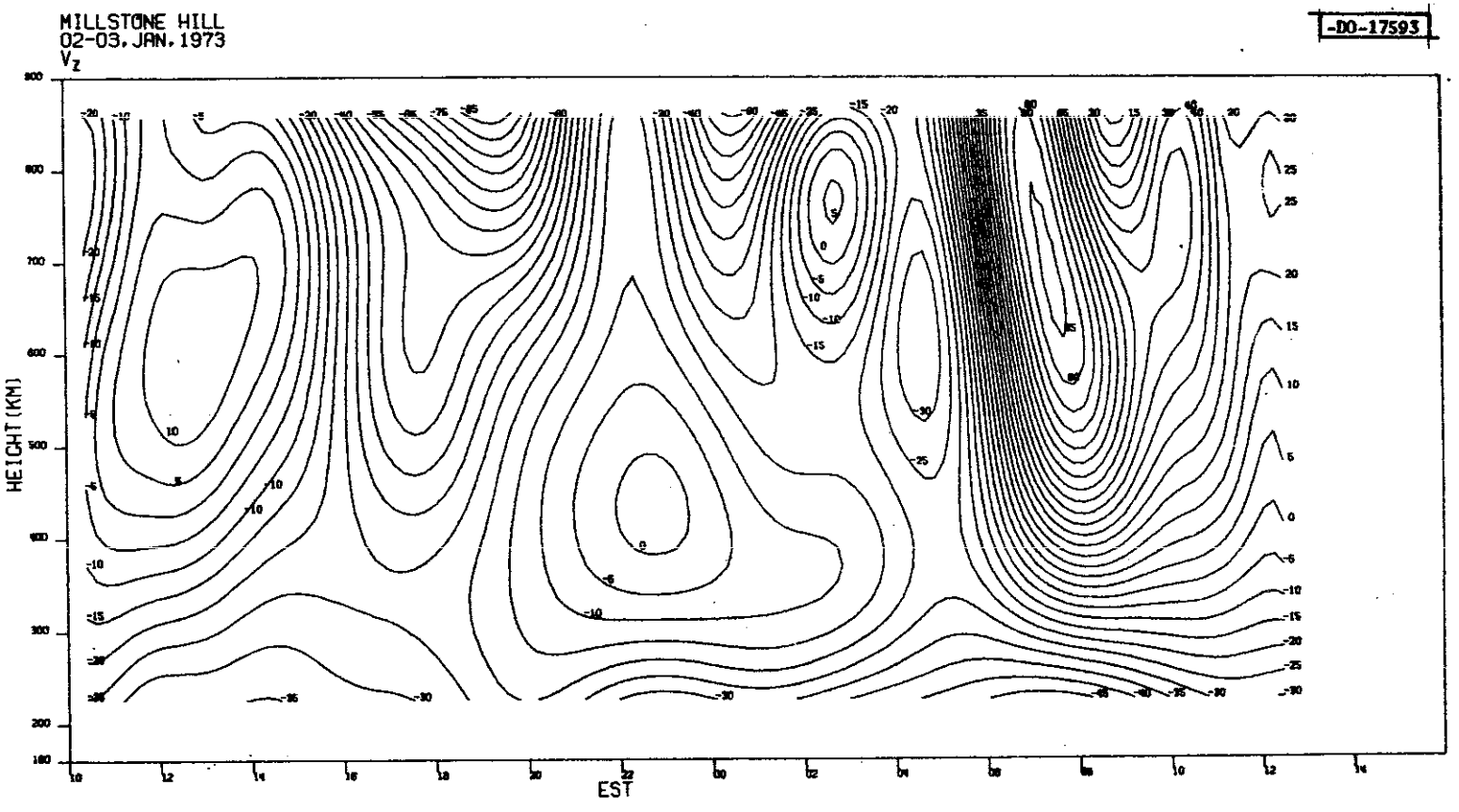

(d) Contours of V_Z.

Fig. 1(a-d). Continued.

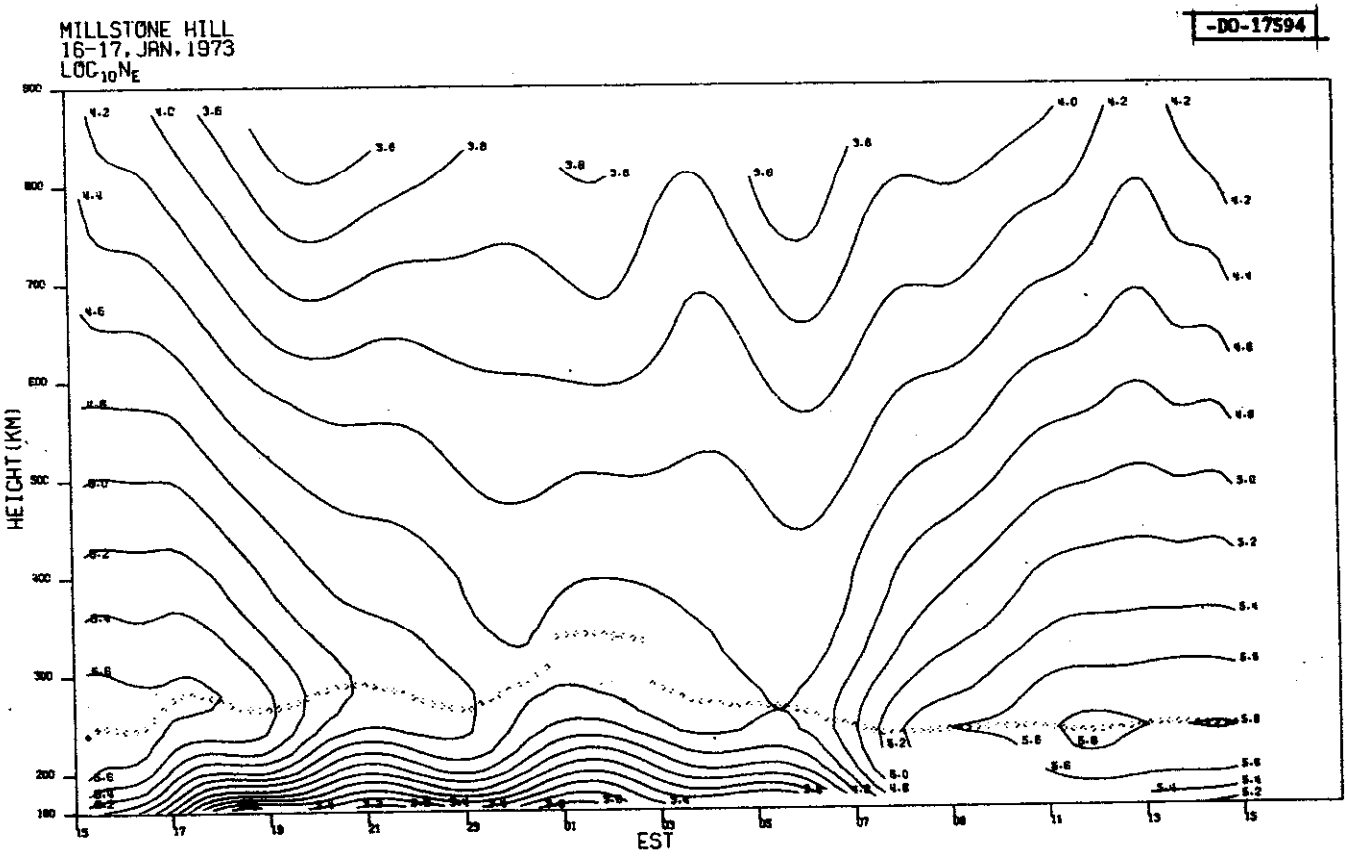

(a) Contours of $Log_{10} N_e$.

Fig. 2(a-d). Results for 16-17 January.

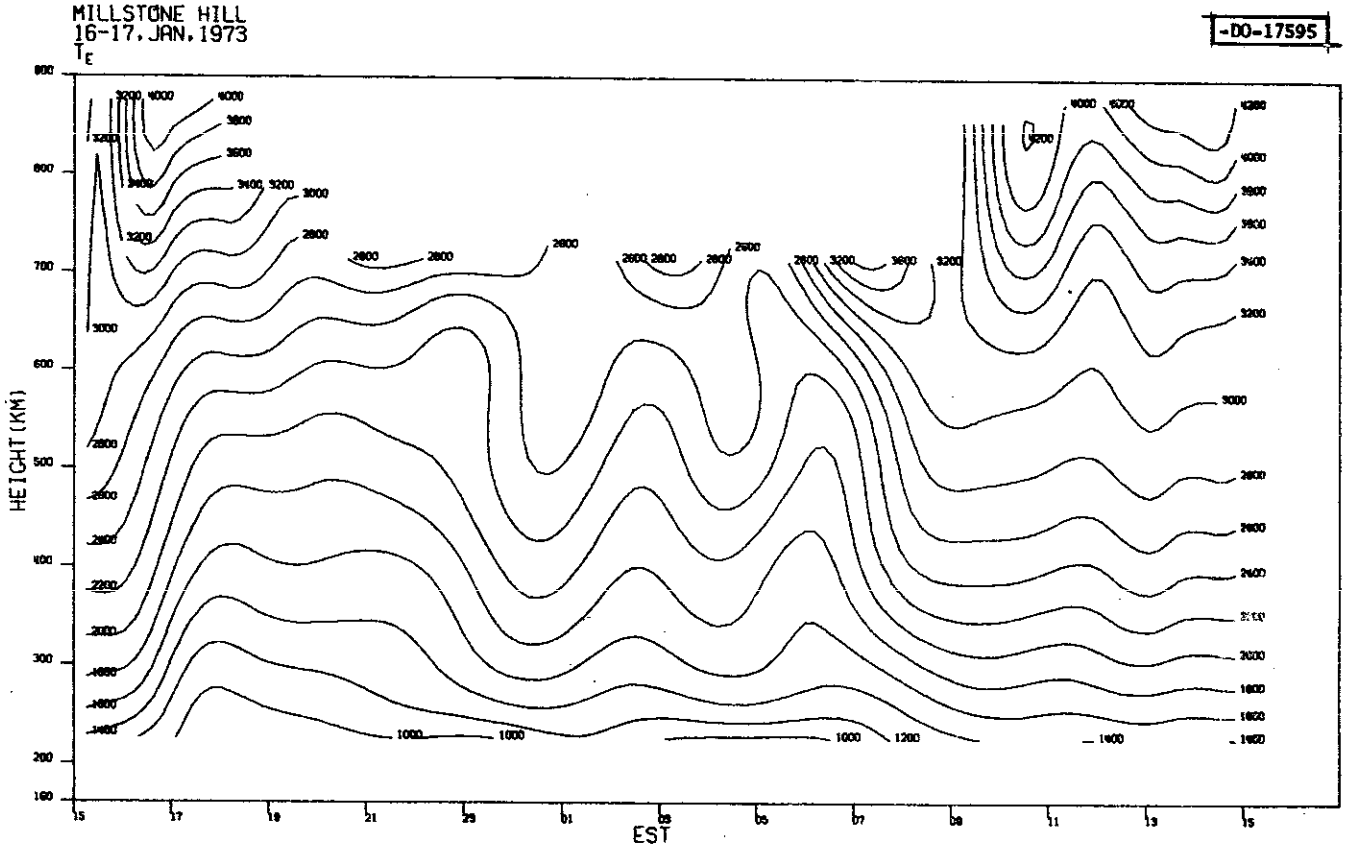

(b) Contours of T_e.

Fig. 2(a-d). Continued.

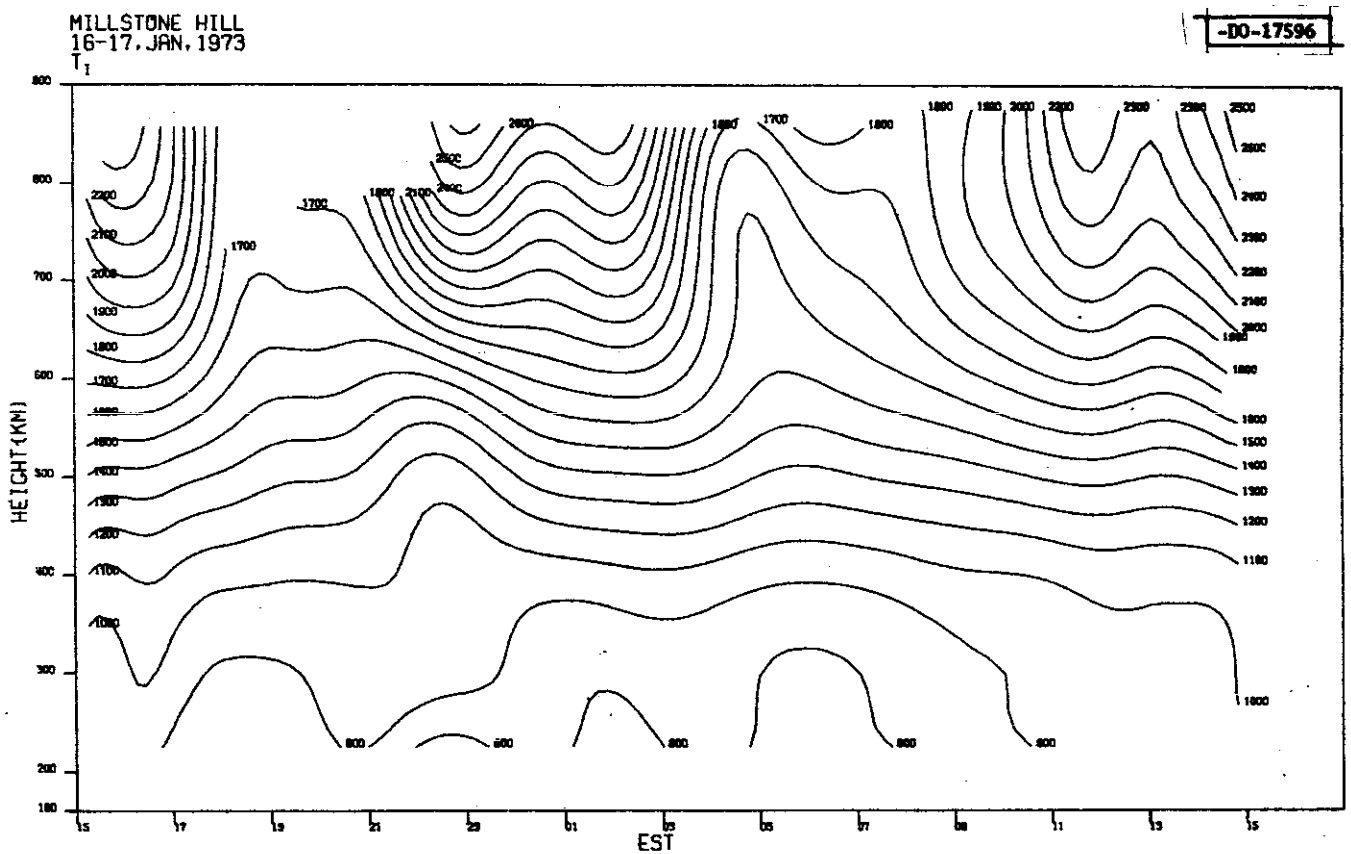

(c) Contours of T_i.

Fig. 2(a-d). Continued.

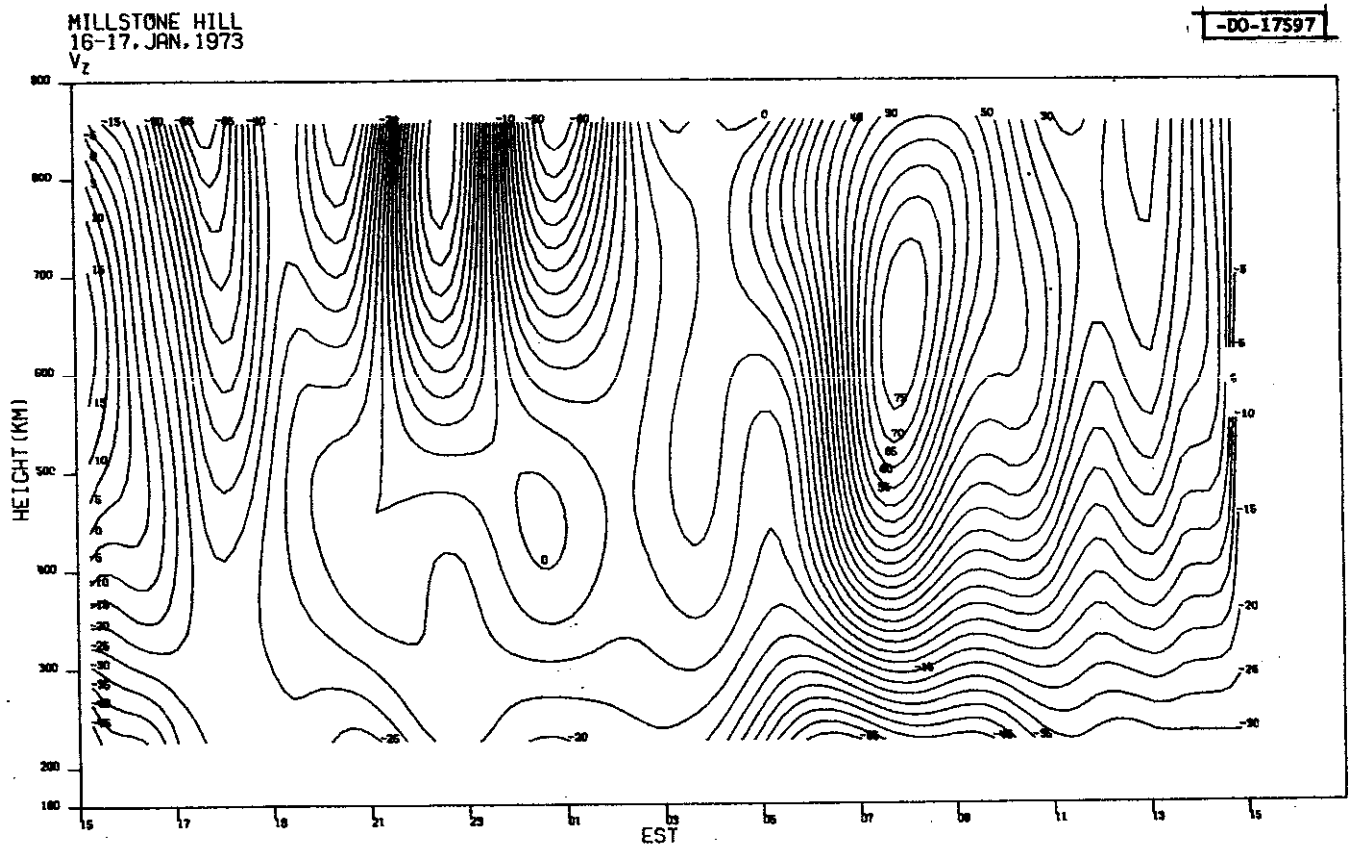

(d) Contours of V_z.

Fig. 2(a-d). Continued.

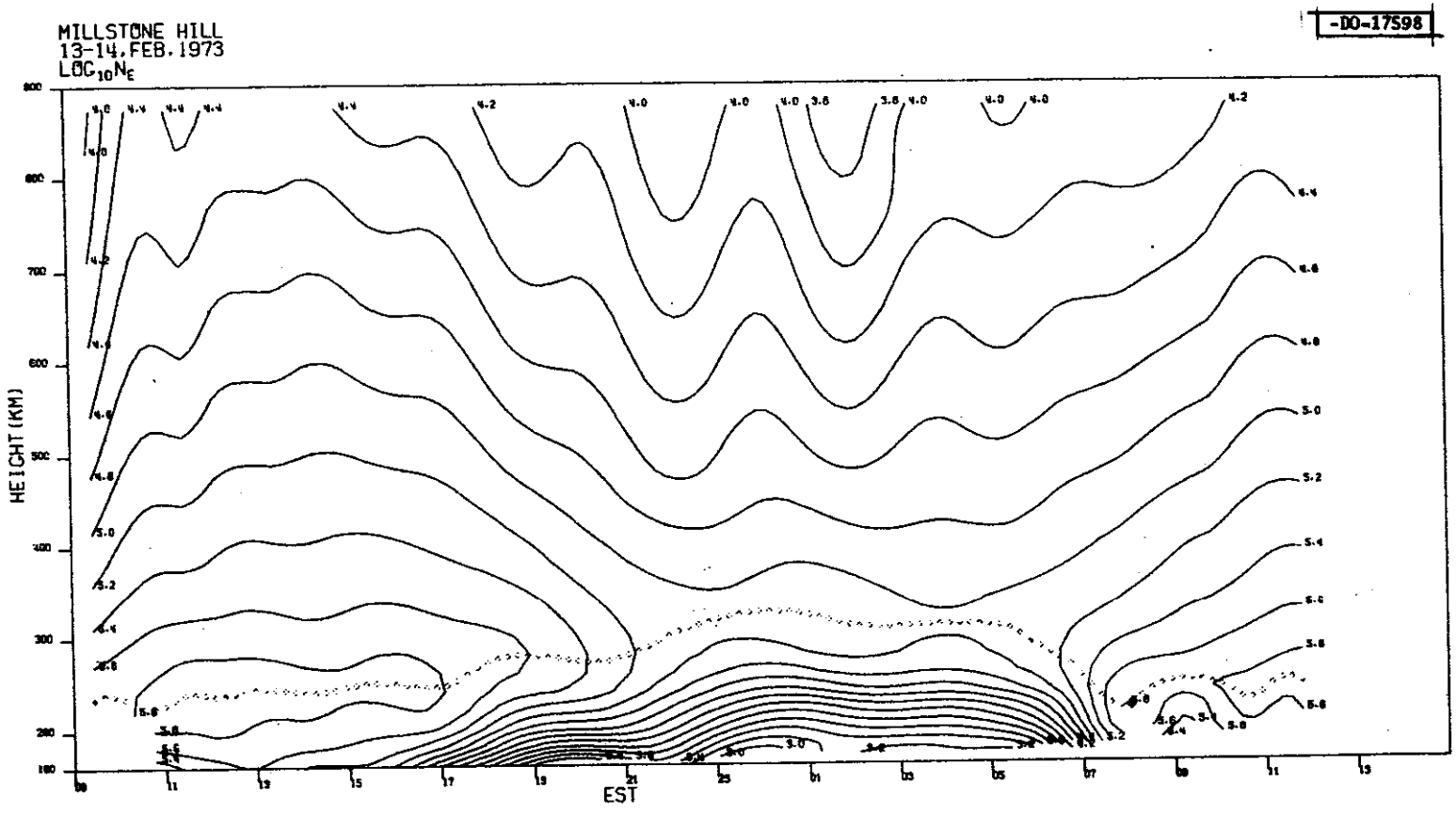

(a) Contours of $Log_{10}\ N_e$.

Fig. 3(a-d). Results for 13-14 February.

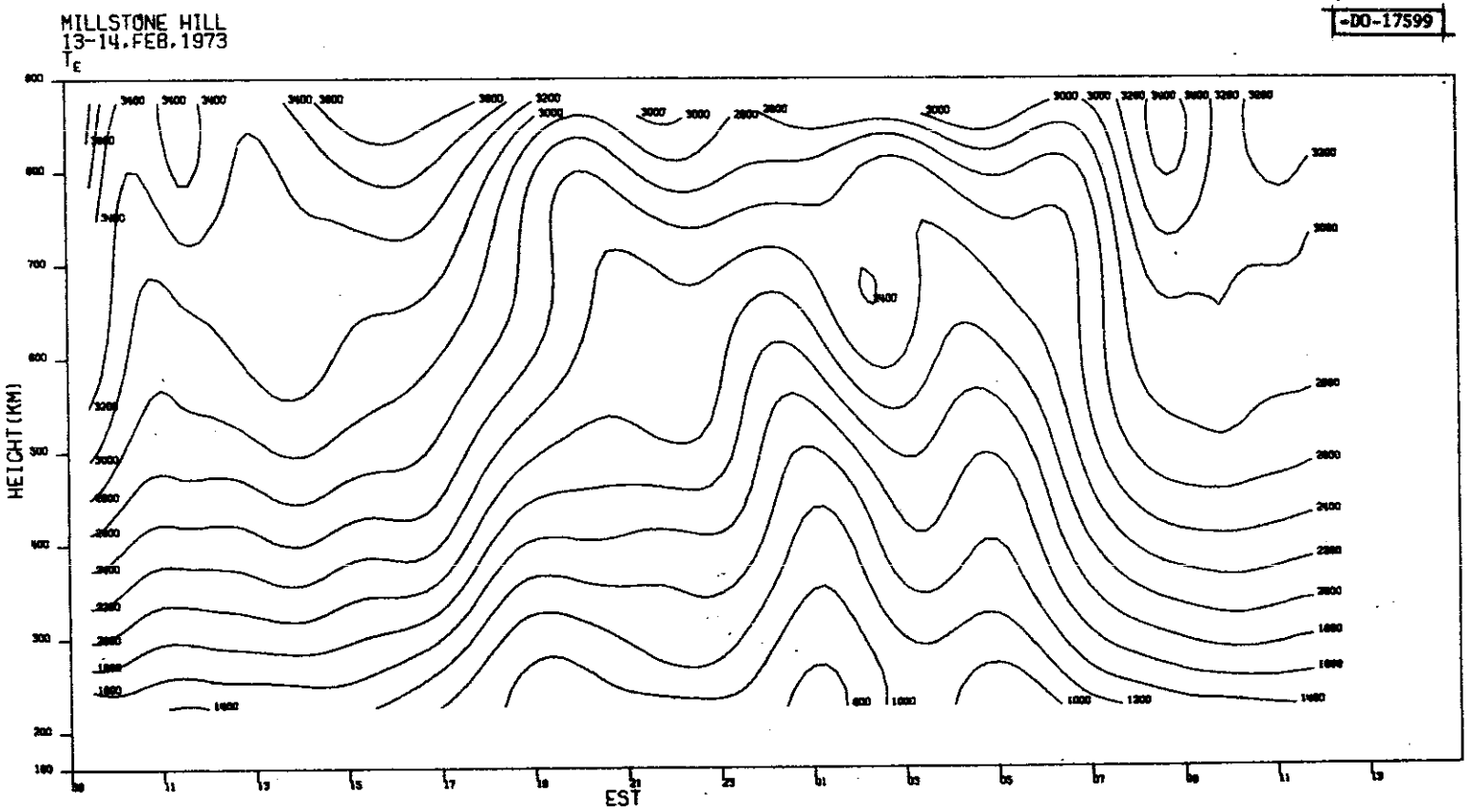

(b) Contours of T_e.

Fig. 3(a-d). Continued.

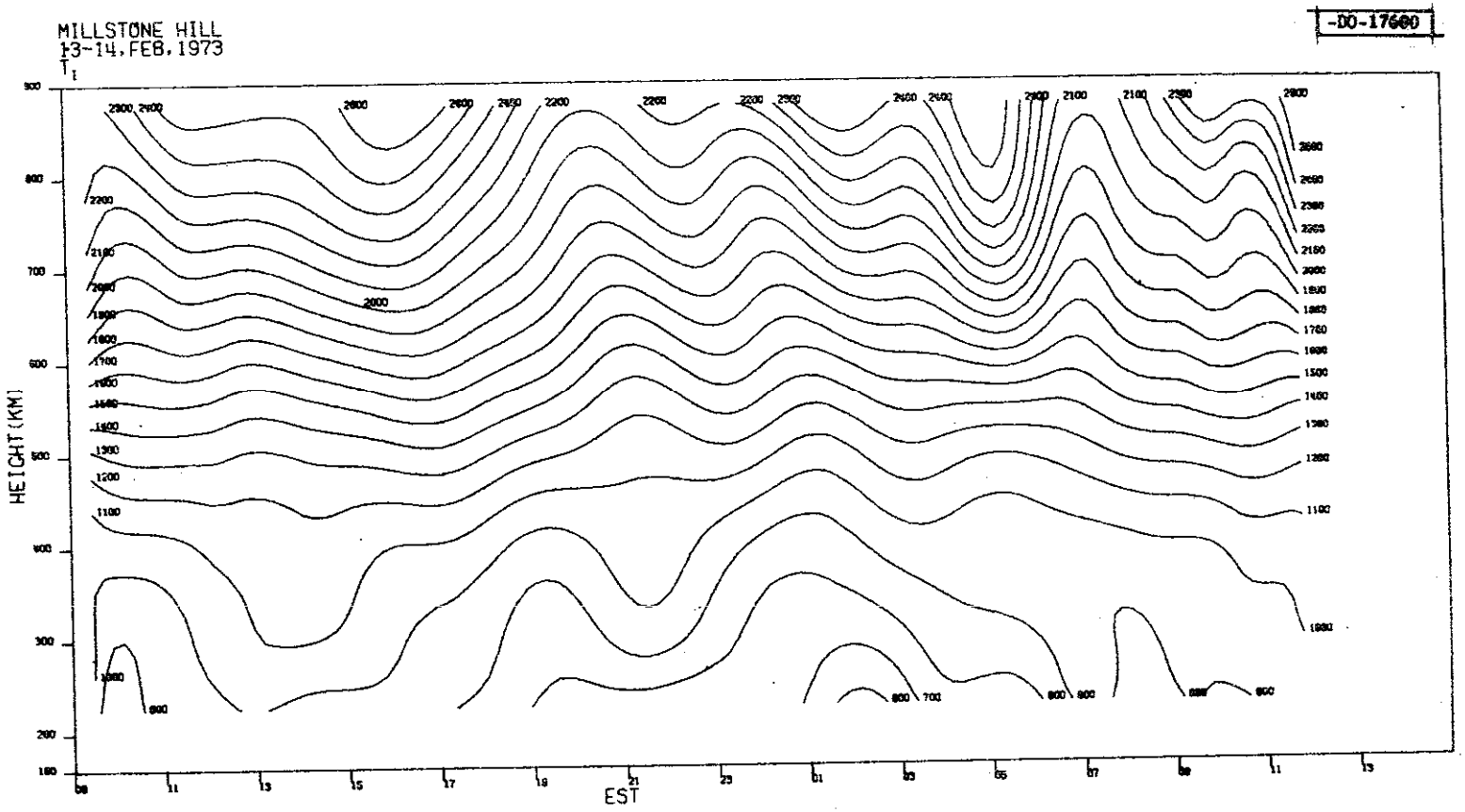

(c) Contours of T_i.

Fig. 3(a-d). Continued.

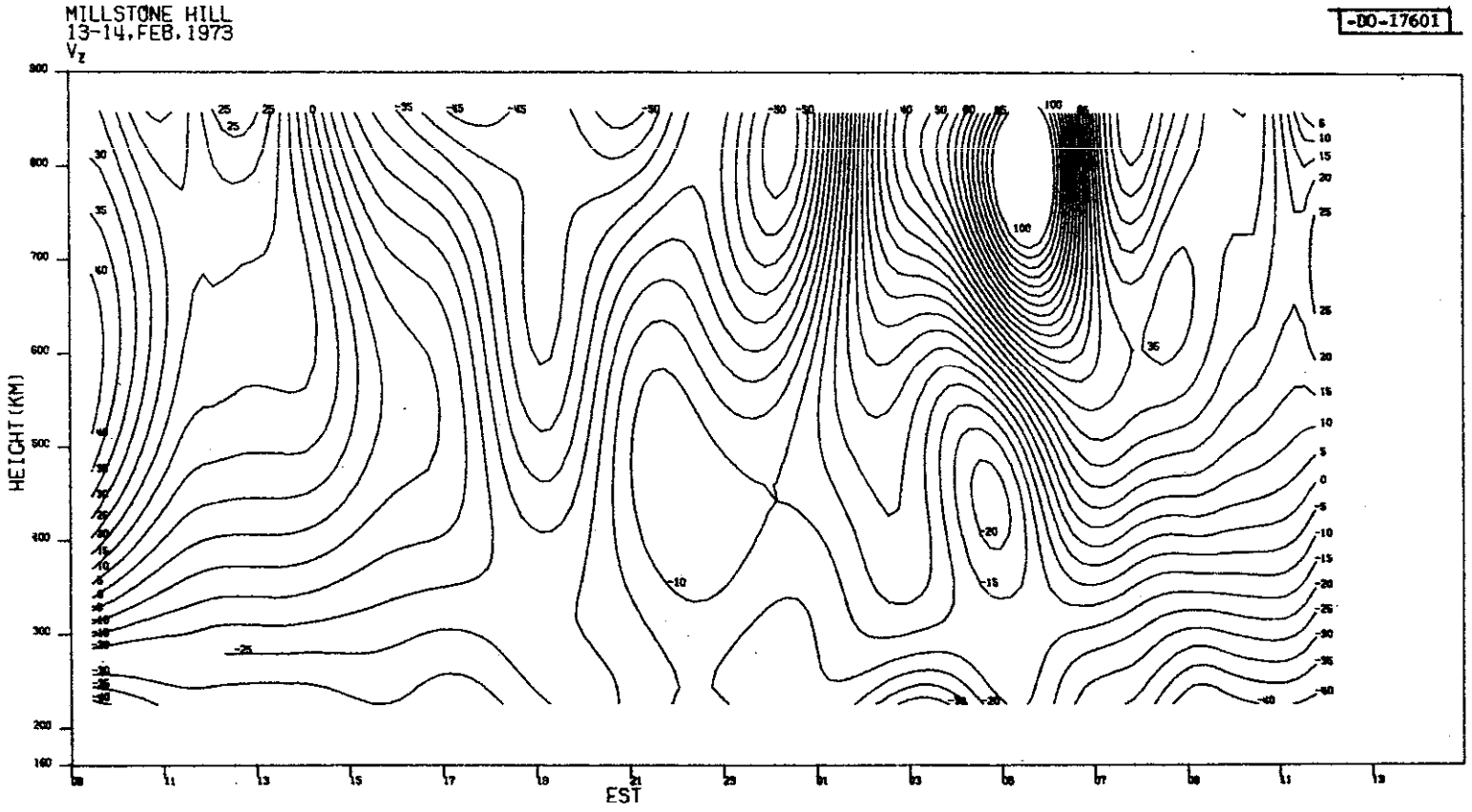

(d) Contours of V_z.

Fig. 3(a-d). Continued.

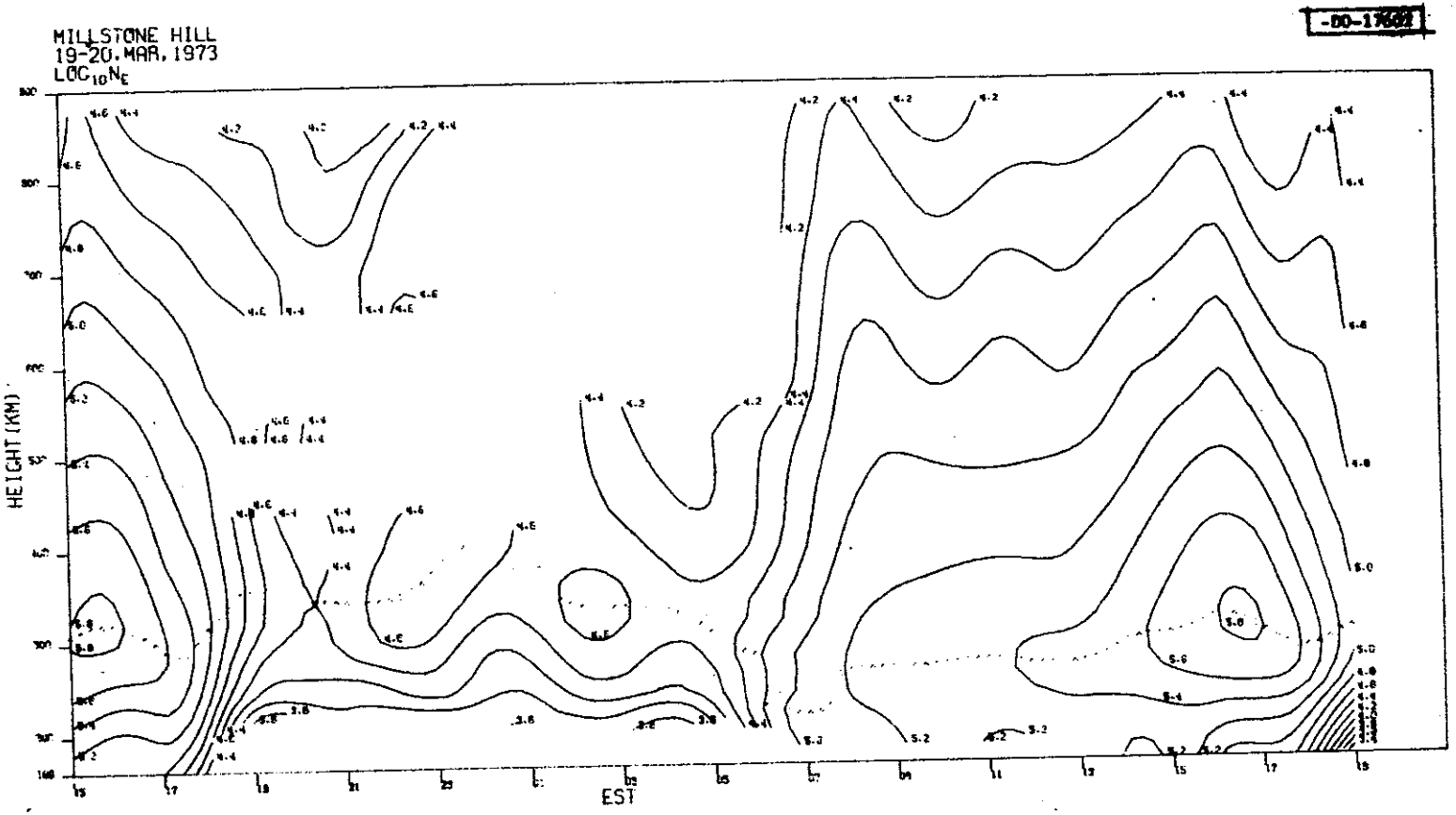

(a) Contours of $Log_{10}\ N_e$.

Fig. 4(a-d). Results for 19-20 March.

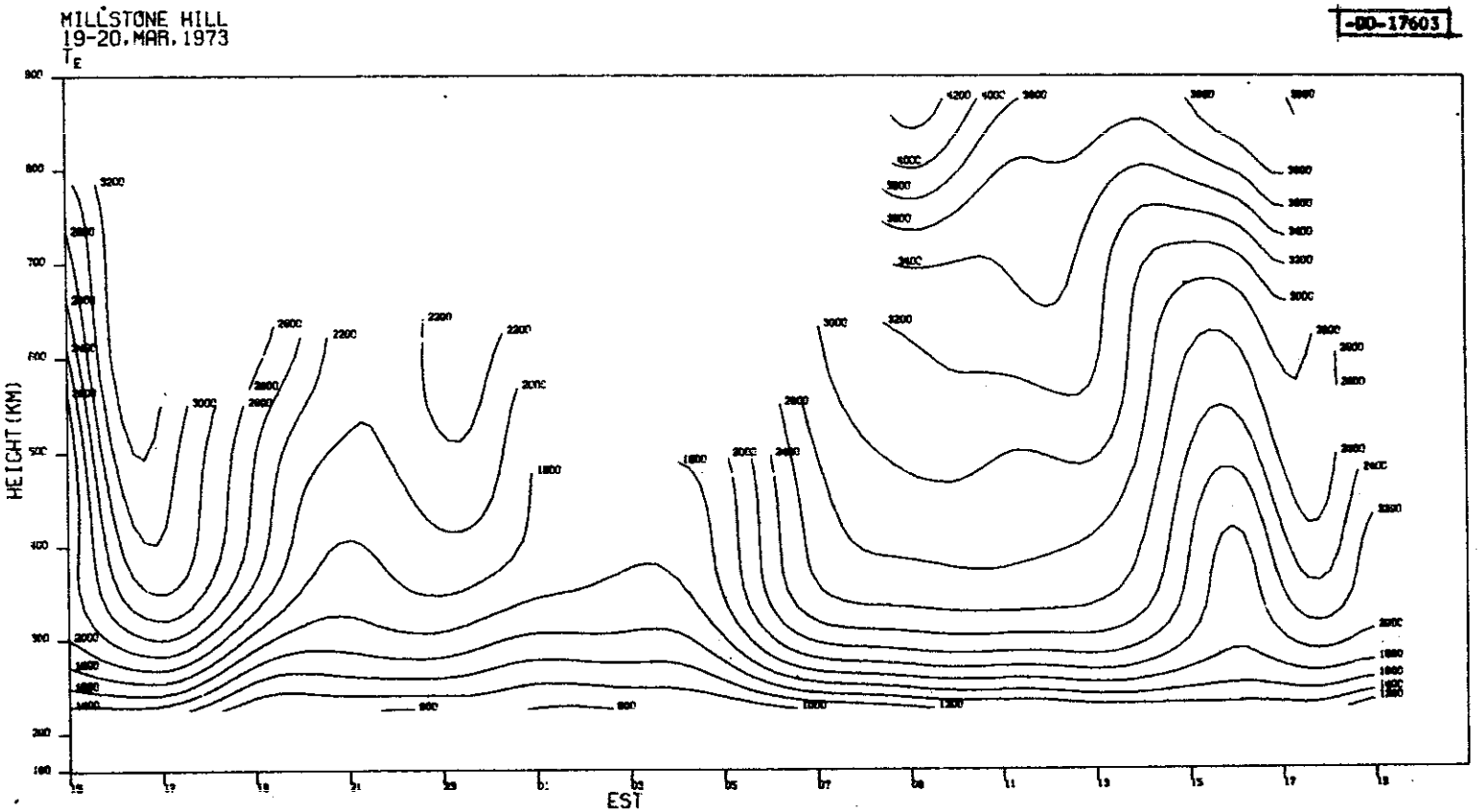

(b) Contours of T_e.

Fig. 4(a-d). Continued.

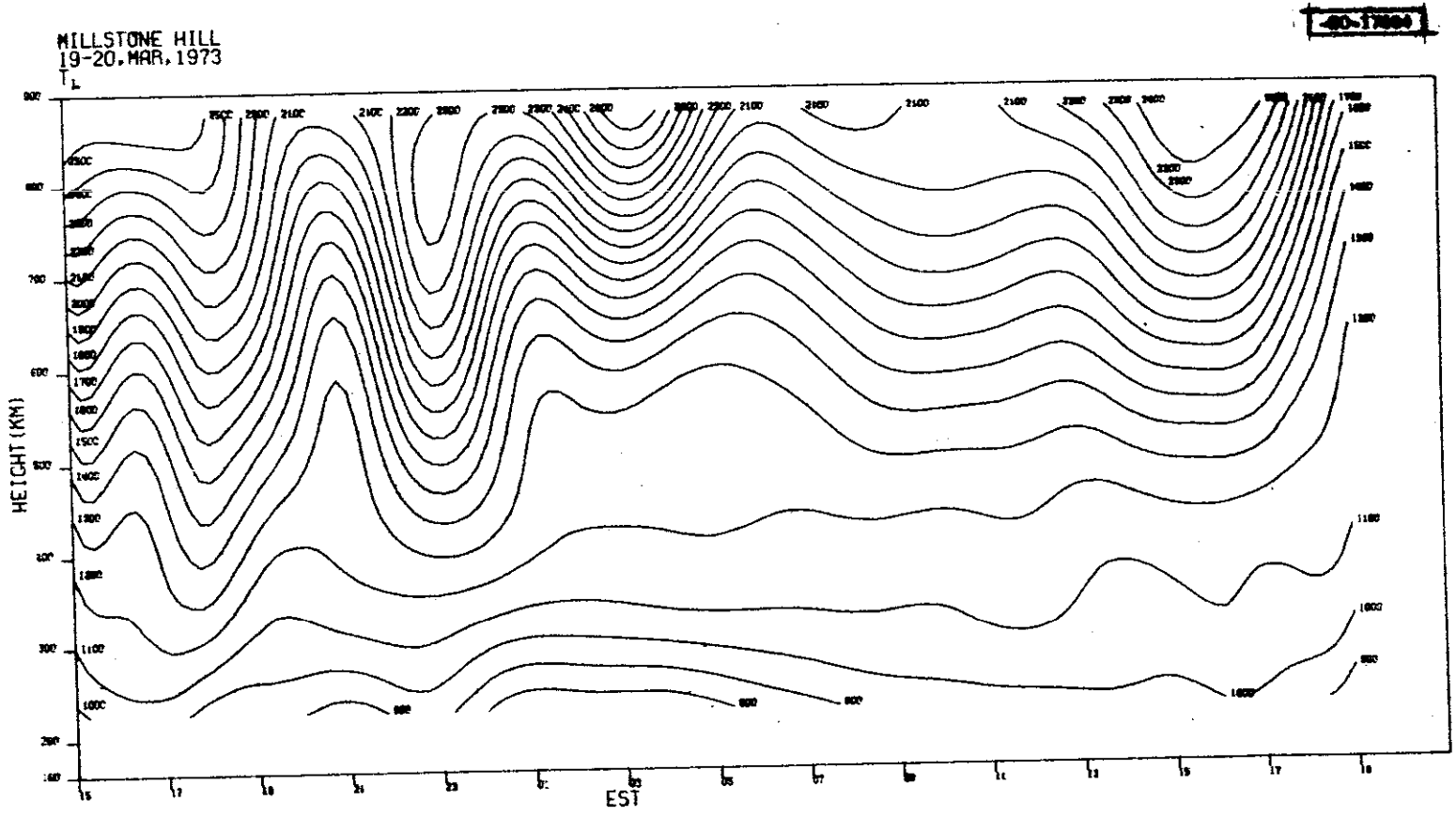

(c) Contours of T_i.

Fig. 4(a-d). Continued.

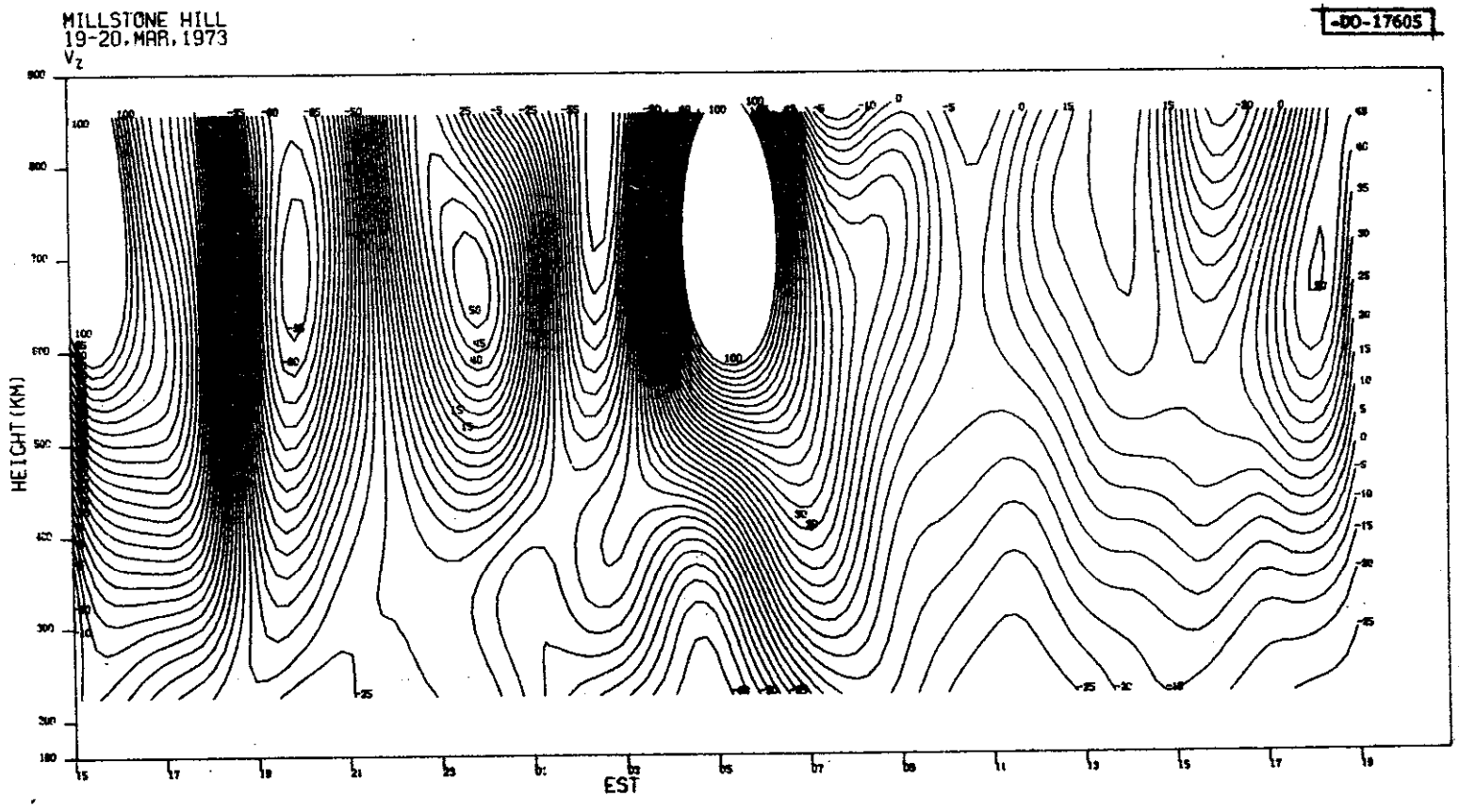

(d) Contours of V_z.

Fig. 4(a-d). Continued.

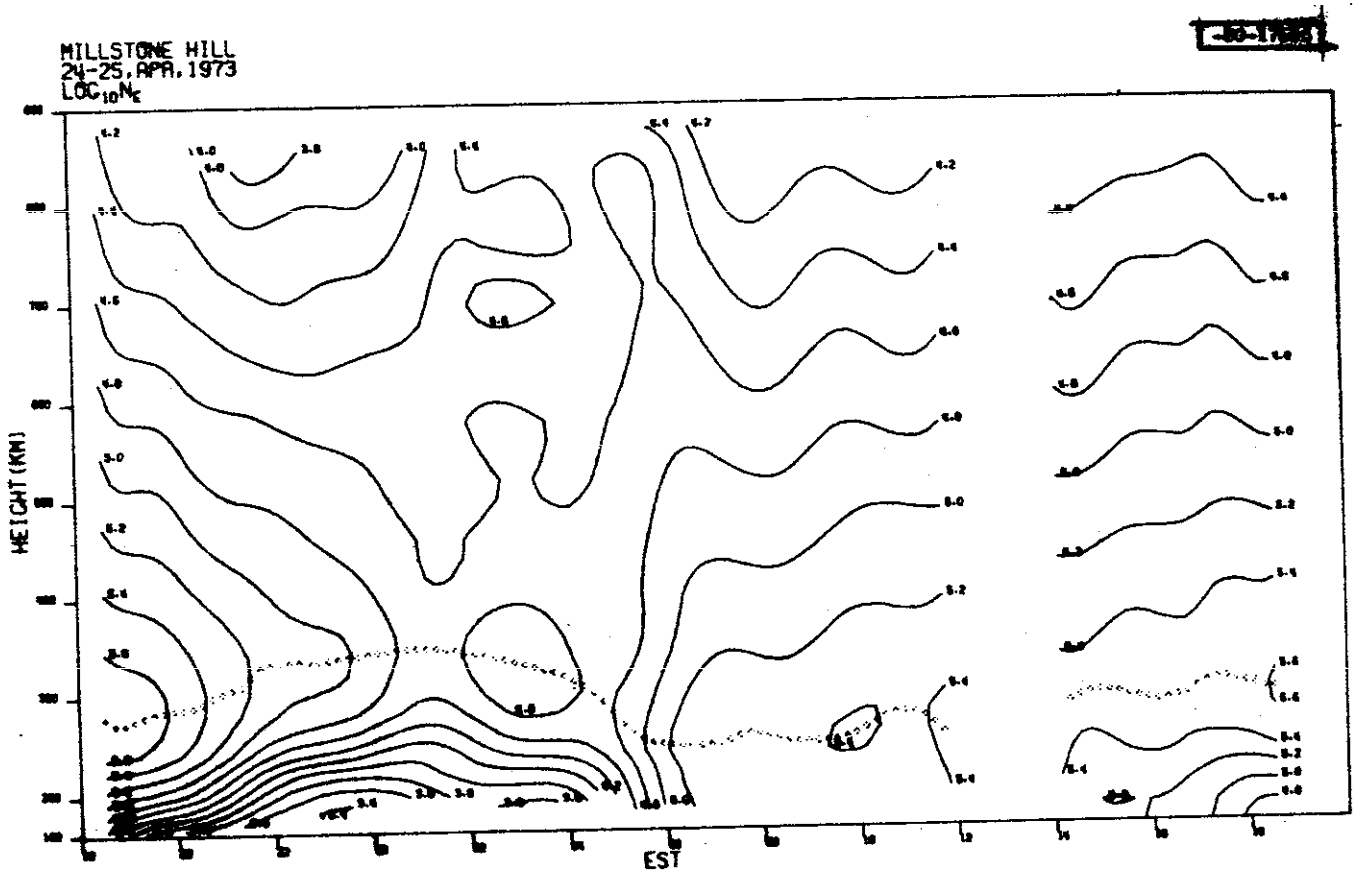

(a) Contours of $Log_{10} N_e$.

Fig. 5(a-d). Results for 24-25 April.

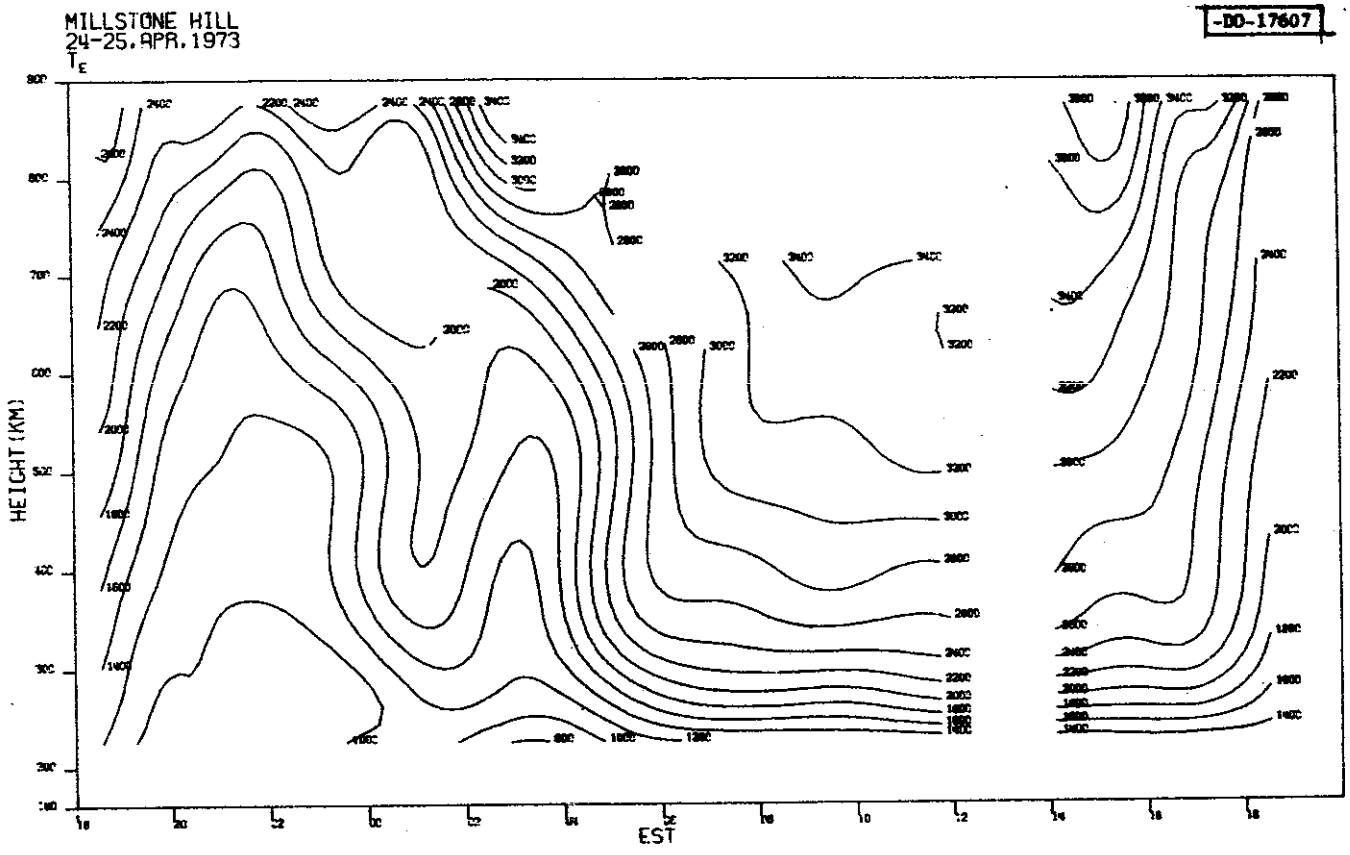

(b) Contours of T_e.

Fig. 5(a-d). Continued.

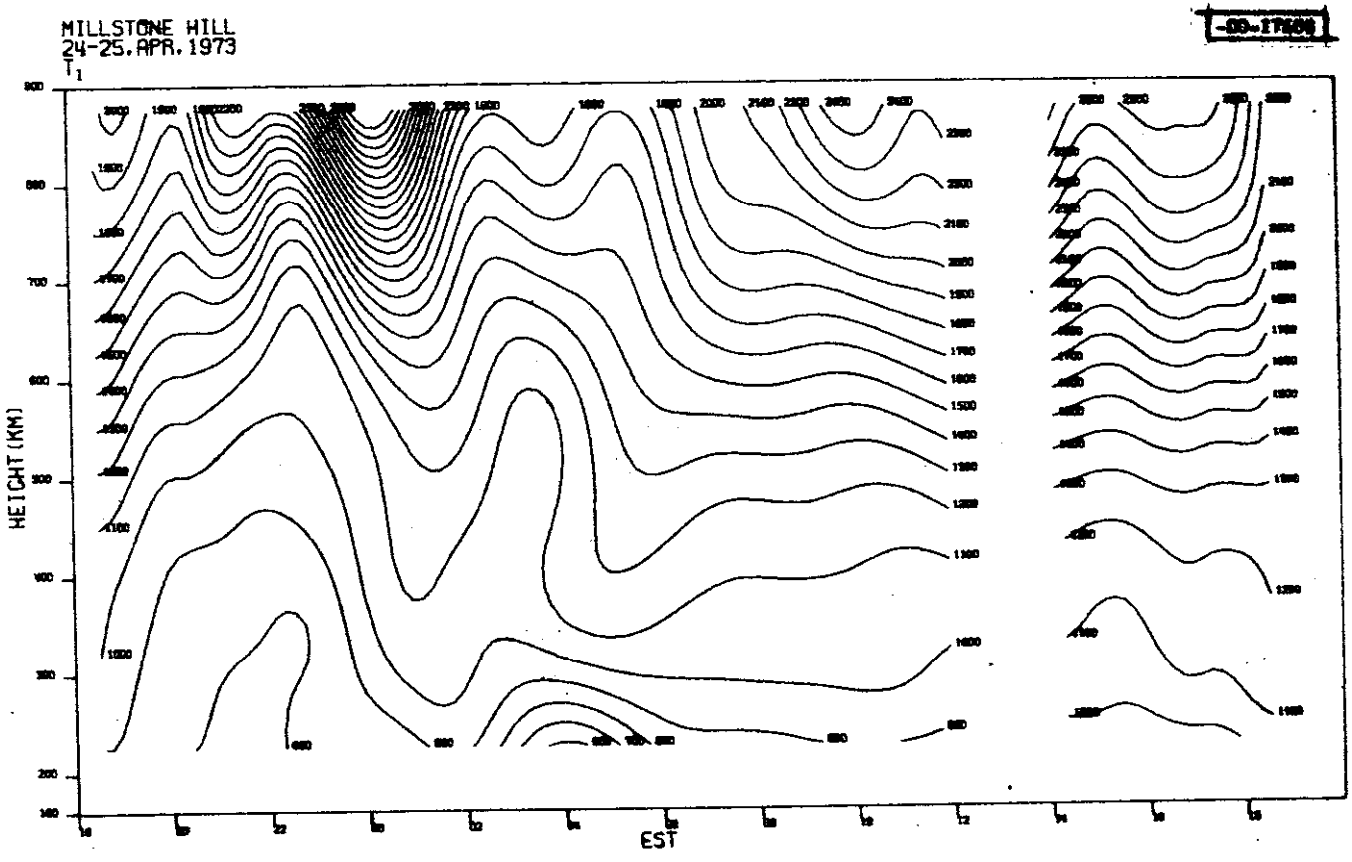

(c) Contours of T_i.

Fig. 5(a-d). Continued.

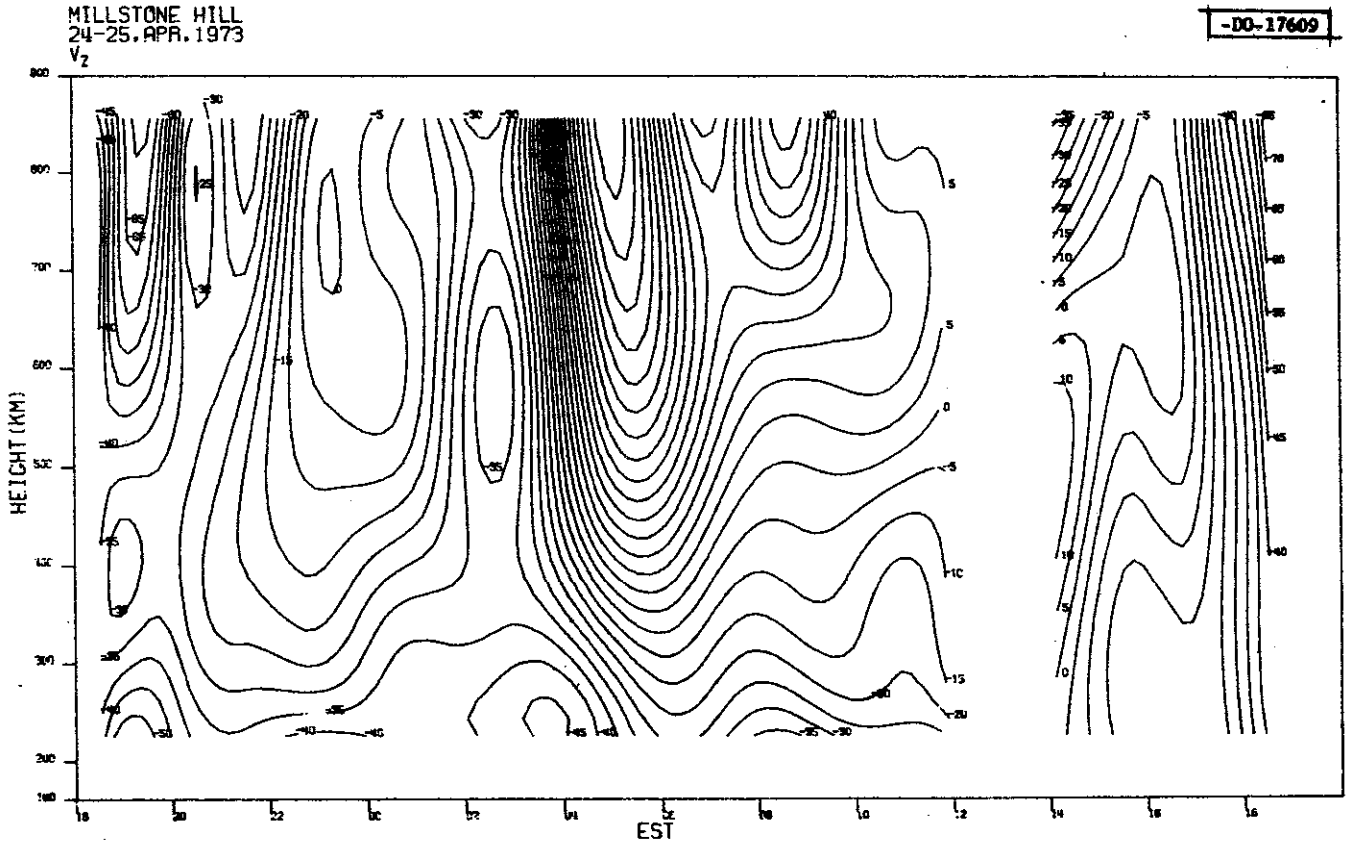

(d) Contours of V_z.

Fig. 5(a-d). Continued.

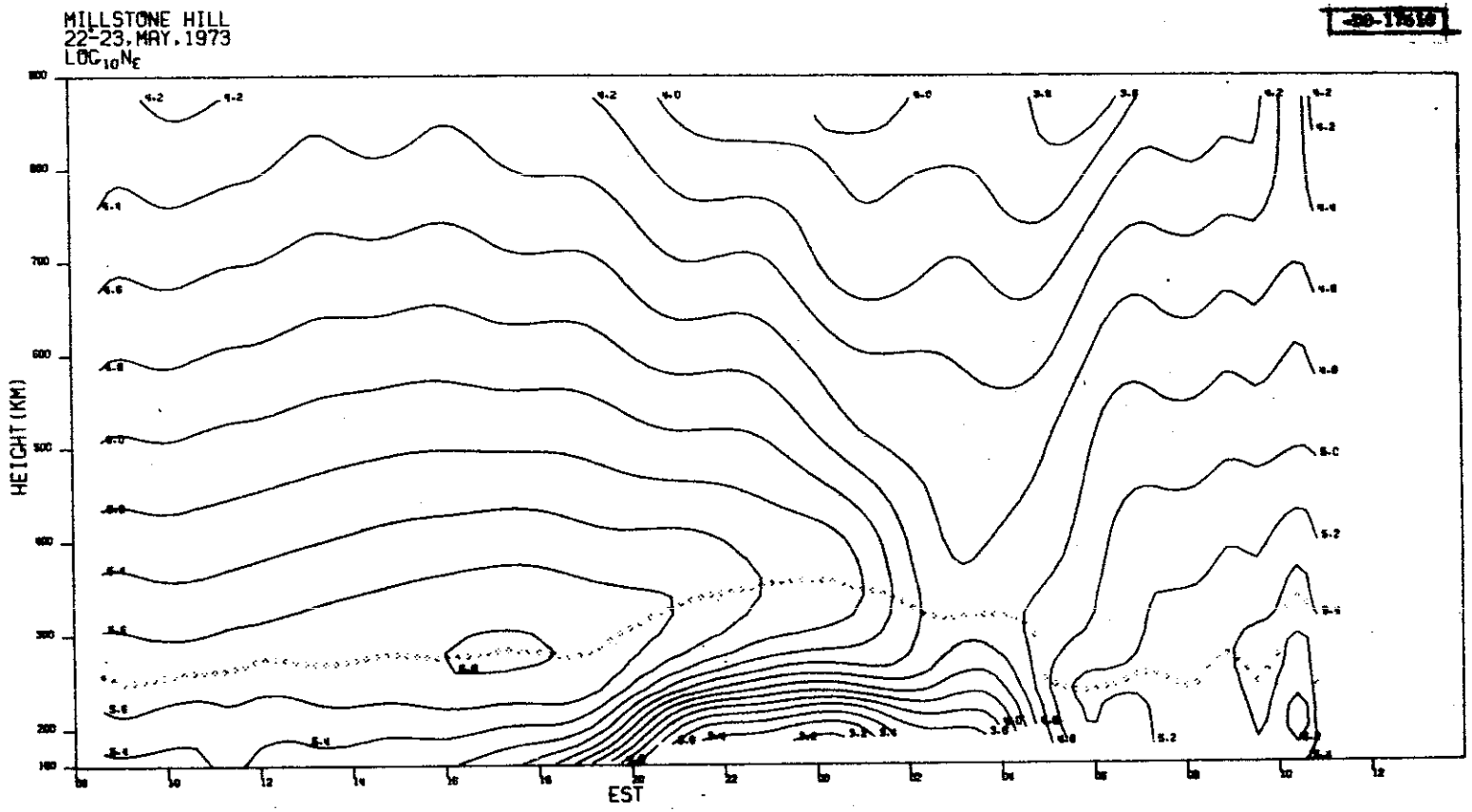

(a) Contours of $Log_{10}\ N_e$.

Fig. 6(a-d). Results for 22-23 May.

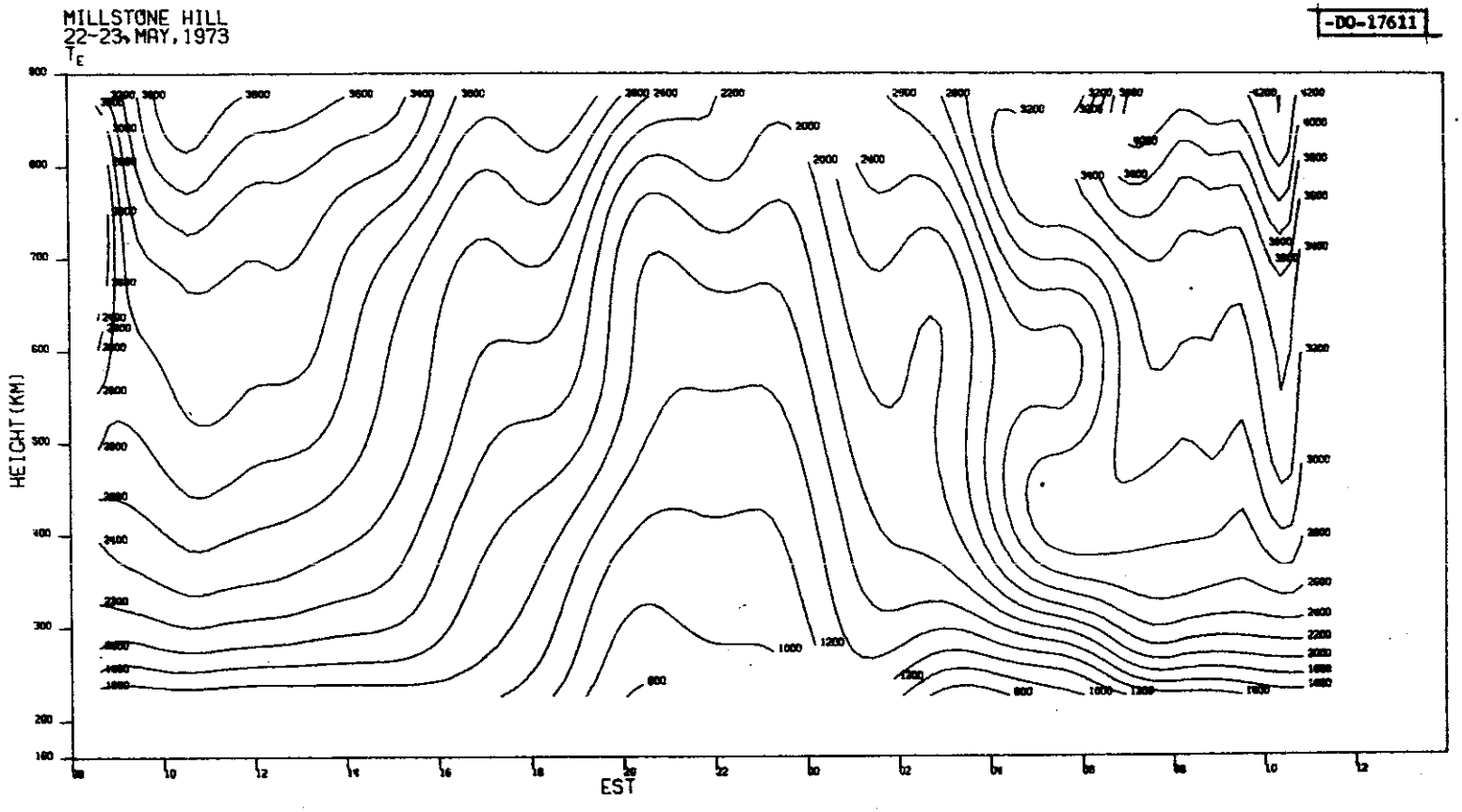

(b) Contours of T_e.

Fig. 6(a-d). Continued.

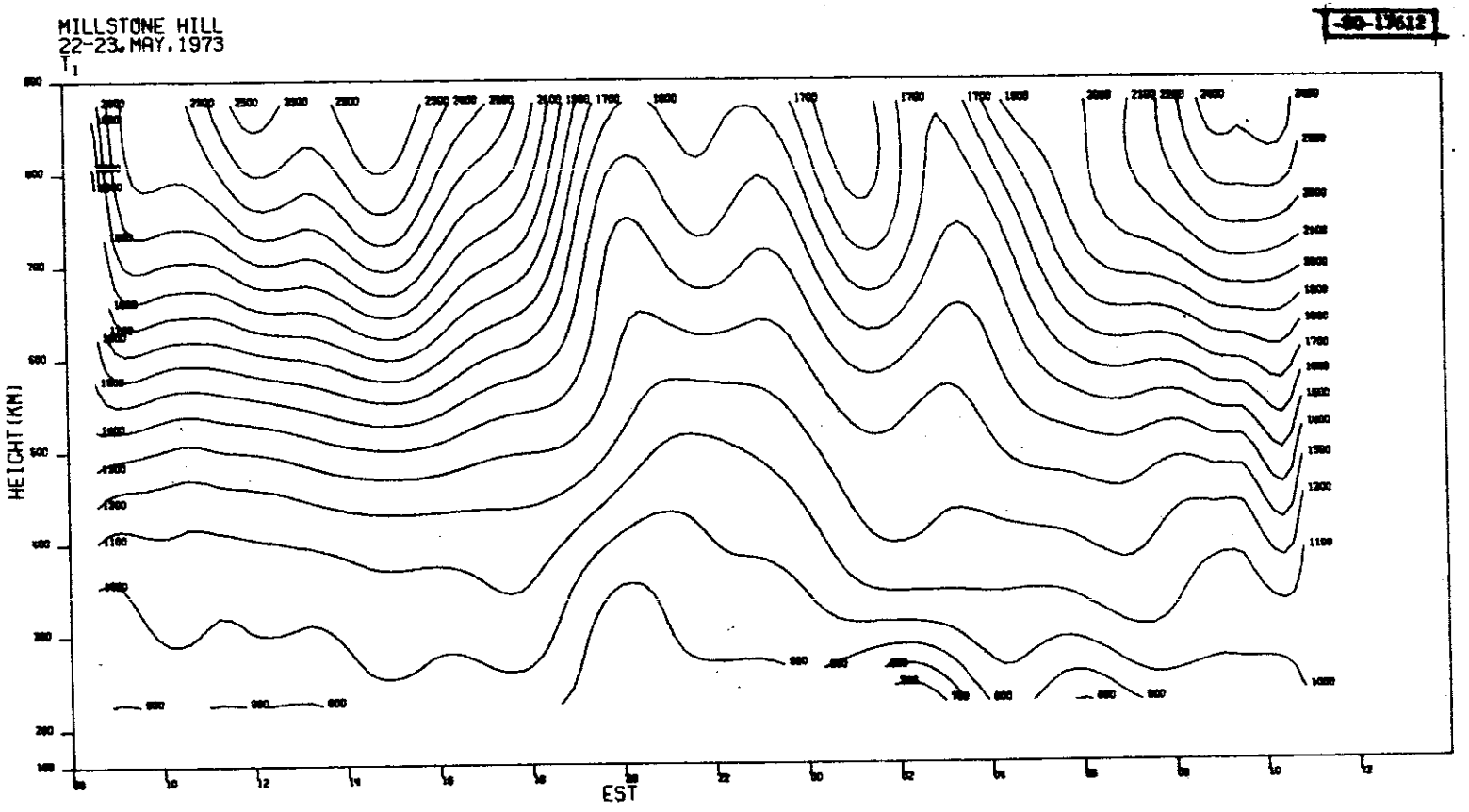

(c) Contours of T_i.

Fig. 6(a-d). Continued.

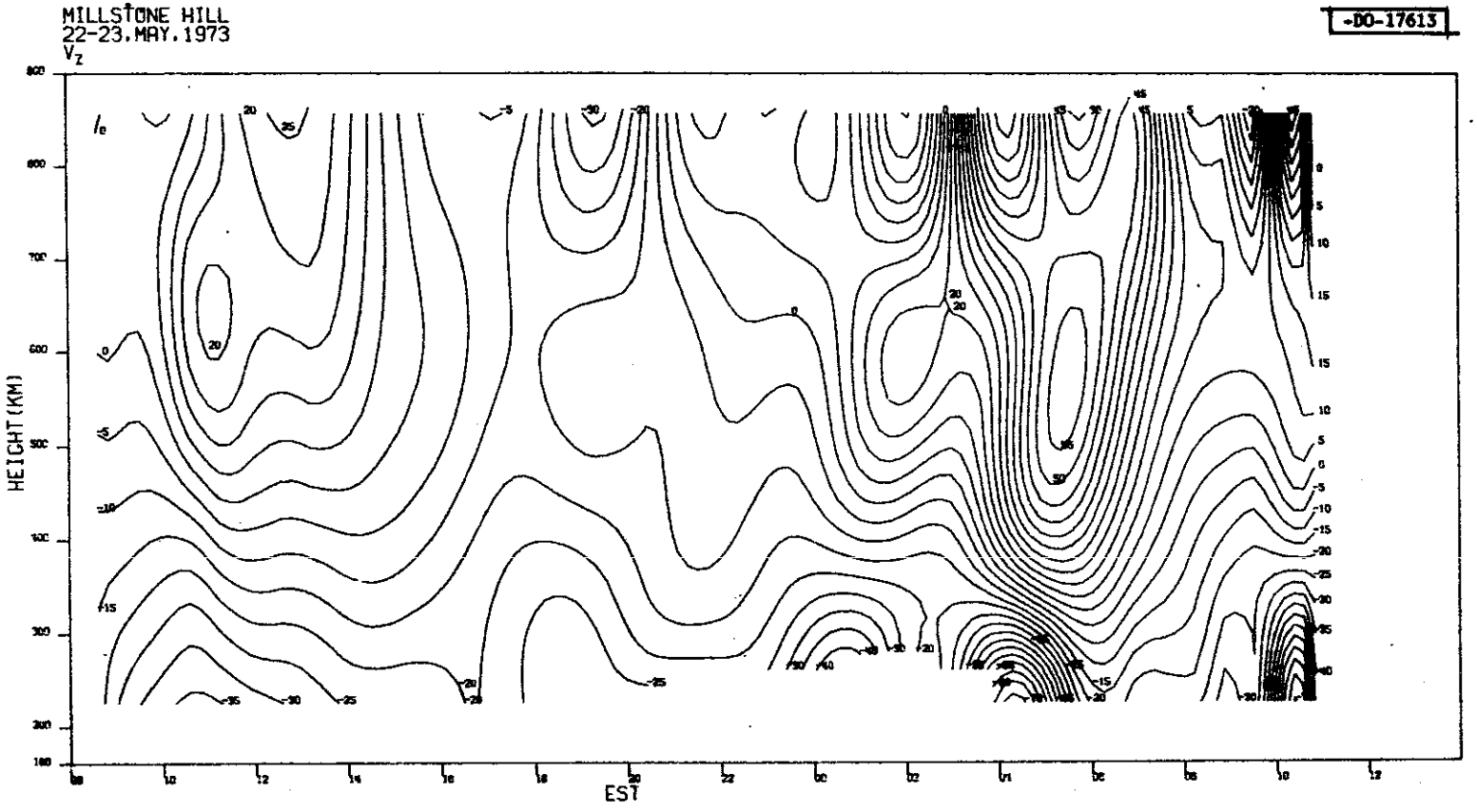

(d) Contours of V_z.

Fig. 6(a-d). Continued.

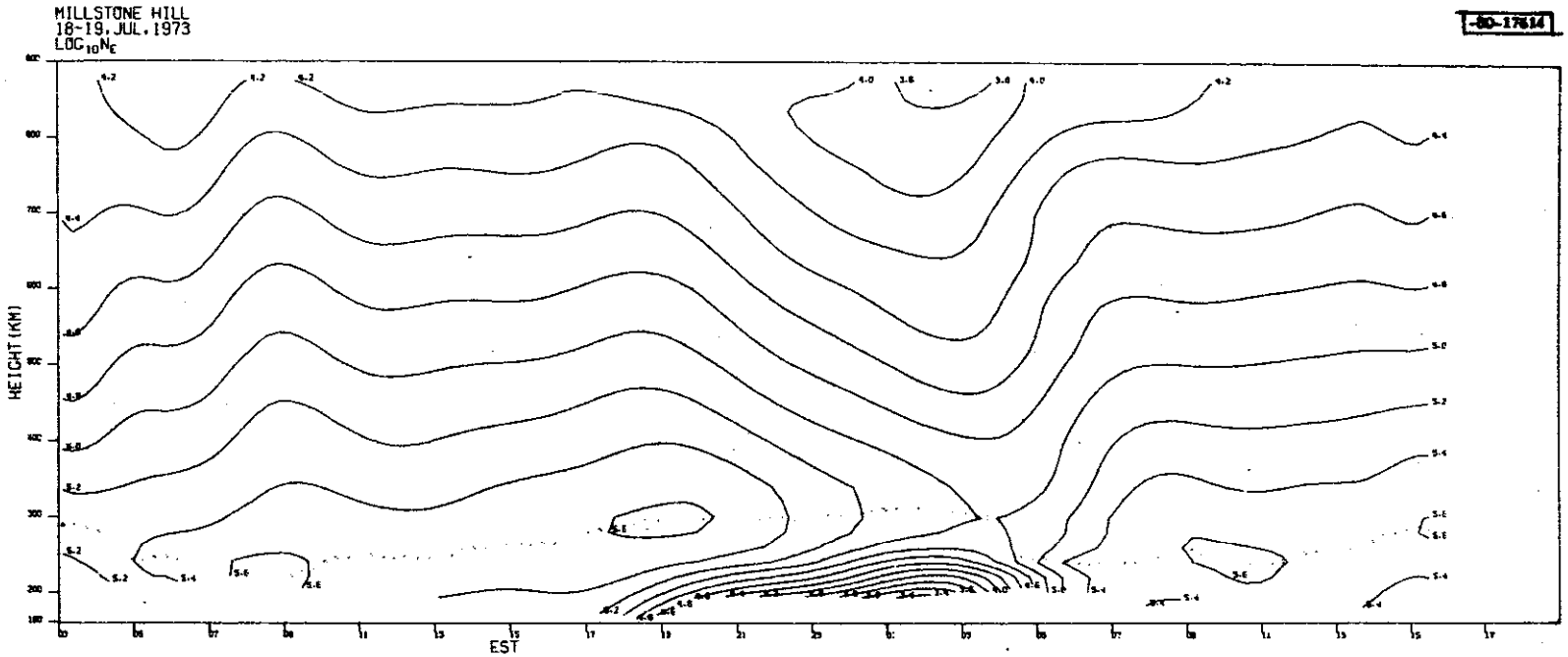

(a) Contours of $Log_{10}\ N_e$.

Fig. 7(a-d). Results for 18-19 July.

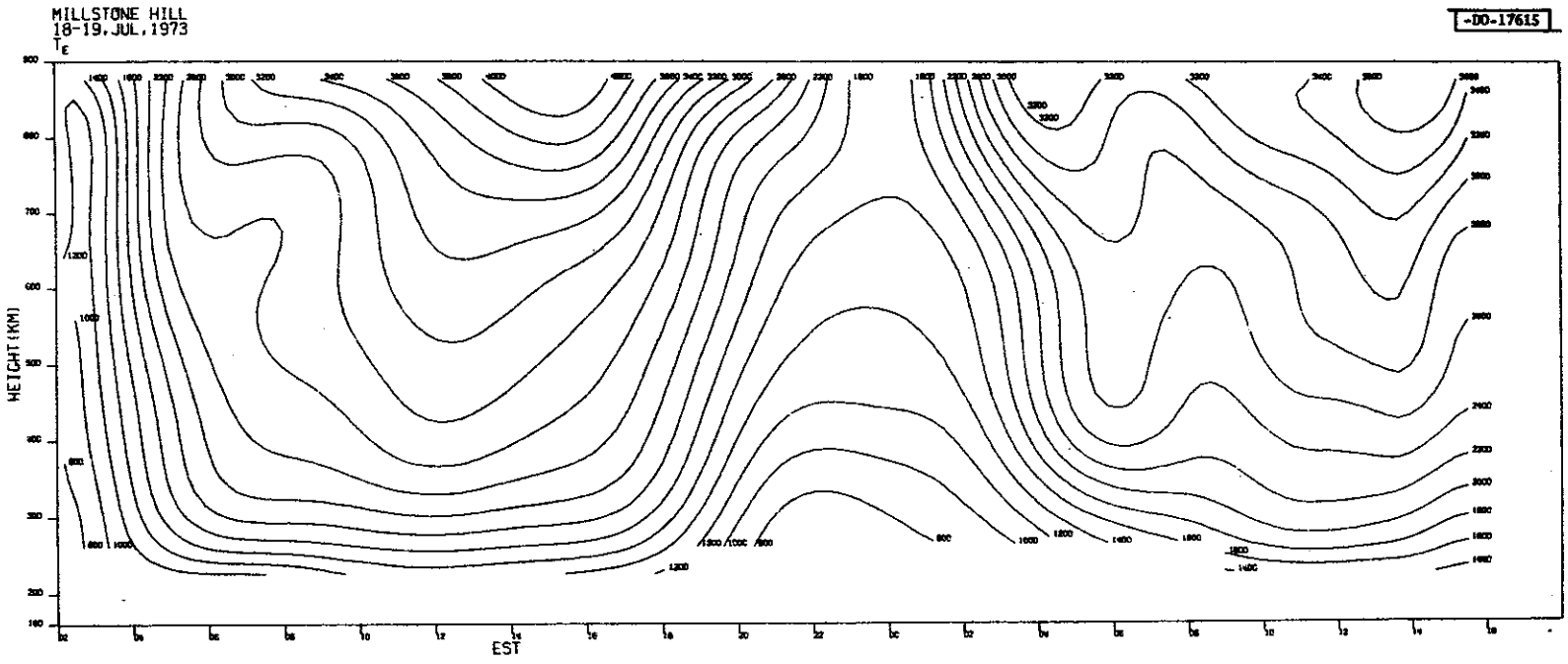

(b) Contours of T_e.

Fig. 7(a-d). Continued.

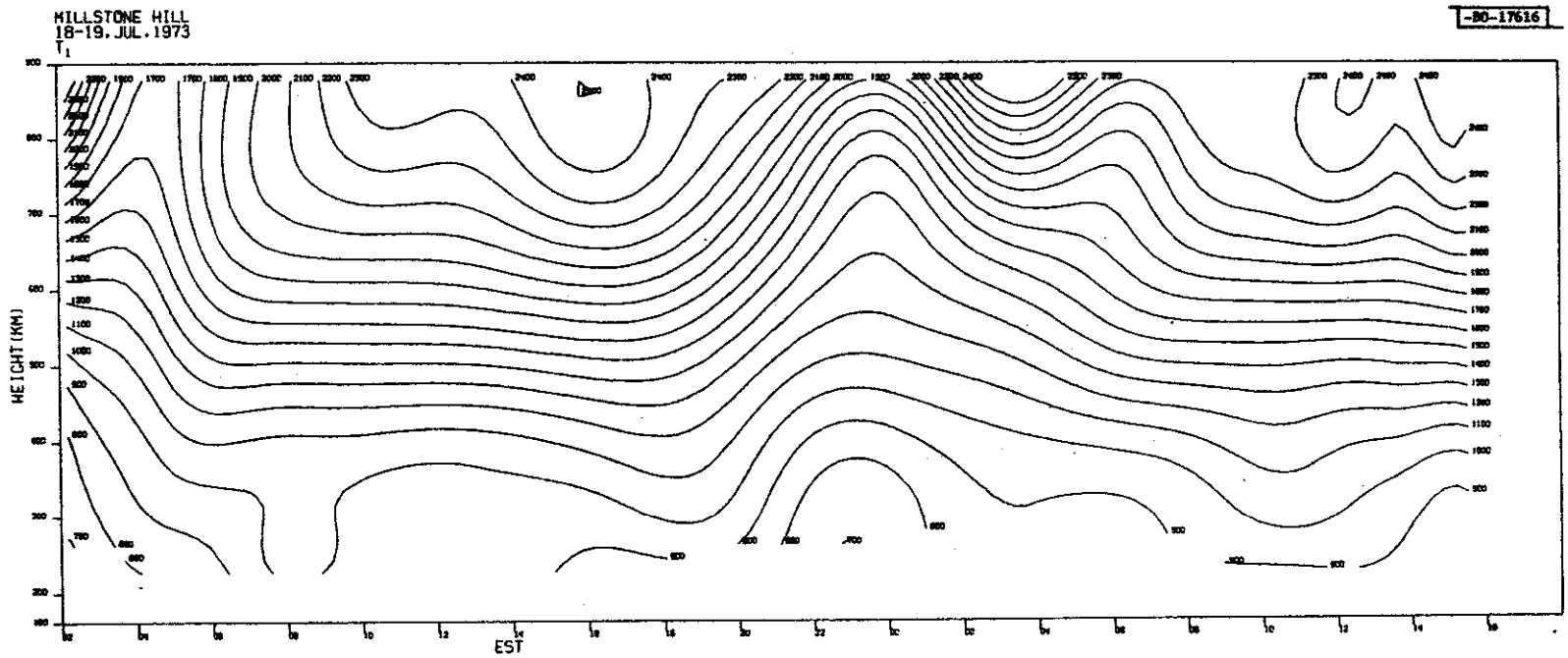

(c) Contours of T_i.

Fig. 7(a-d). Continued.

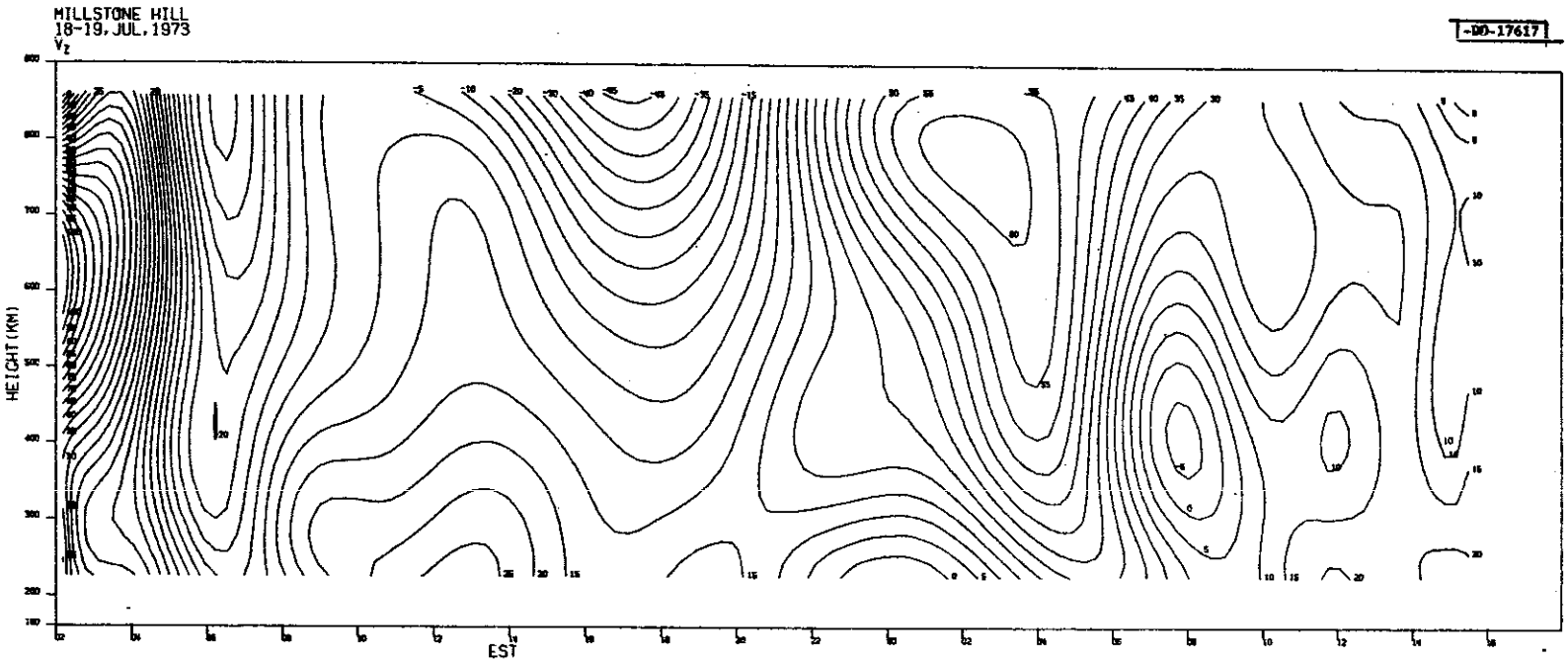

(d) Contours of V_z.

Fig. 7(a-d). Continued.

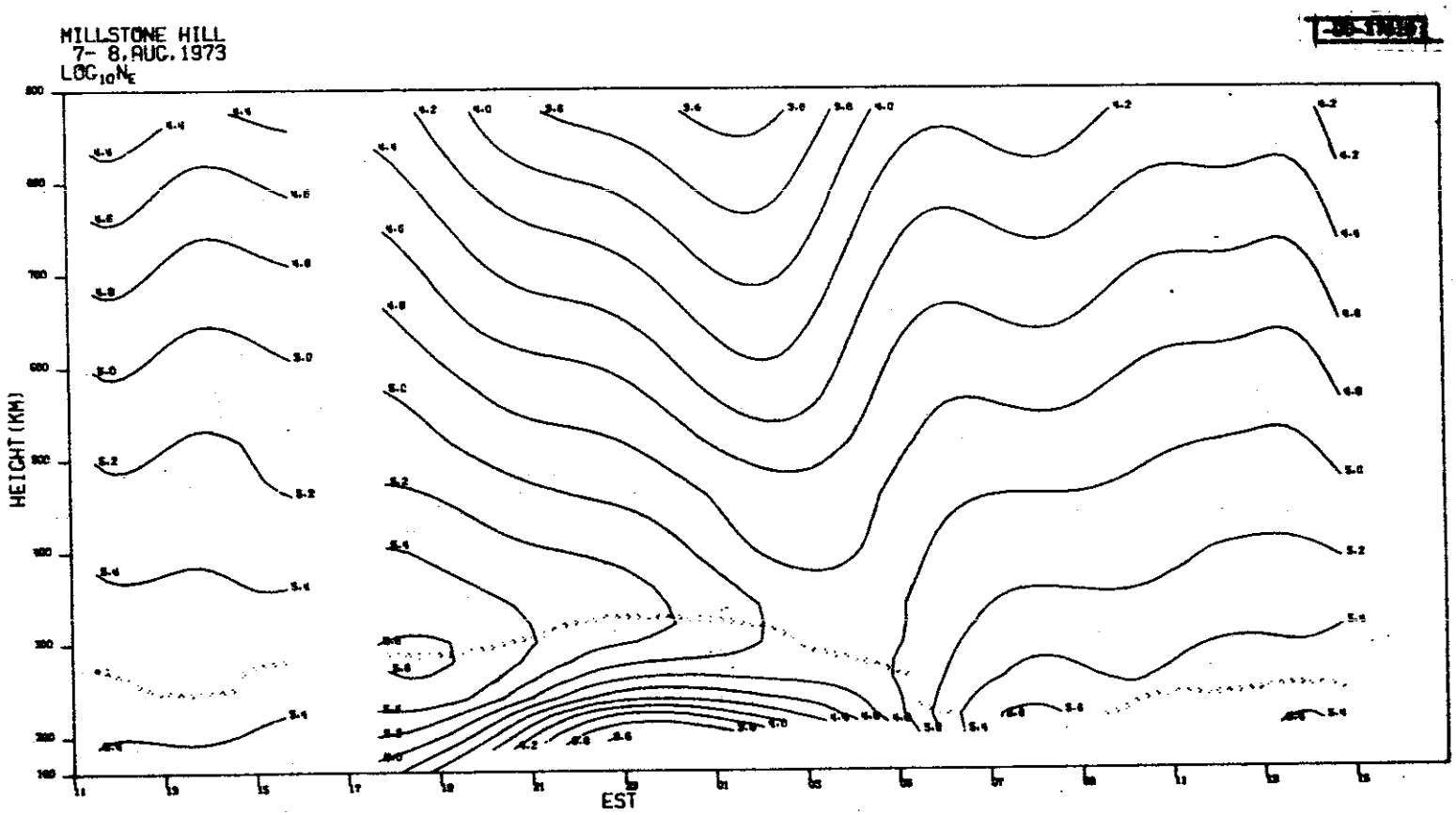

(a) Contours of Log_{10} N_e.

Fig. 8(a-d). Results for 7-8 August.

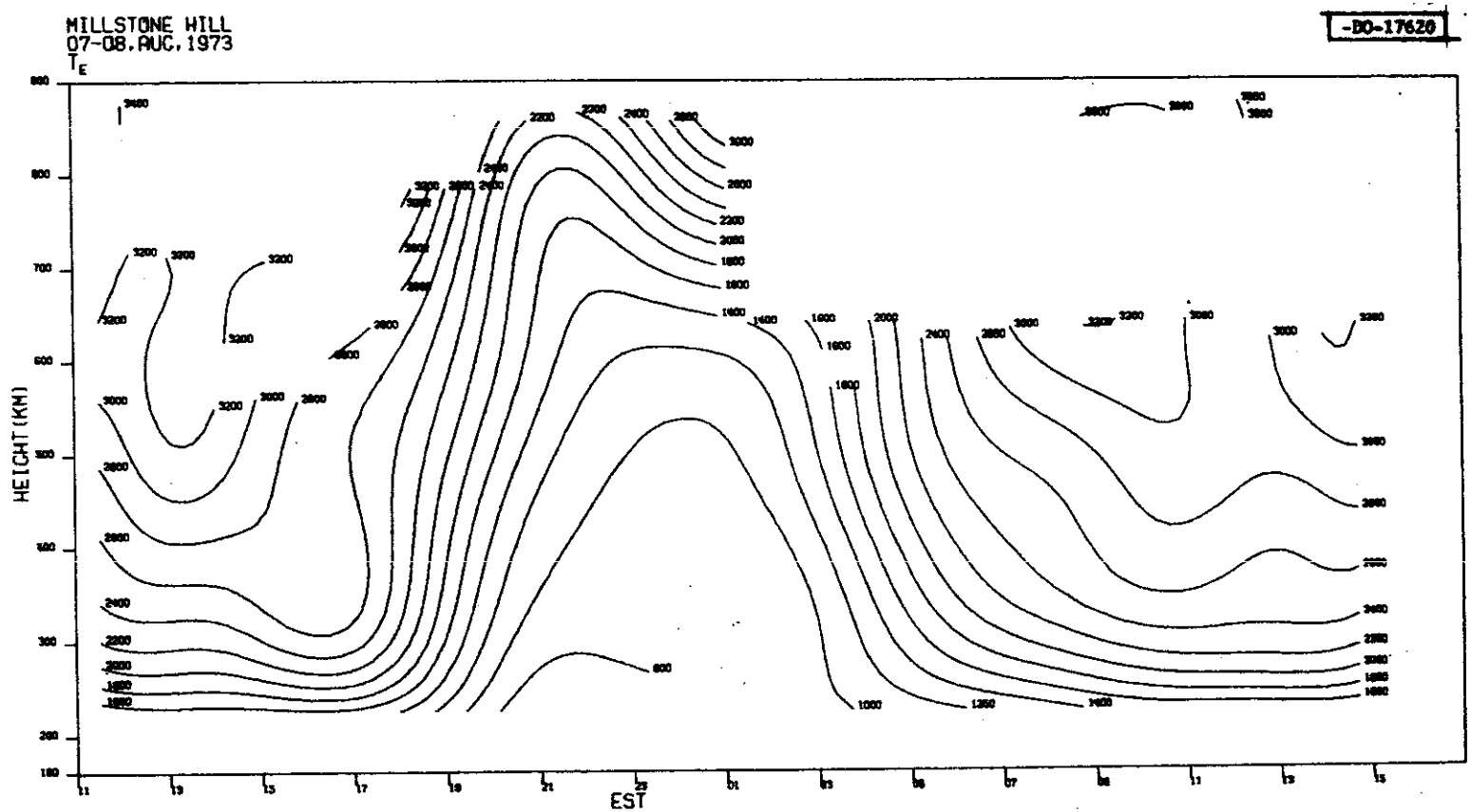

(b) Contours of T_e.

Fig. 8(a-d). Continued.

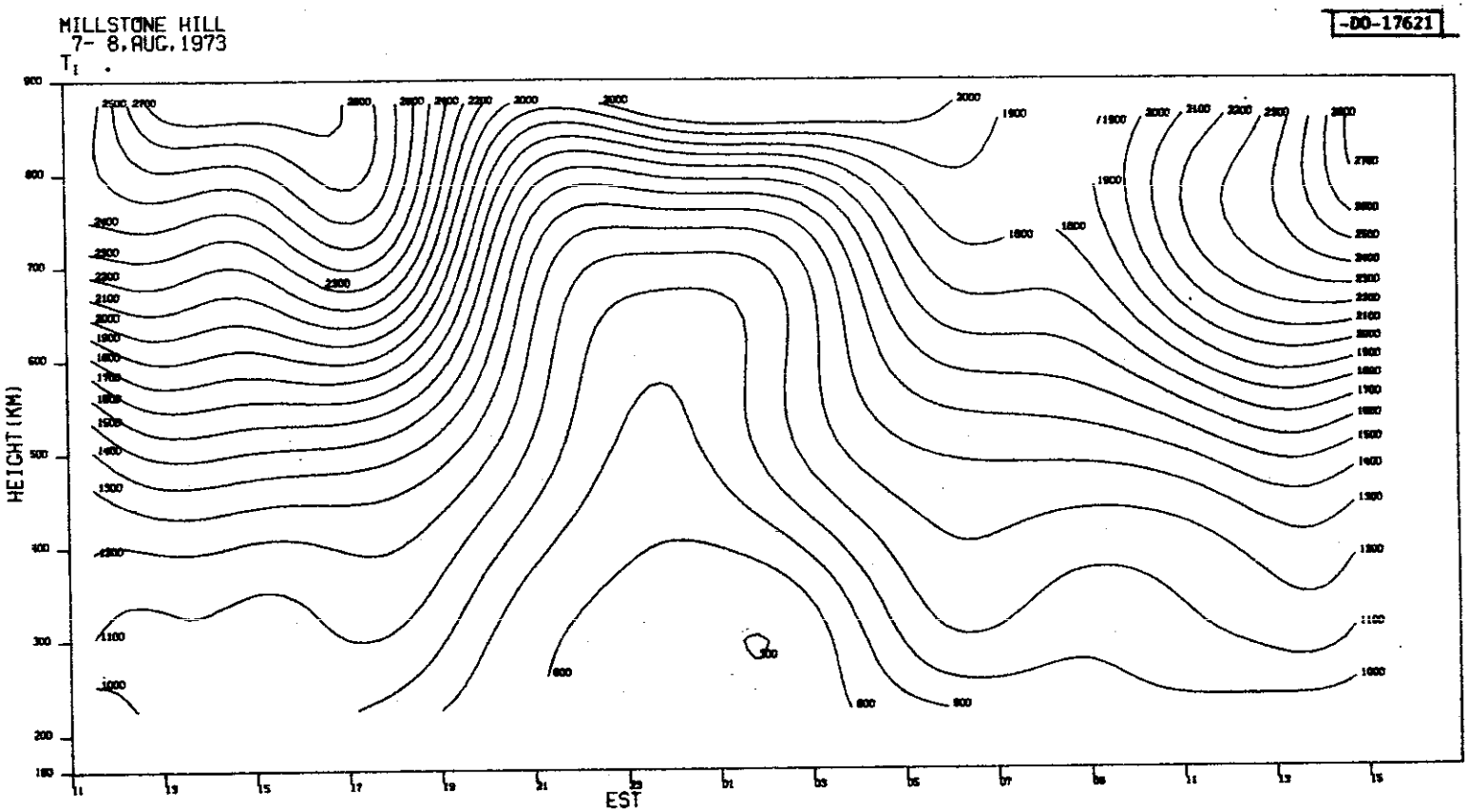

(c) Contours of T_i.

Fig. 8(a-d). Continued.

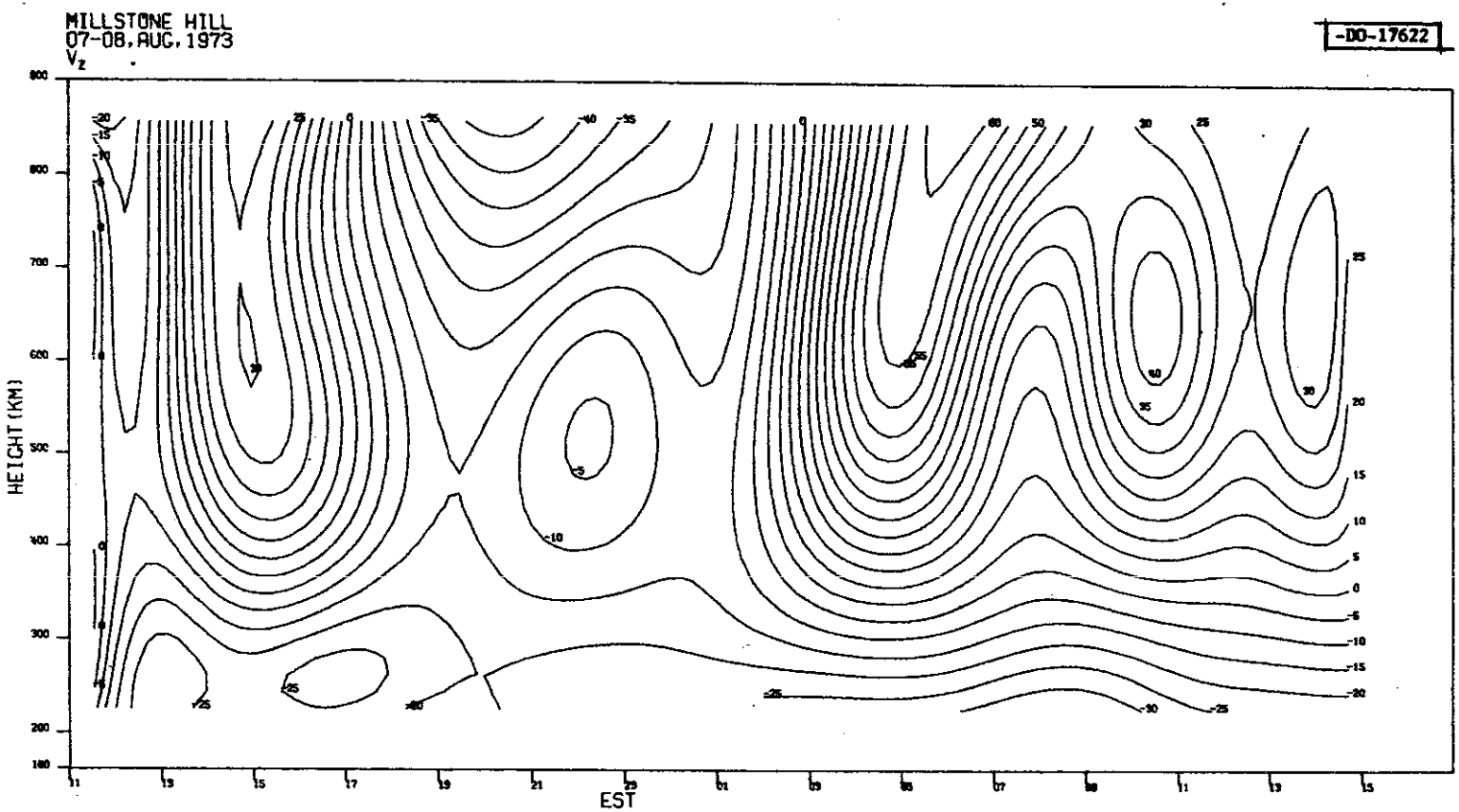

(d) Contours of V_z.

Fig. 8(a-d). Continued.

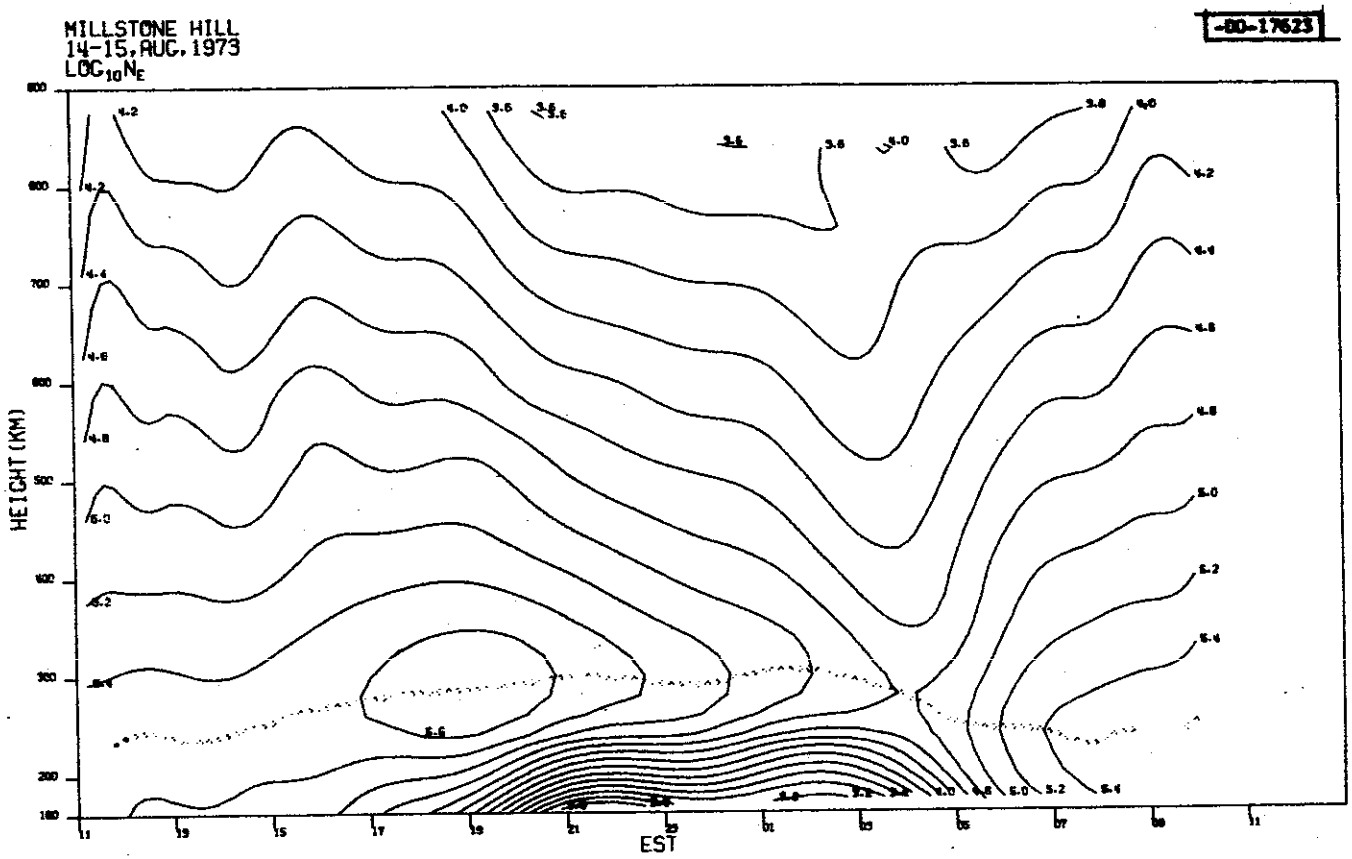

(a) Contours of $Log_{10}\ N_e$.

Fig. 9(a-d). Results for 14-15 August.

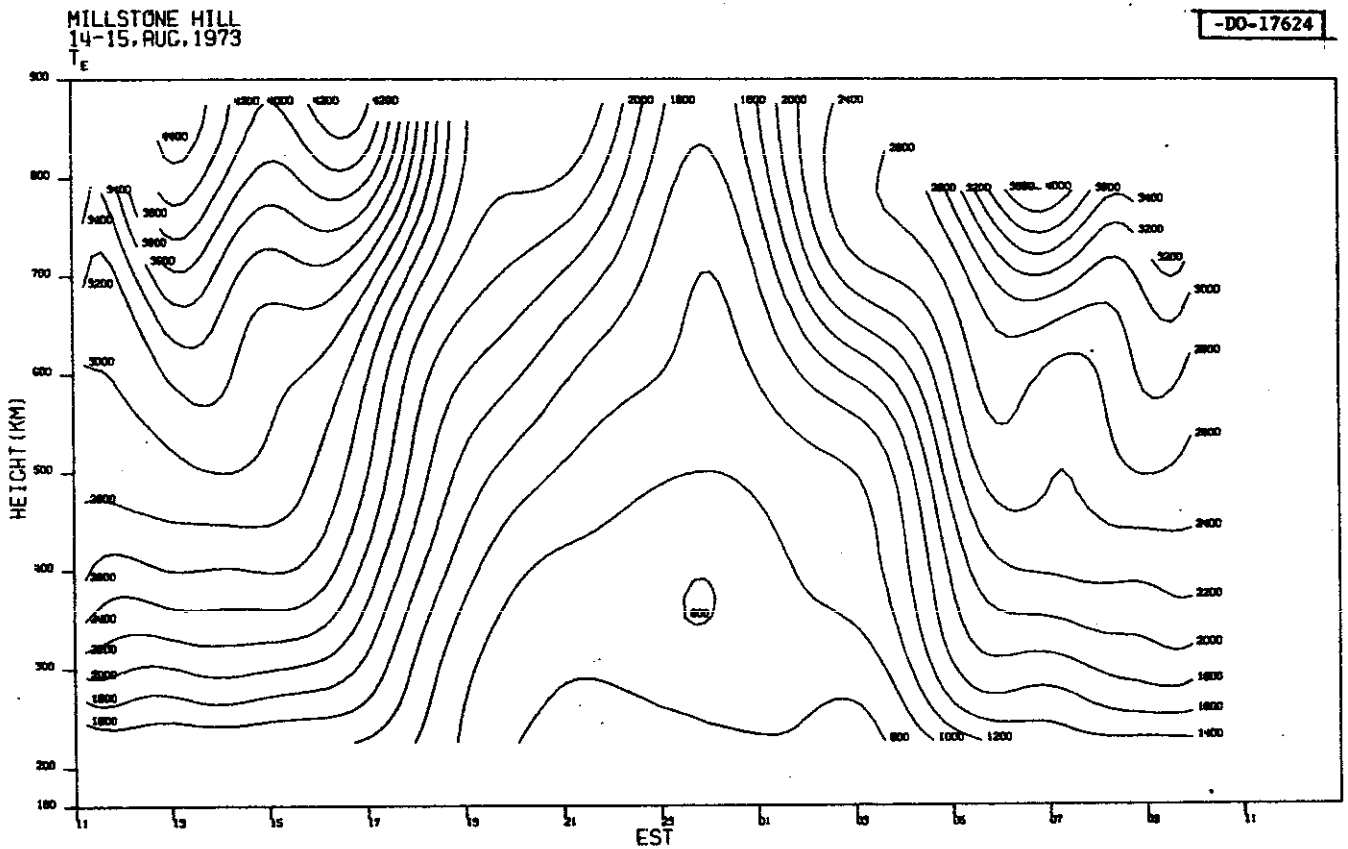

(b) Contours of T_e.

Fig. 9(a-d). Continued.

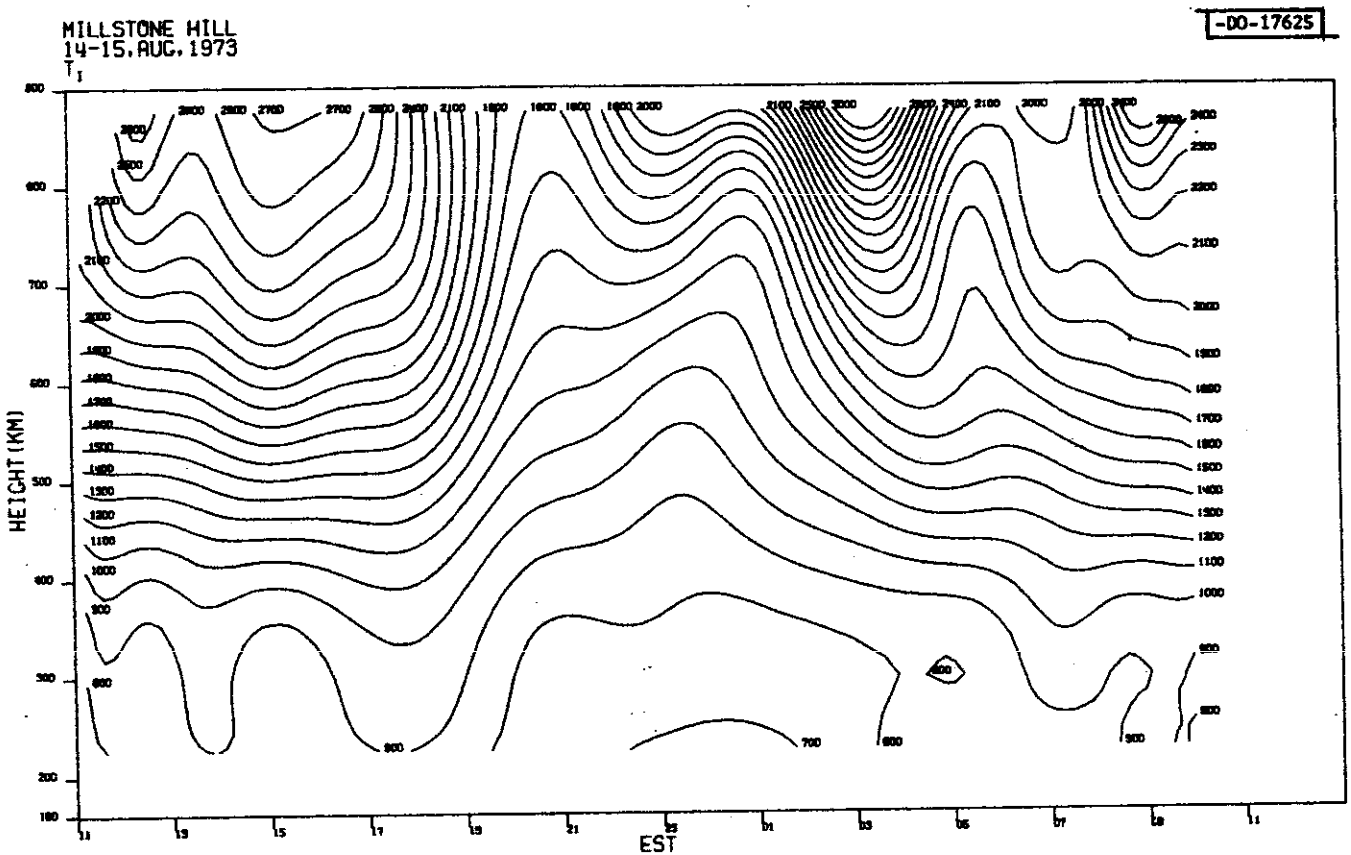

(c) Contours of T_i.

Fig. 9(a-d). Continued.

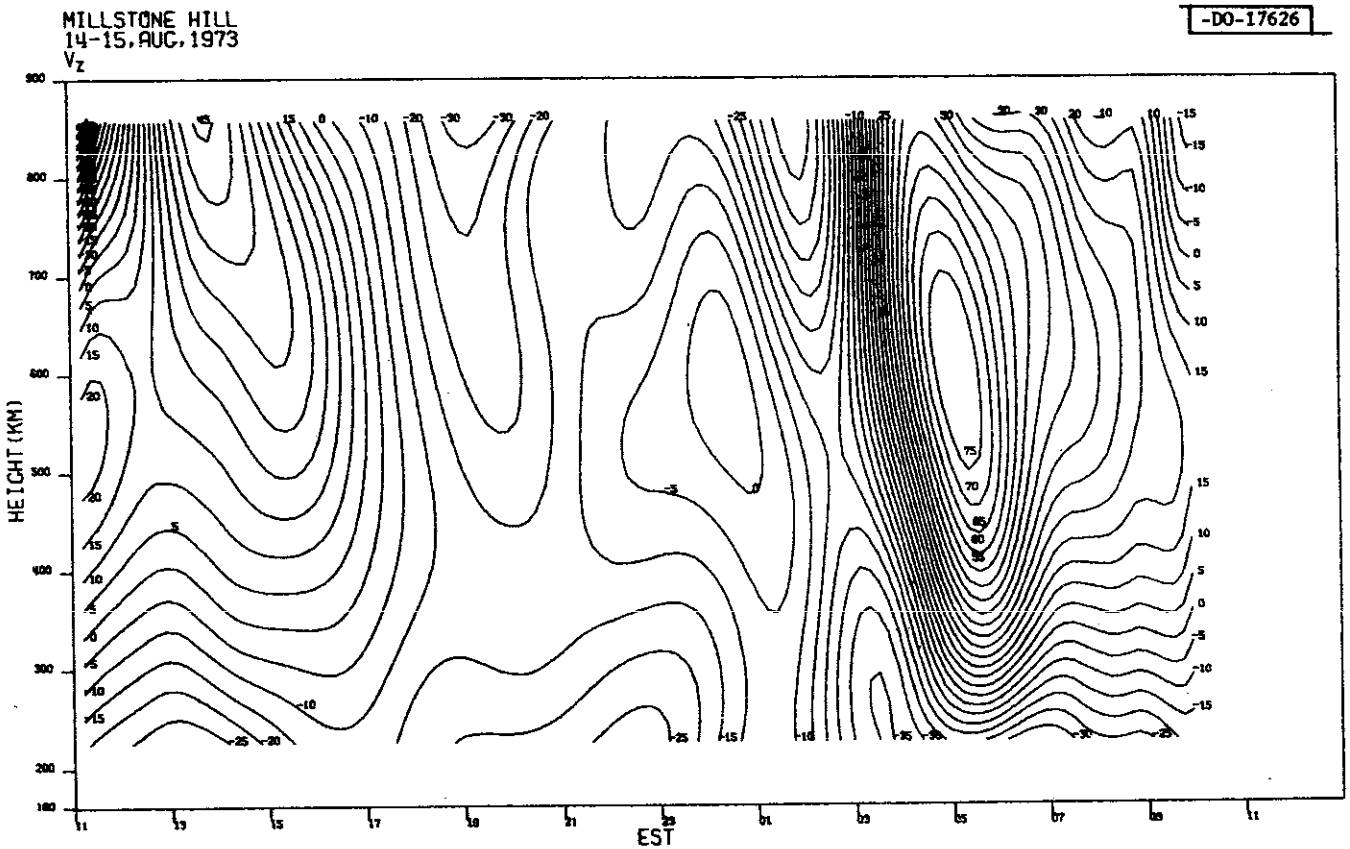

(d) Contours of V_Z.

Fig. 9(a-d). Continued.

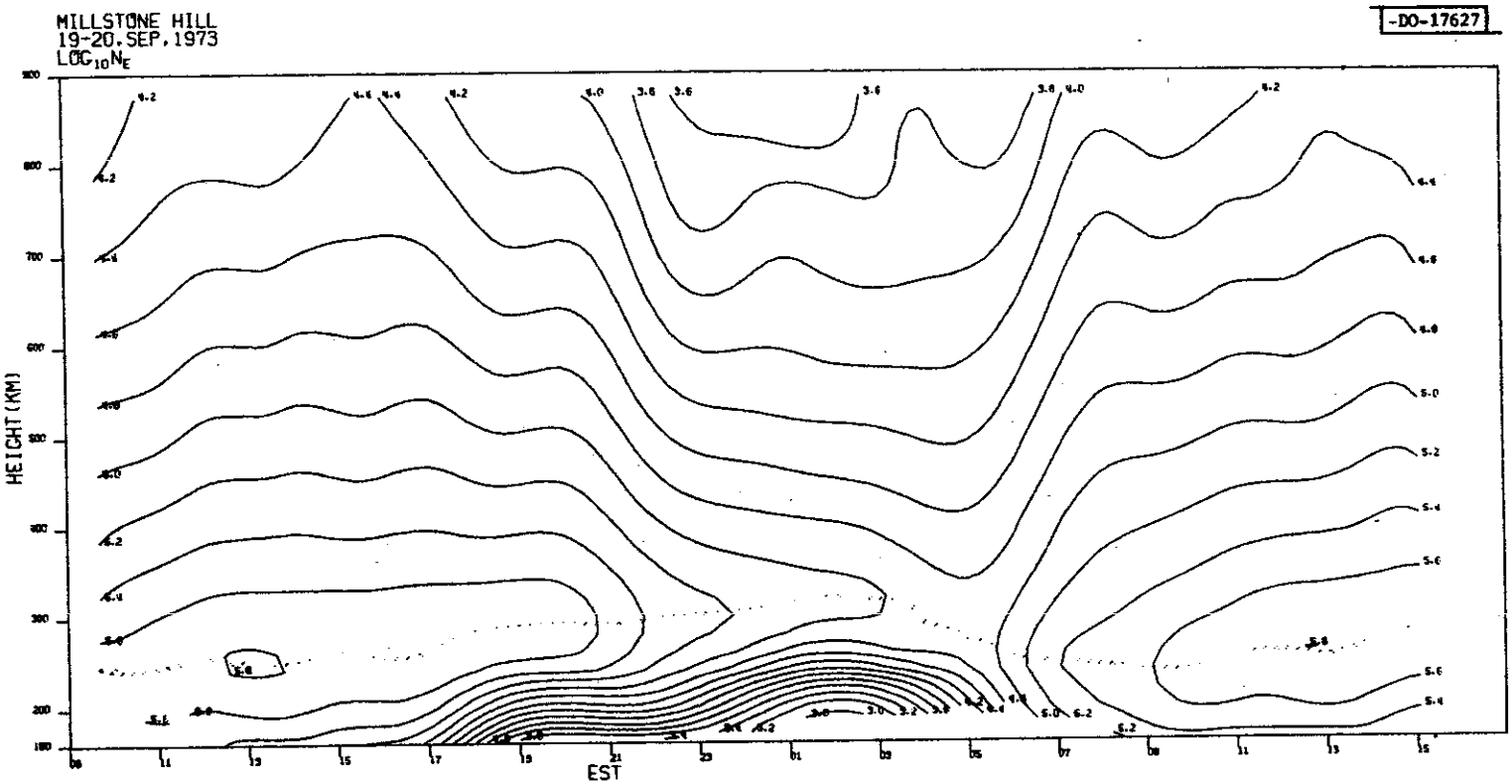

(a) Contours of $Log_{10} N_e$.

Fig. 10(a-d). Results for 19-20 September.

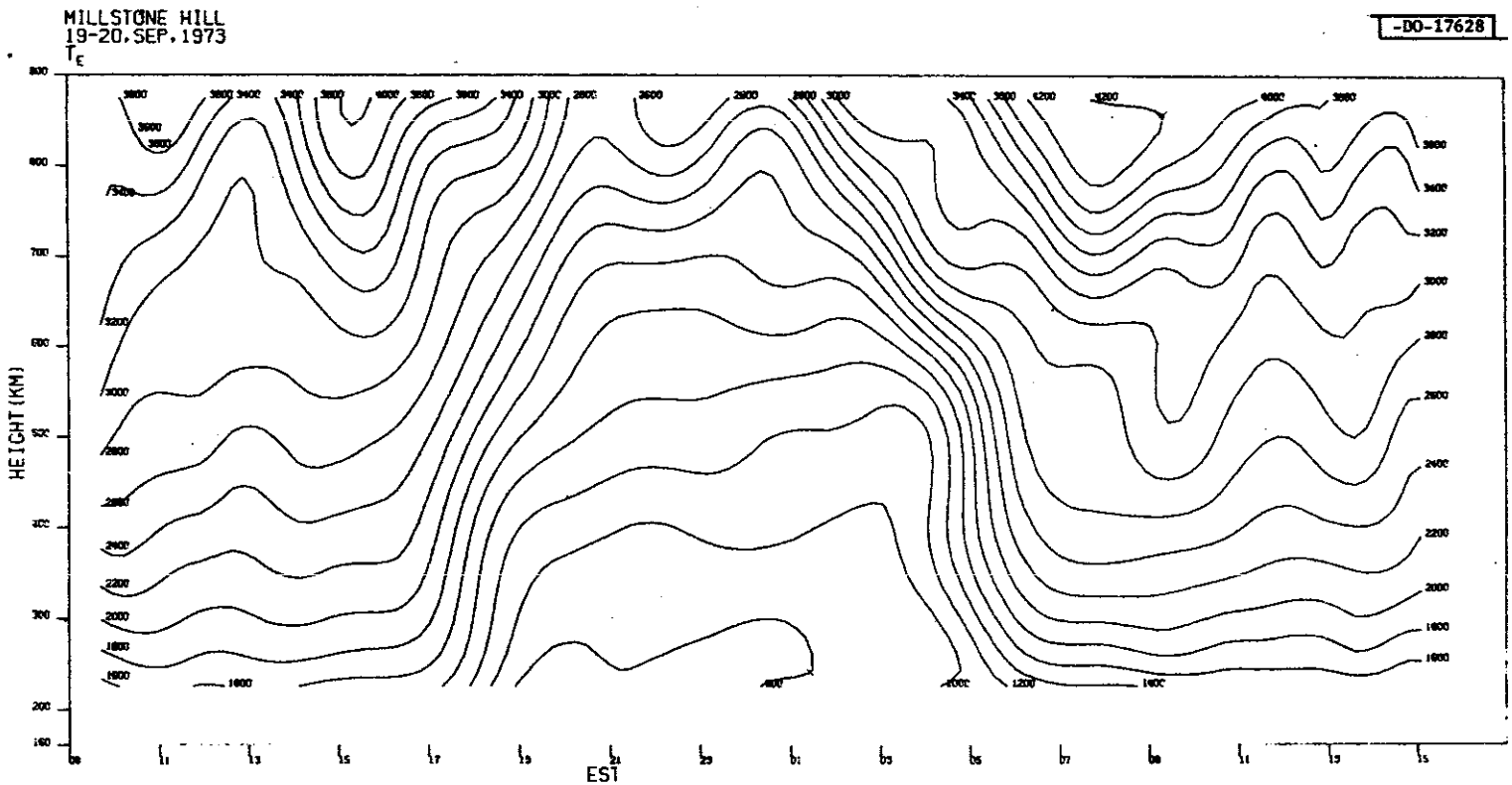

(b) Contours of T_e.

Fig. 10(a-d). Continued.

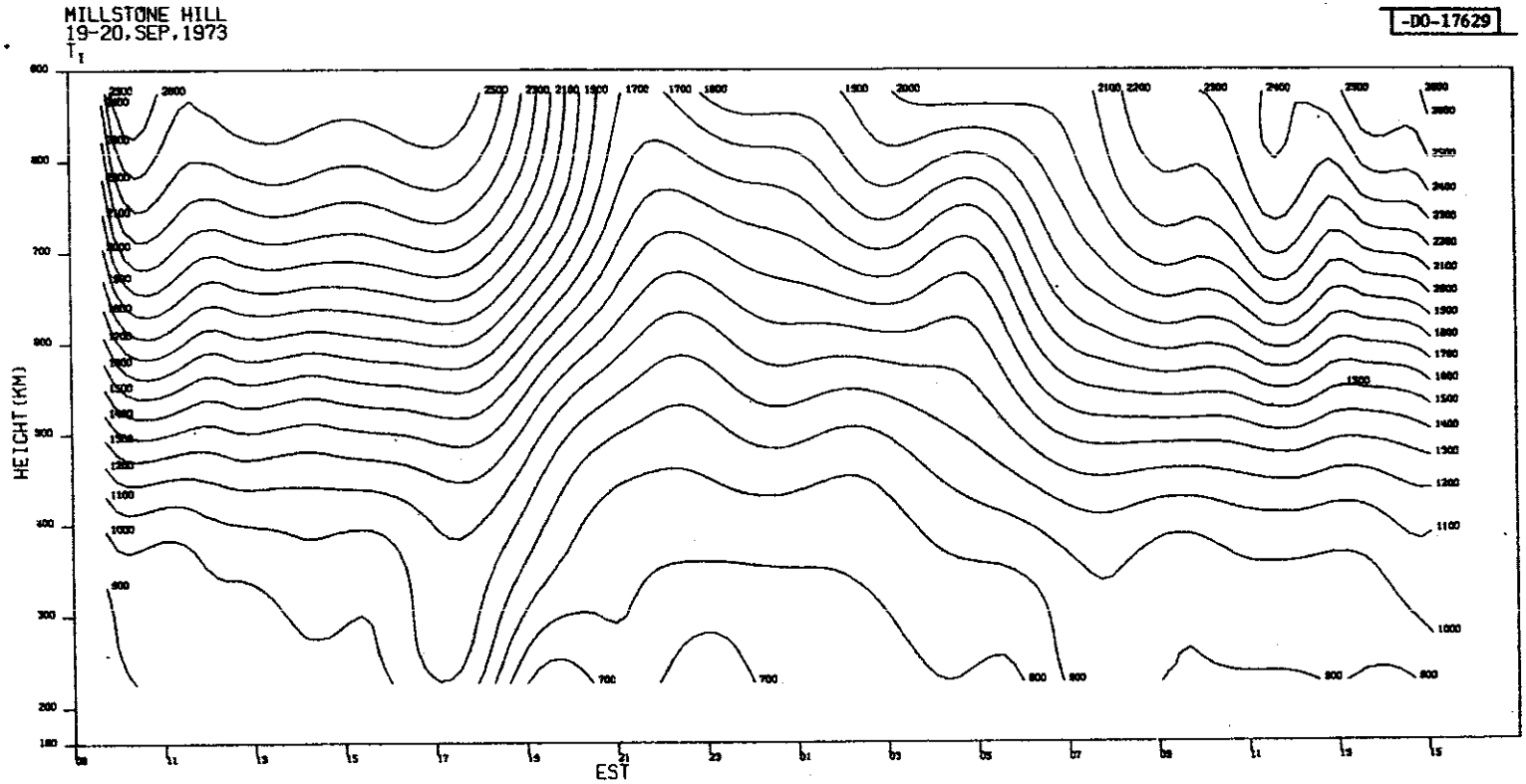

(c) Contours of T_i.

Fig. 10(a-d). Continued.

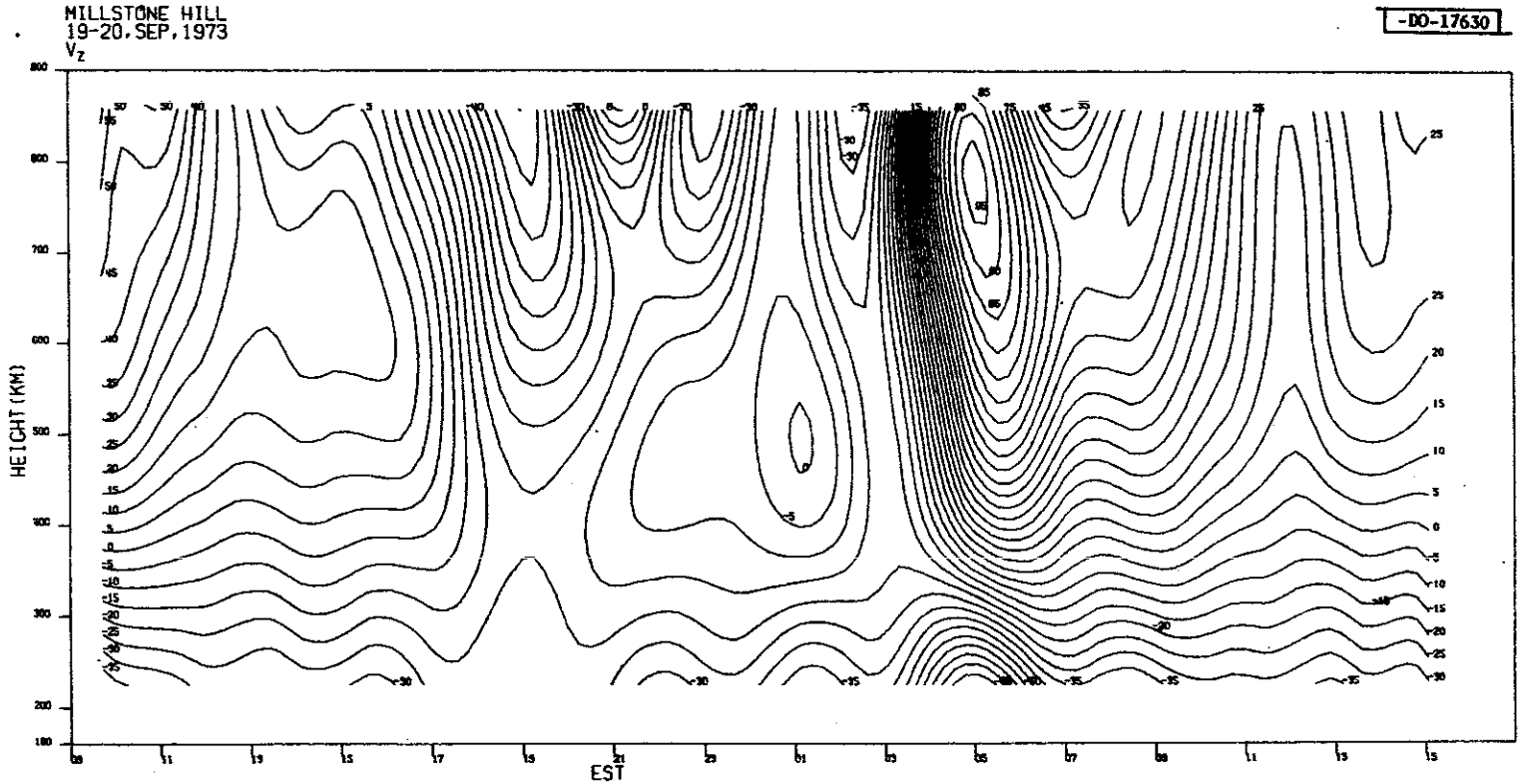

(d) Contours of V_z.

Fig. 10(a-d). Continued.

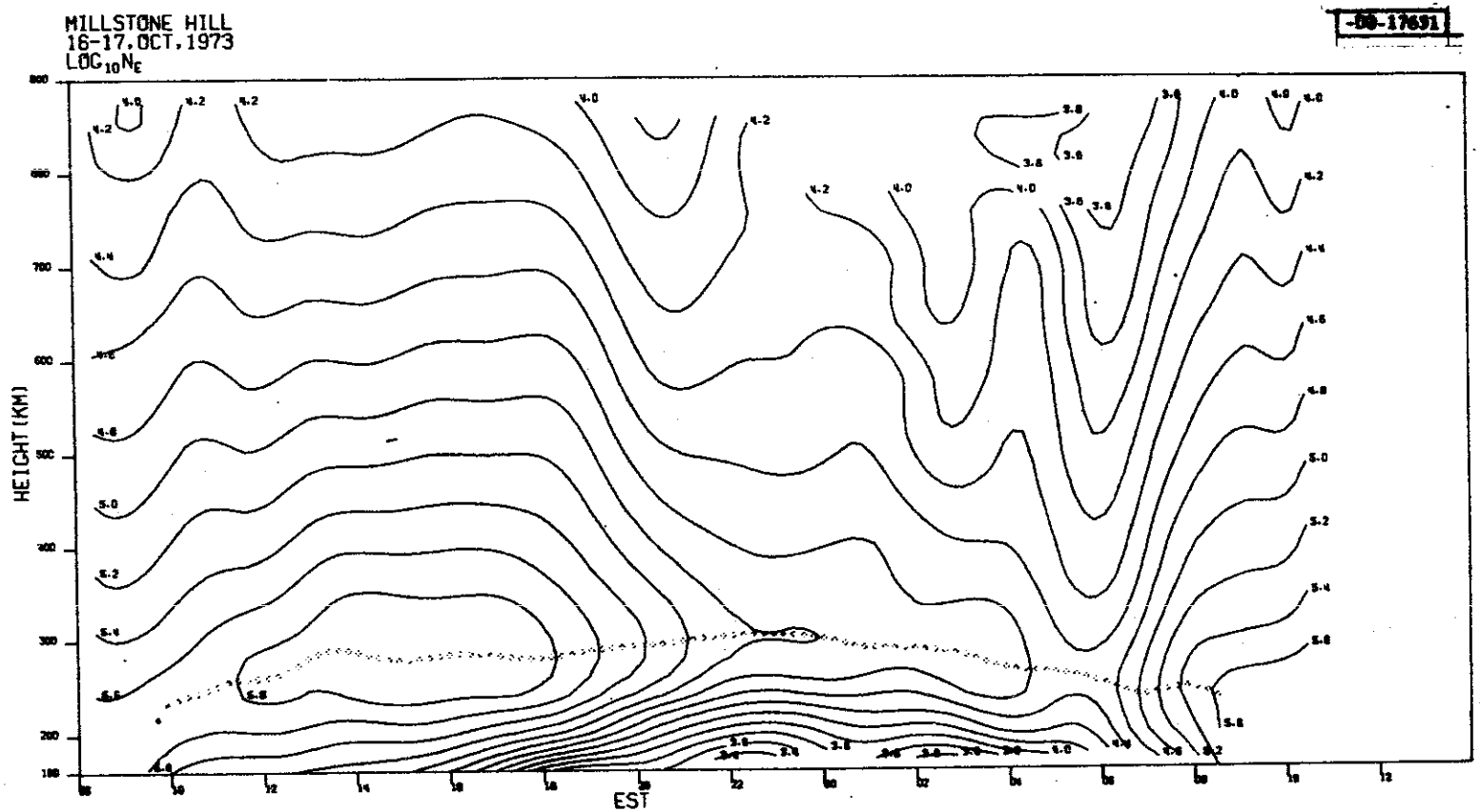

(a) Contours of $Log_{10}\ N_e$.

Fig. 11(a-d). Results for 16-17 October.

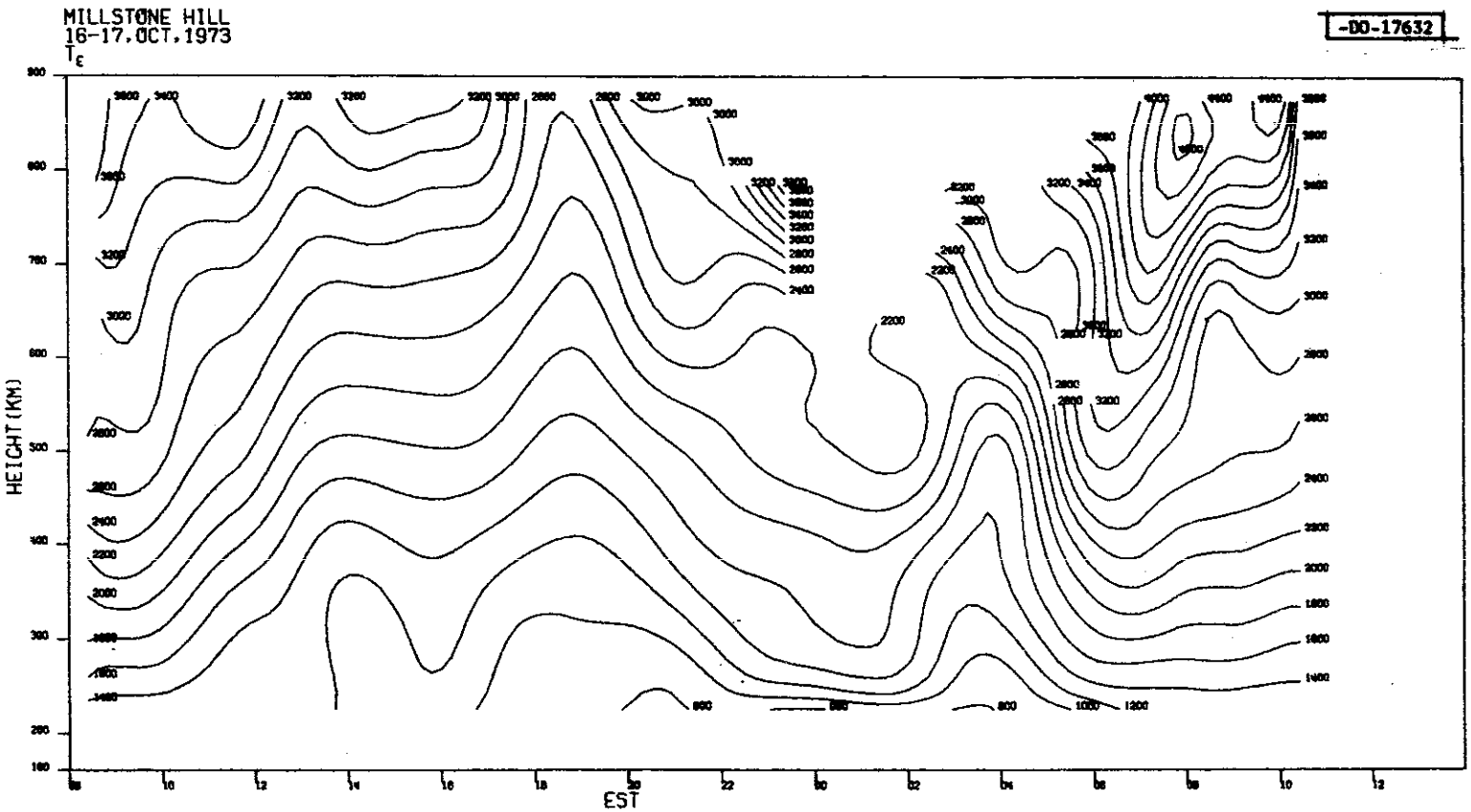

(b) Contours of T_e.

Fig. 11(a-d). Continued.

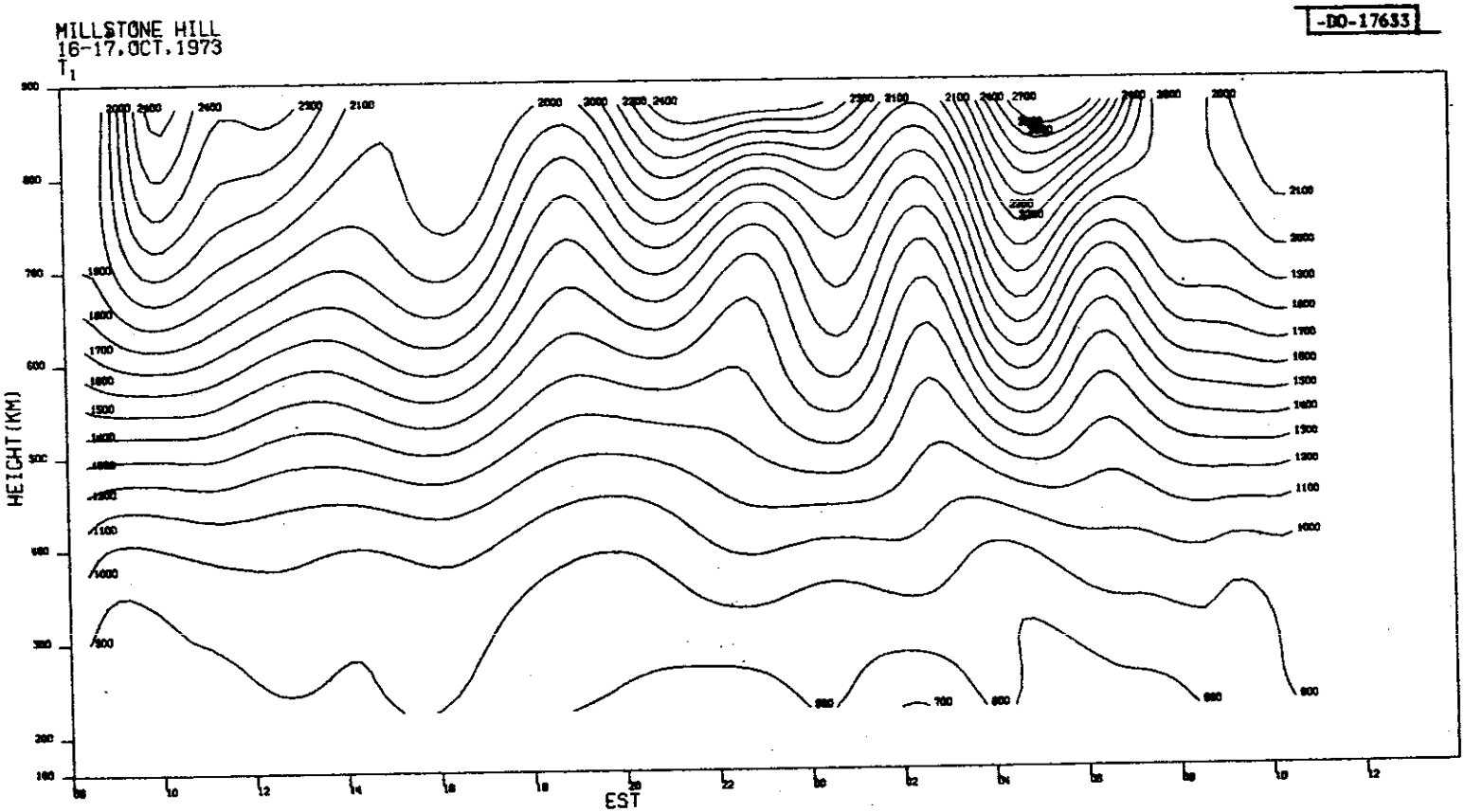

(c) Contours of T_i.

Fig. 11(a-d). Continued.

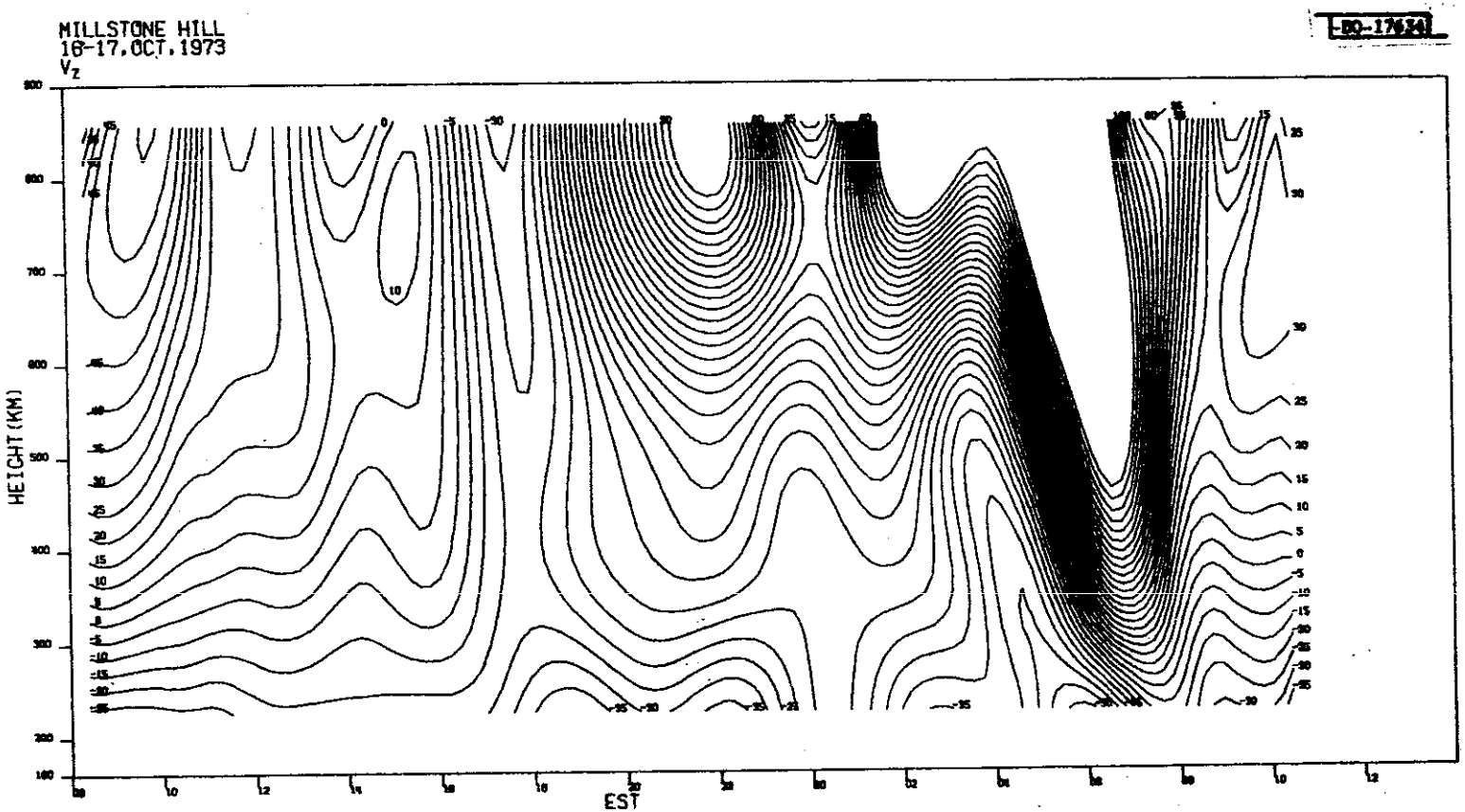

(d) Contours of V_z.

Fig. 11(a-d). Continued.

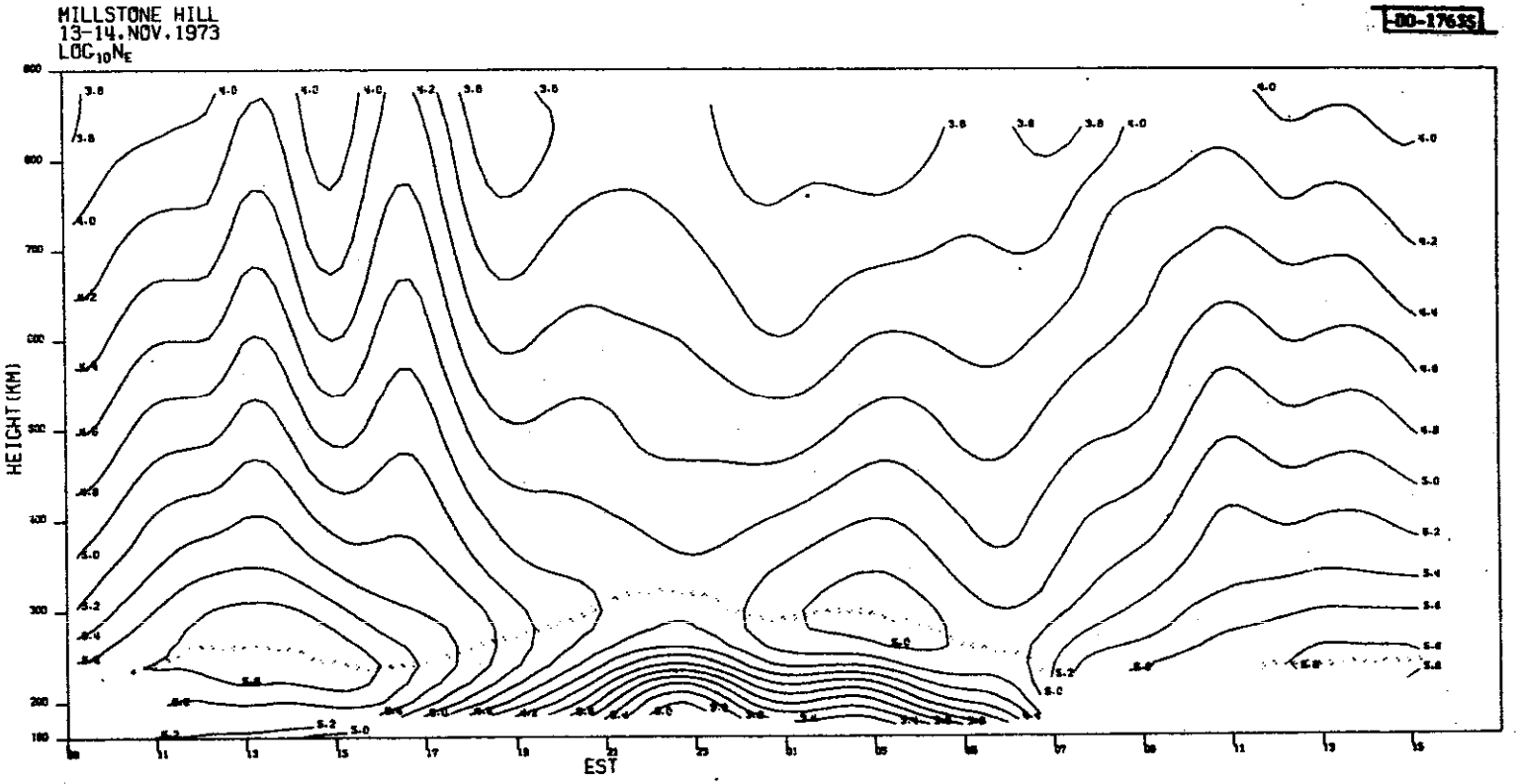

(a) Contours of $Log_{10} N_e$.

Fig. 12(a-d). Results for 13-14 November.

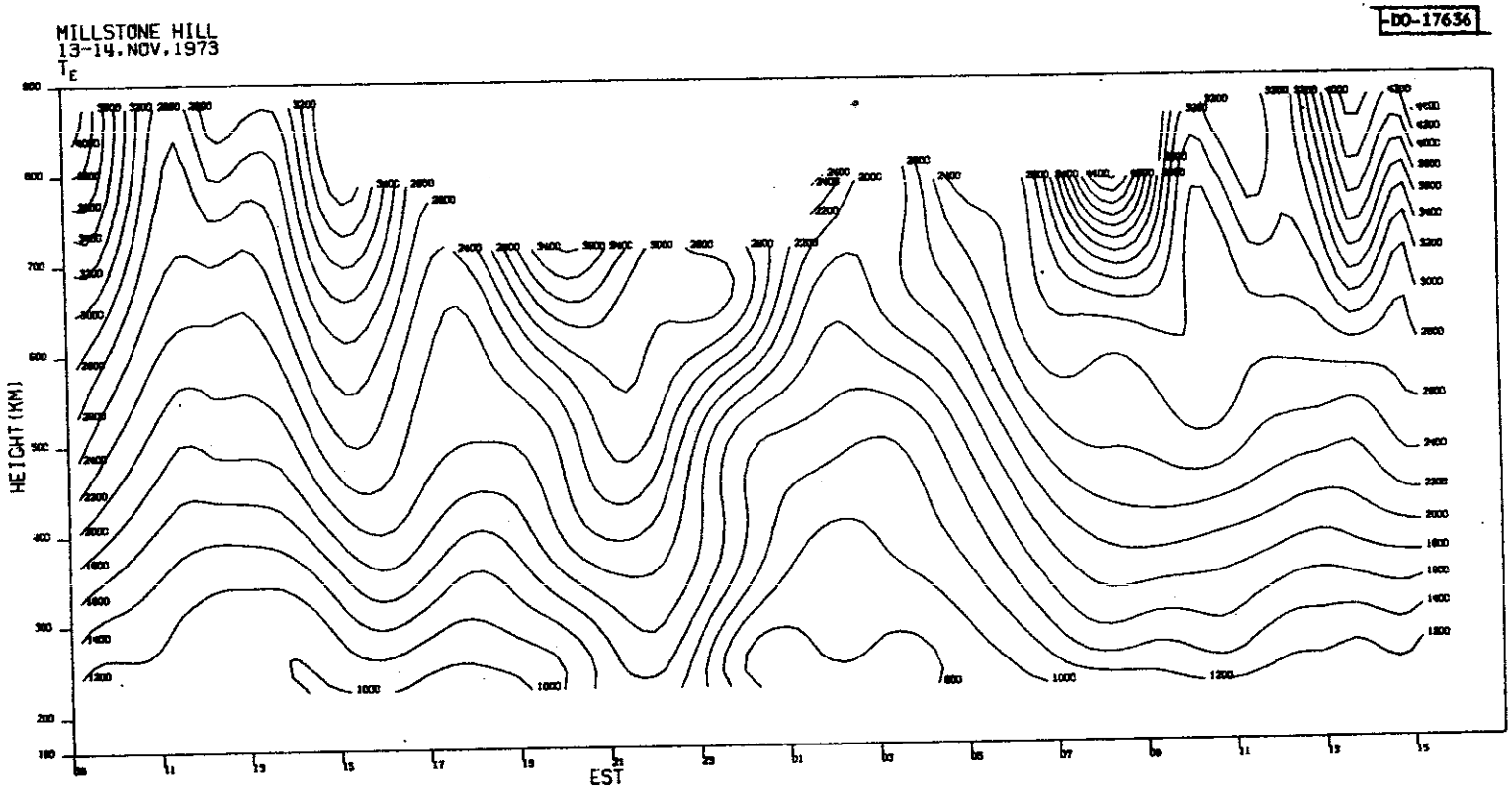

(b) Contours of T_e.

Fig. 12(a-d). Continued.

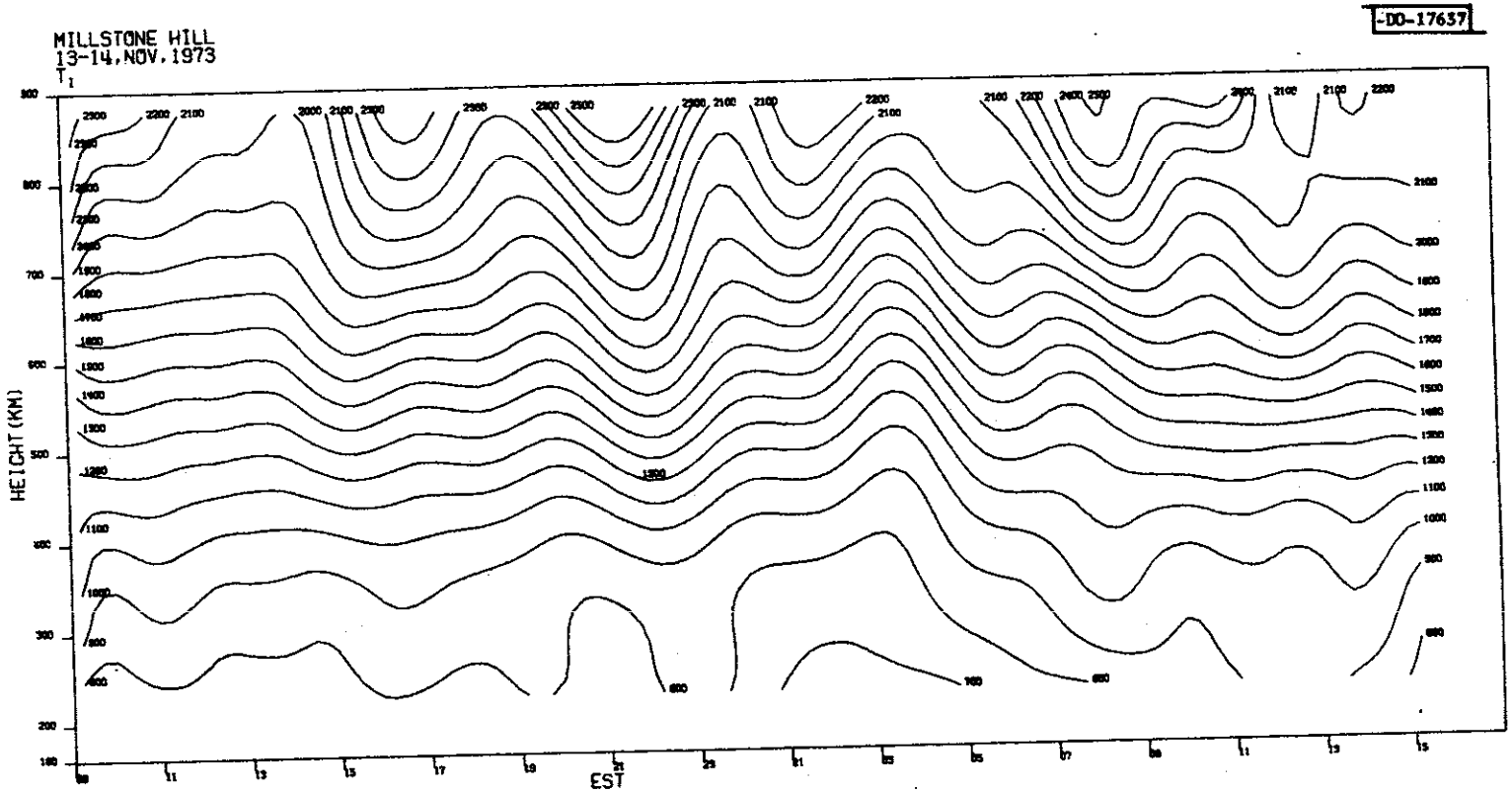

(c) Contours of T_i.

Fig. 12(a-d). Continued.

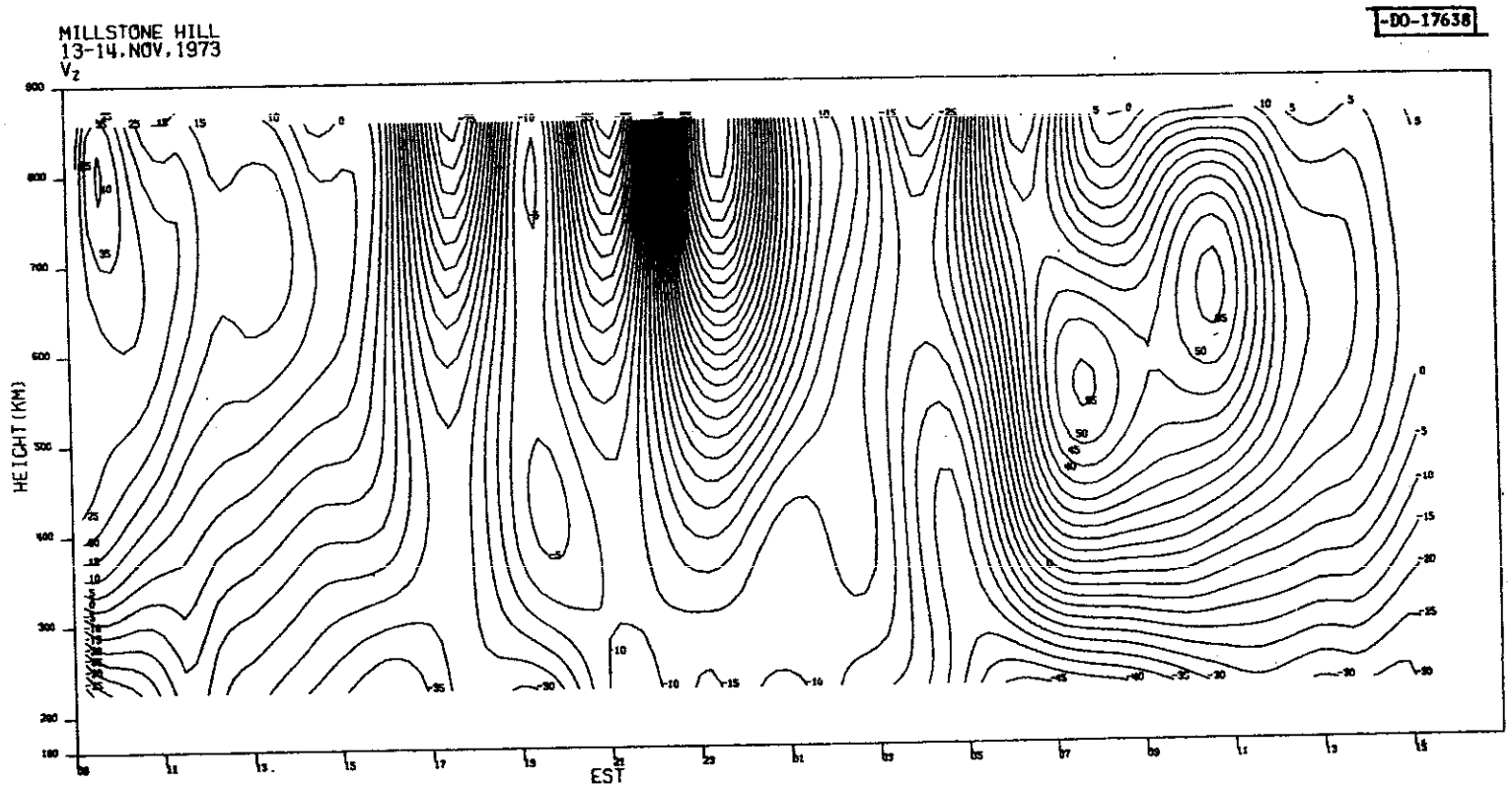

(d) Contours of V_z.

Fig. 12(a-d). Continued.

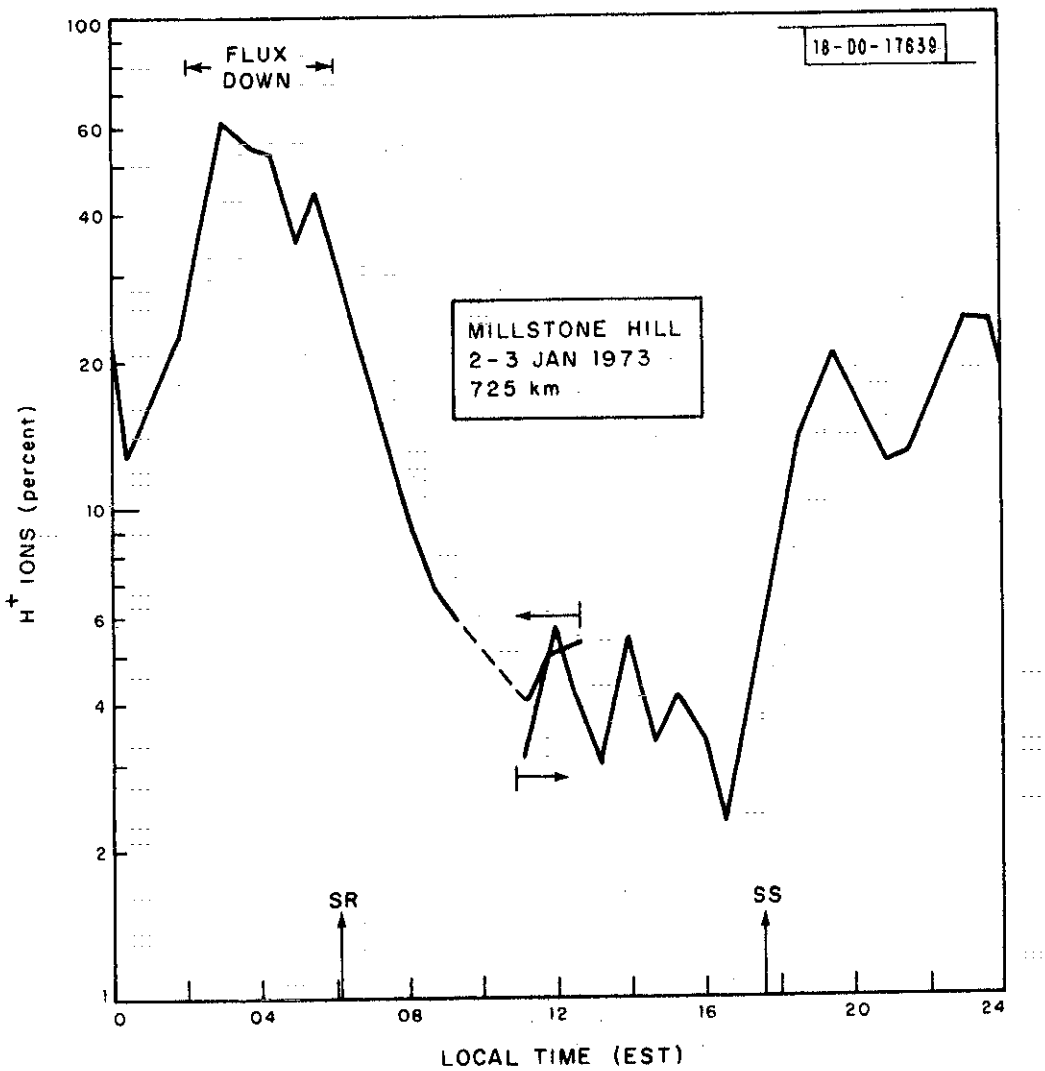

(a) 725 km on 2-3 January.

Fig. 13(a-f). Percentage concentration of H^+ ions for some days in 1973.

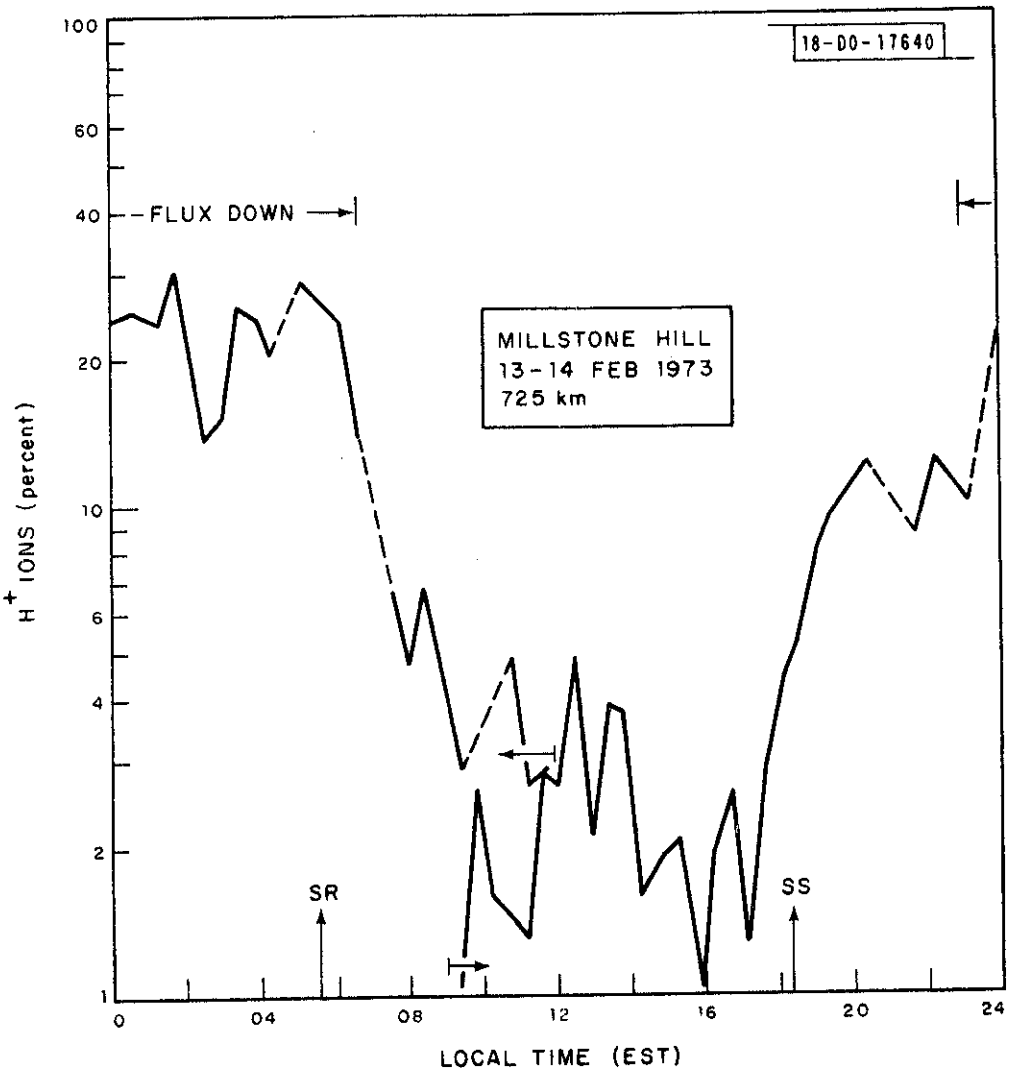

(b) 725 km on 13-14 February.

Fig. 13(a-g). Continued.

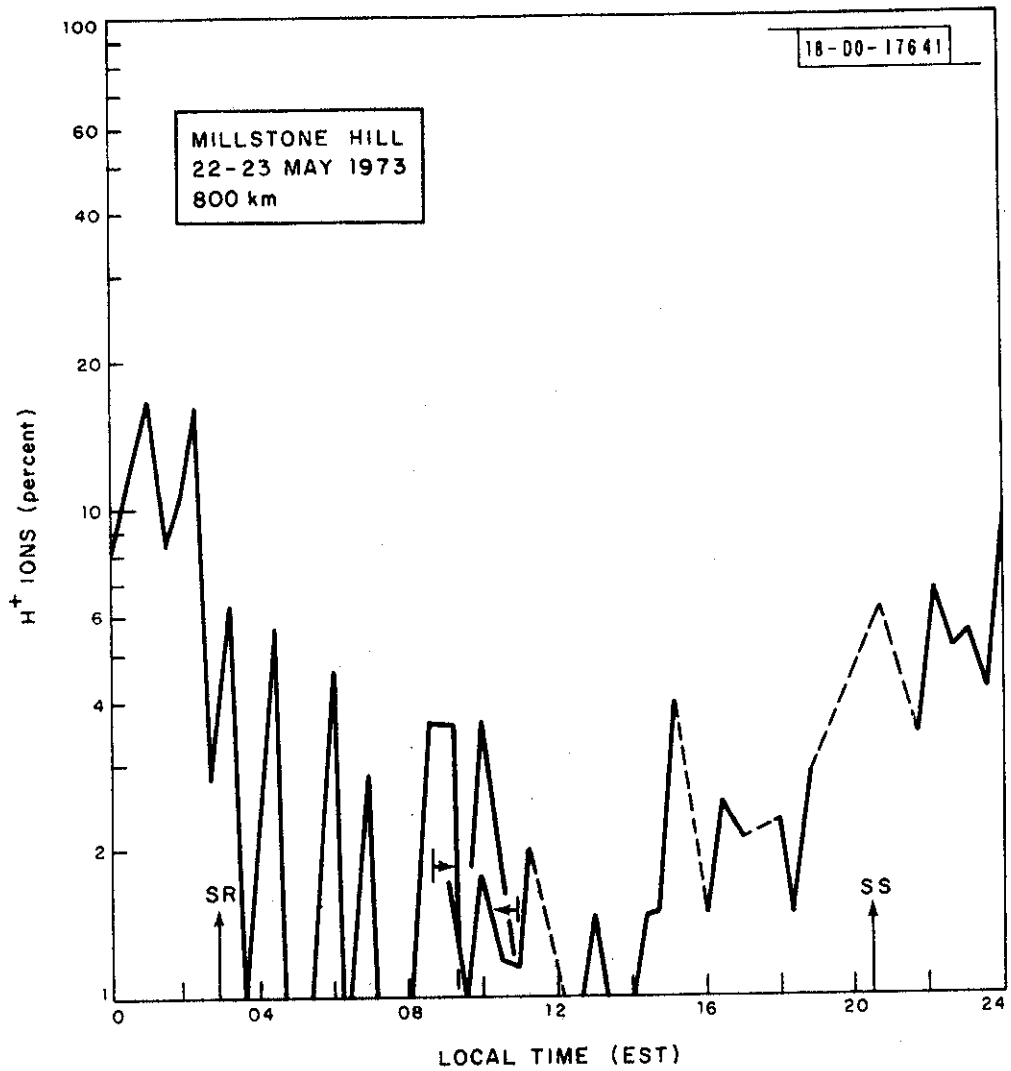

(c) 800 km on 22-23 May.

Fig. 13(a-g). Continued.

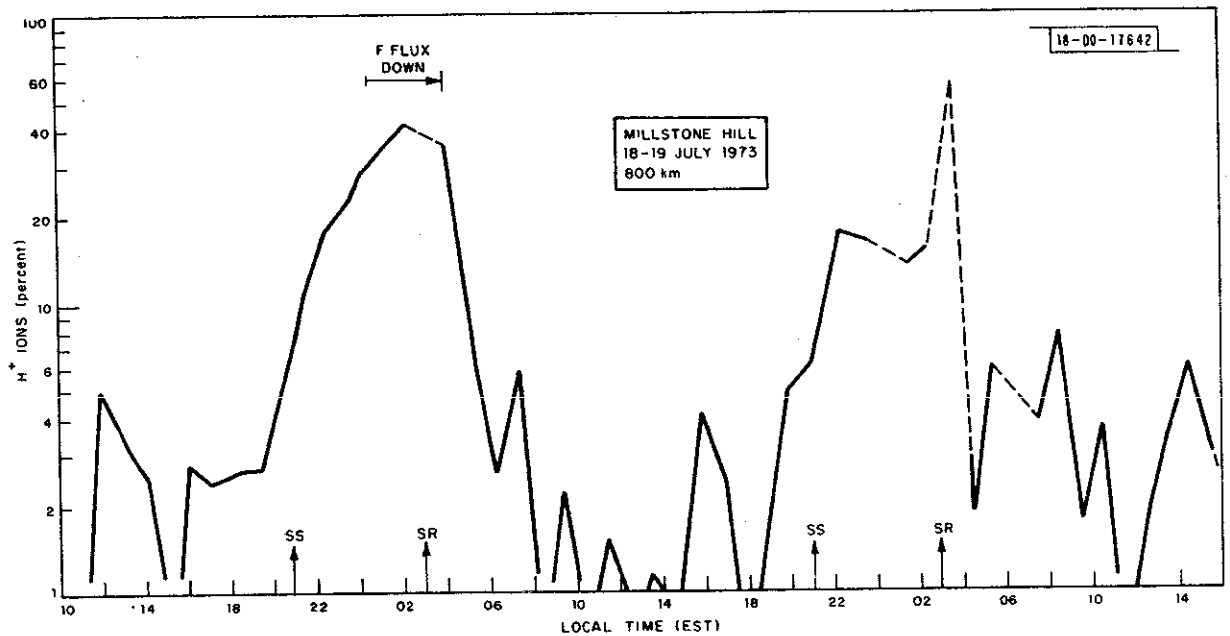

(d) 800 km on 18-19 July.

Fig. 13(a-g). Continued.

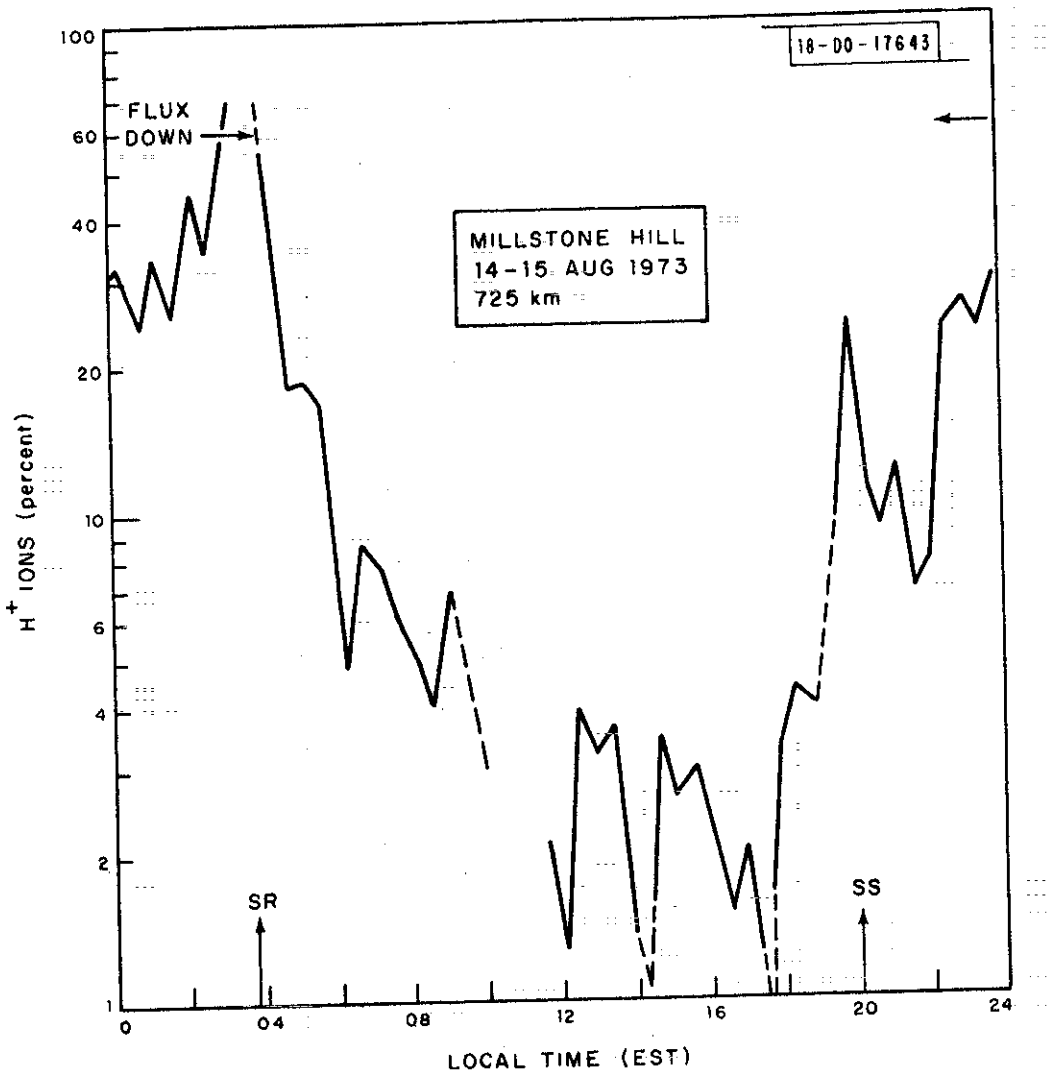

(e) 725 km on 14-15 August.

Fig. 13(a-g). Continued.

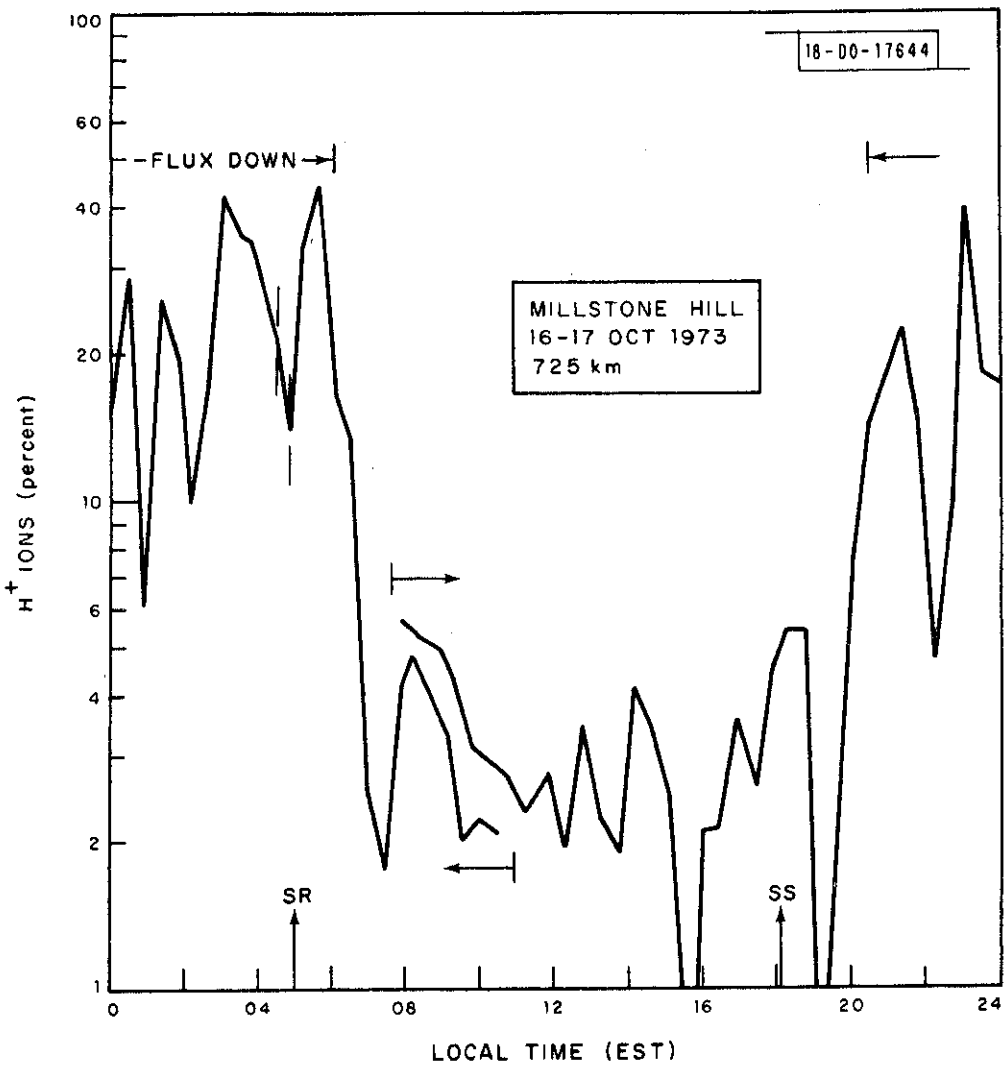

(f) 725 km on 16-17 October.

Fig. 13(a-d). Continued.

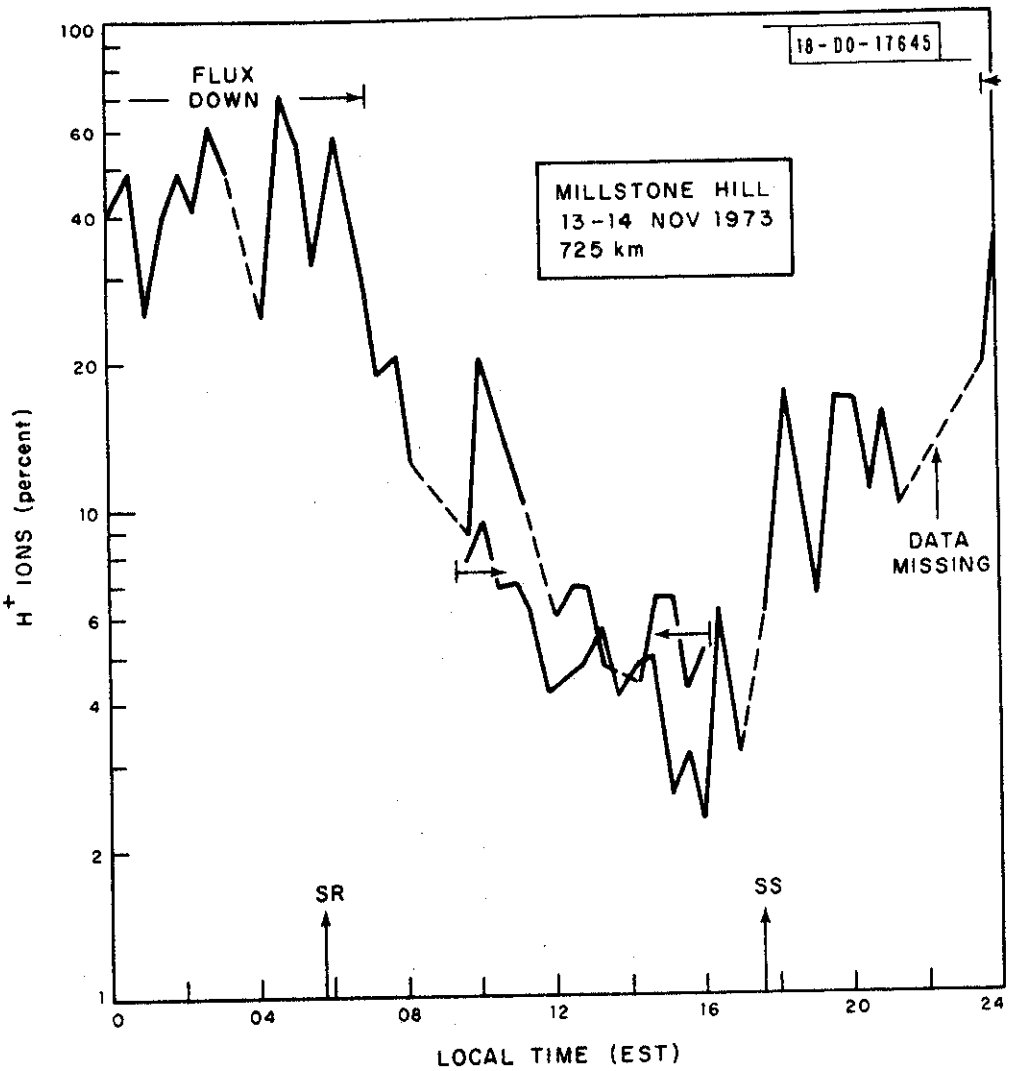

(g) 725 km on 13-14 November.

Fig. 13(a-g). Continued.

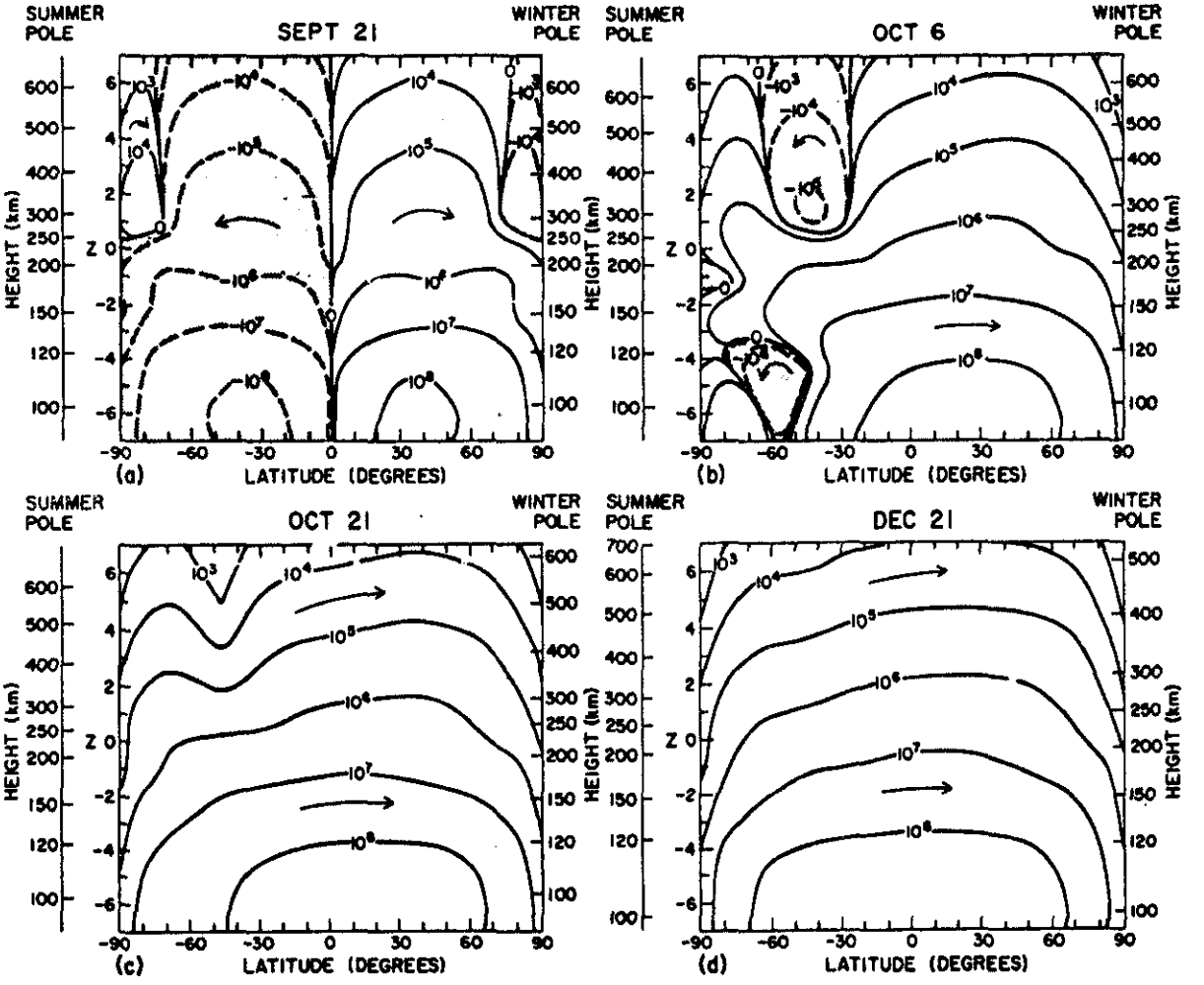

Fig. 14. Plots of the zonal mean thermospheric circulation according to Roble et al[45]. Shown is the transition from the symmetric equinox circulation to the asymmetric solstice circulation. The reverse cell in the high latitude winter hemisphere is driven by auroral heating (from Roble et al[45].

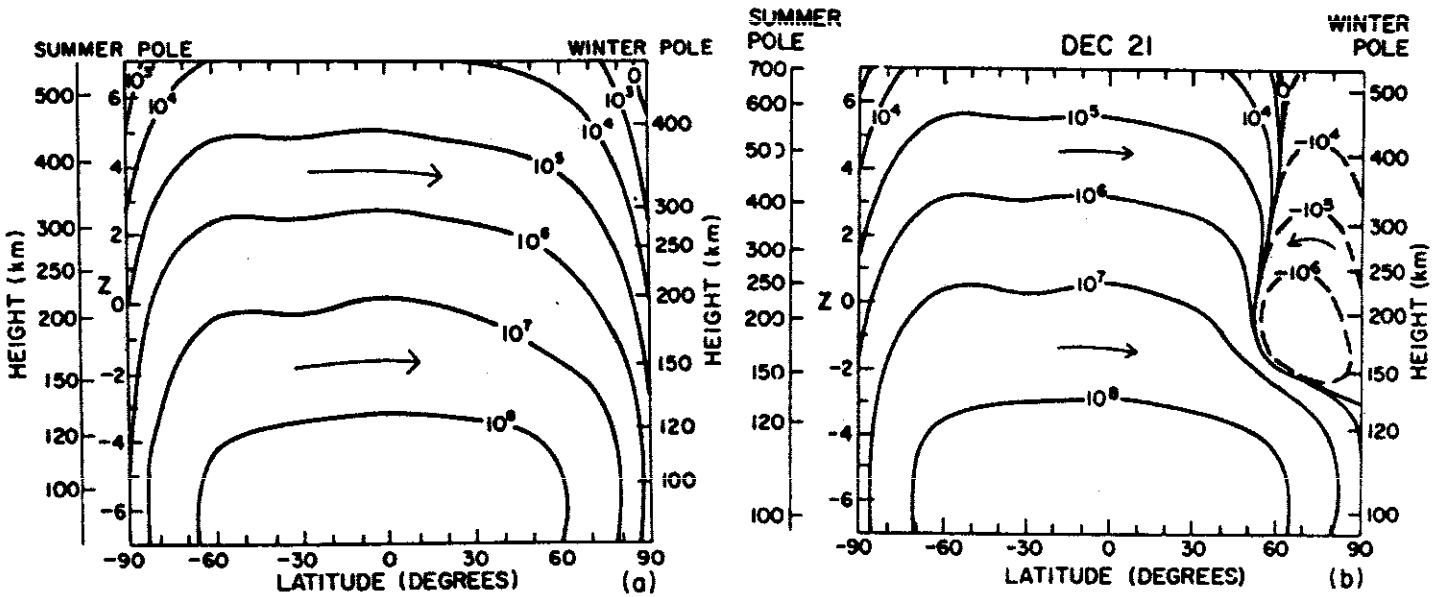

Fig. 15. Comparison of the zonal mean circulation of the thermosphere at solstice for (a) solar minimum and (b) solar maximum according to Roble et al[45]. At solar minimum, the auroral activity is too low to drive a reverse cell in the winter hemisphere (from Roble et al[45]).

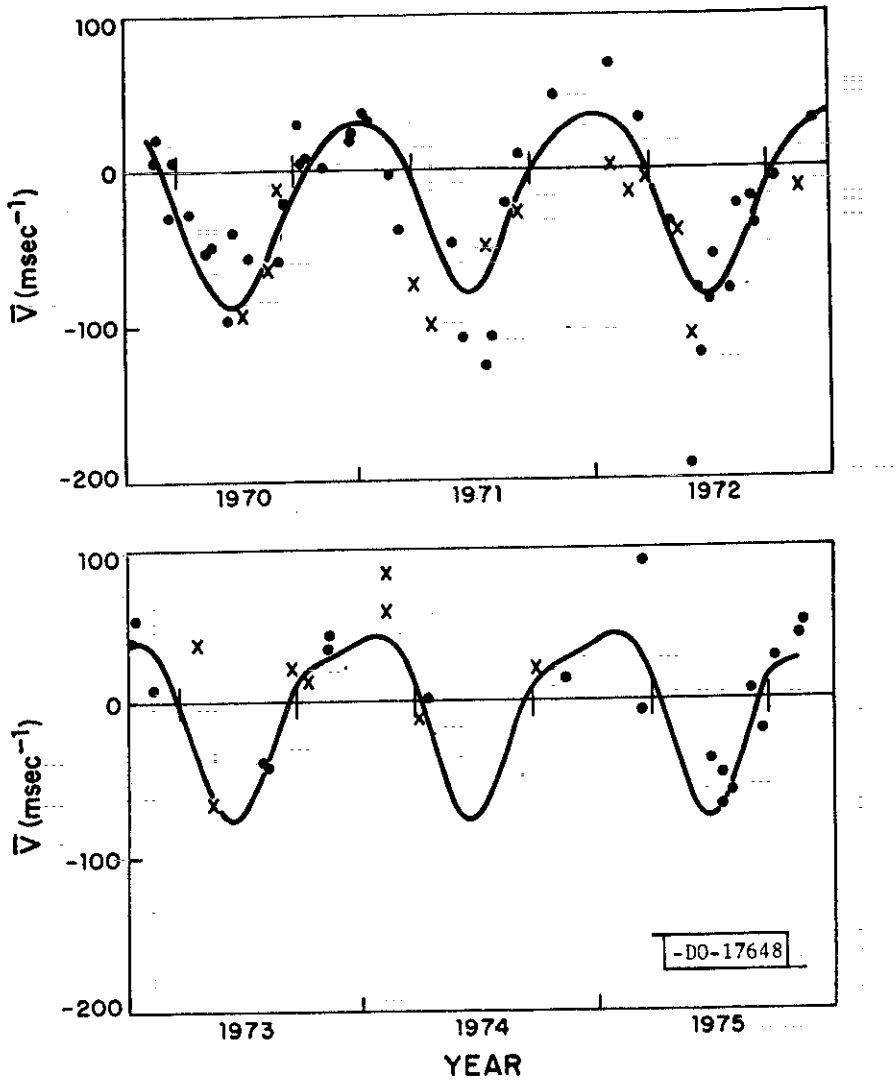

MILLSTONE HILL
MEAN MERIDIONAL WINDS

Fig. 16. The diurnally averaged values of the meridional wind at 300 km over Millstone Hill derived using the model of Emery[40]. The solid line is a least squares fit to the quiet days (dots) given by the sum of a mean and the first three harmonics (Eq.2). Crosses represent disturbed days that were not included in fitting the curve. Note the change in the equinox winds from generally equatorward at solar maximum to generally poleward at solar minimum.

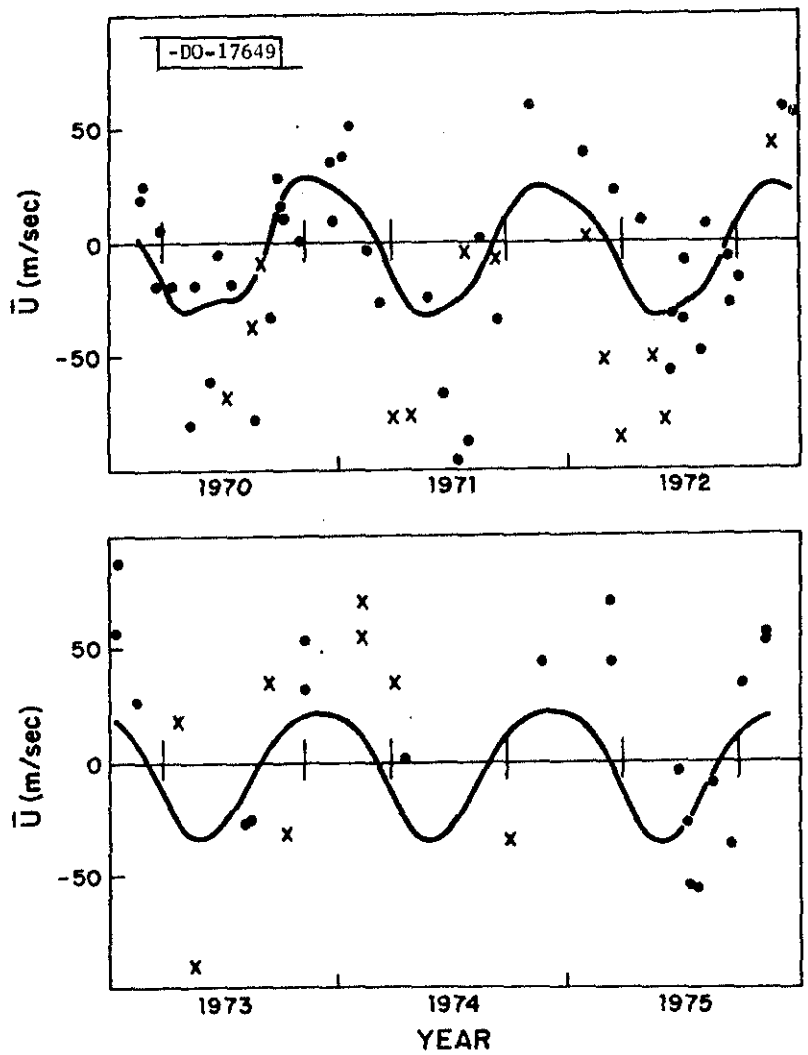

MILLSTONE HILL
MEAN ZONAL WINDS

Fig. 17. The diurnally averaged values of the zonal winds at 300 km over Millstone Hill. The solid line is a least squares fit to the data given by the sum of a mean and the first three harmonics (Eq.3). Because of the large scatter in the data, the fit is not statistically significant; however, there is a general trend of eastward winds in winter and westward winds in summer, with no apparent change in the pattern over the solar cycle. Crosses represent disturbed days and were not included in the fit.

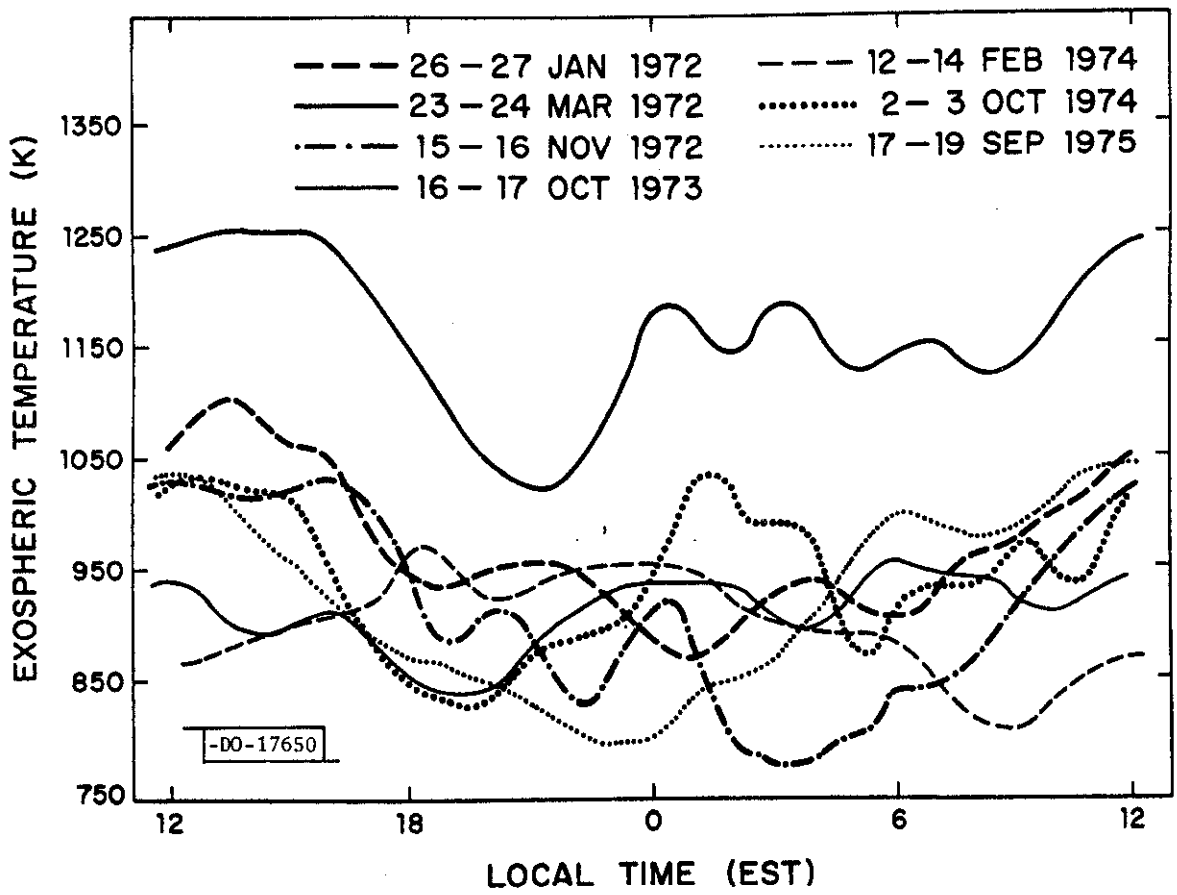

Fig. 18. The diurnal temperature pattern on seven geomagnetically disturbed days as derived from Millstone Hill data. The nighttime temperatures are markedly enhanced over the normal quiettime values, particularly in the midnight and post midnight sectors. For 12-13 February 1974, the nighttime temperature is higher than the daytime temperature.

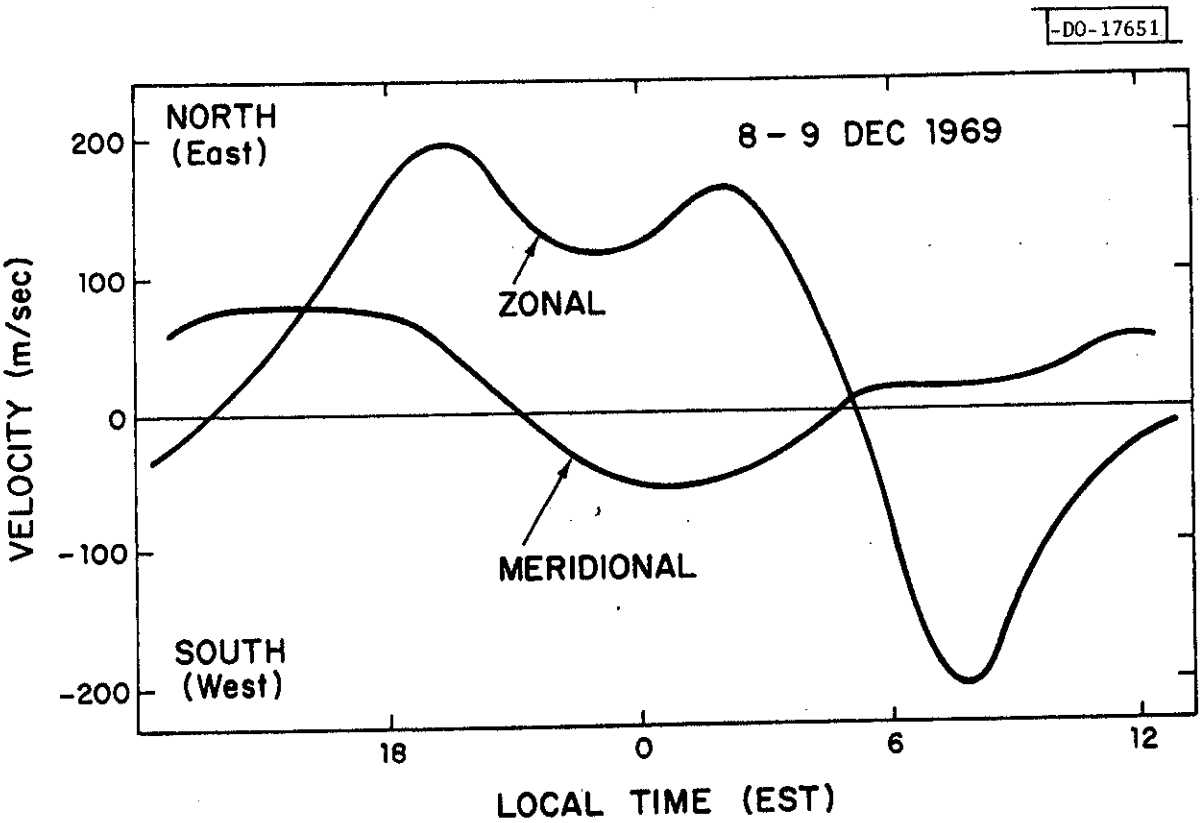

Fig. 19. The diurnal zonal and meridional wind patterns for a typical quiet winter day.

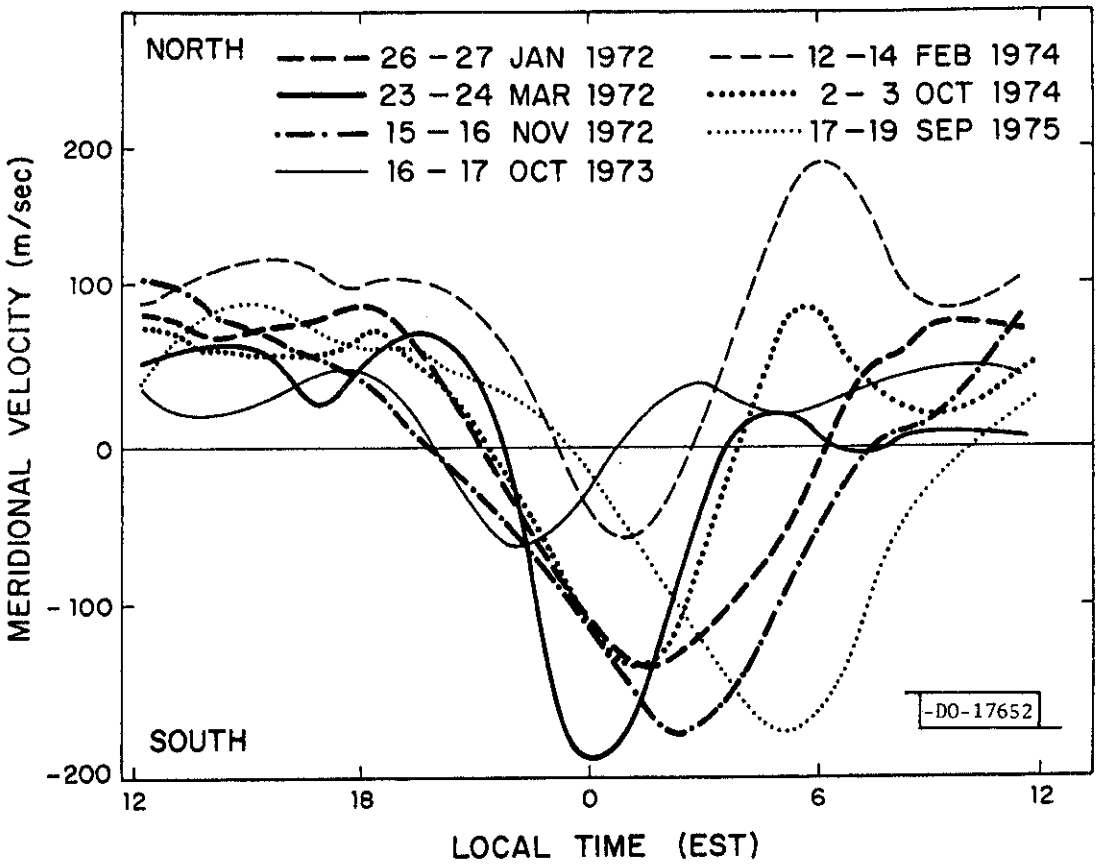

Fig. 20. The meridional wind patterns for the seven geomagnetically disturbed days shown in Figure 18. The equatorward winds in the midnight and postmidnight sectors are enhanced markedly over the quiettime pattern shown in Figure 19.

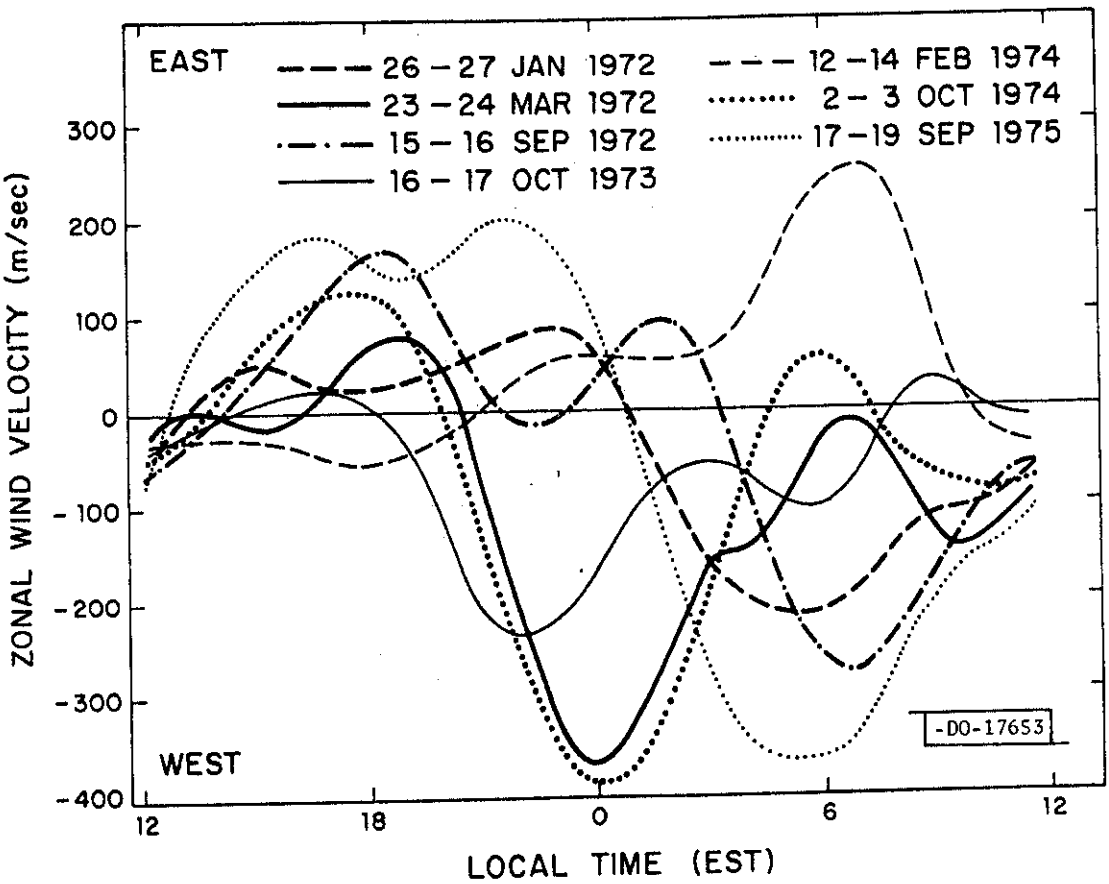

Fig. 21. The zonal wind pattern for the seven geomagnetically disturbed days shown in Figure 18. The westward winds in the morning sector are significantly stronger than on quiet days, and the time of reversal from eastward to westward winds has shifted to the pre-midnight sector on most days. For 12-13 February 1974, the derived wind pattern is reversed from the normal pattern, with westward winds in the morning and eastward winds in the evening.

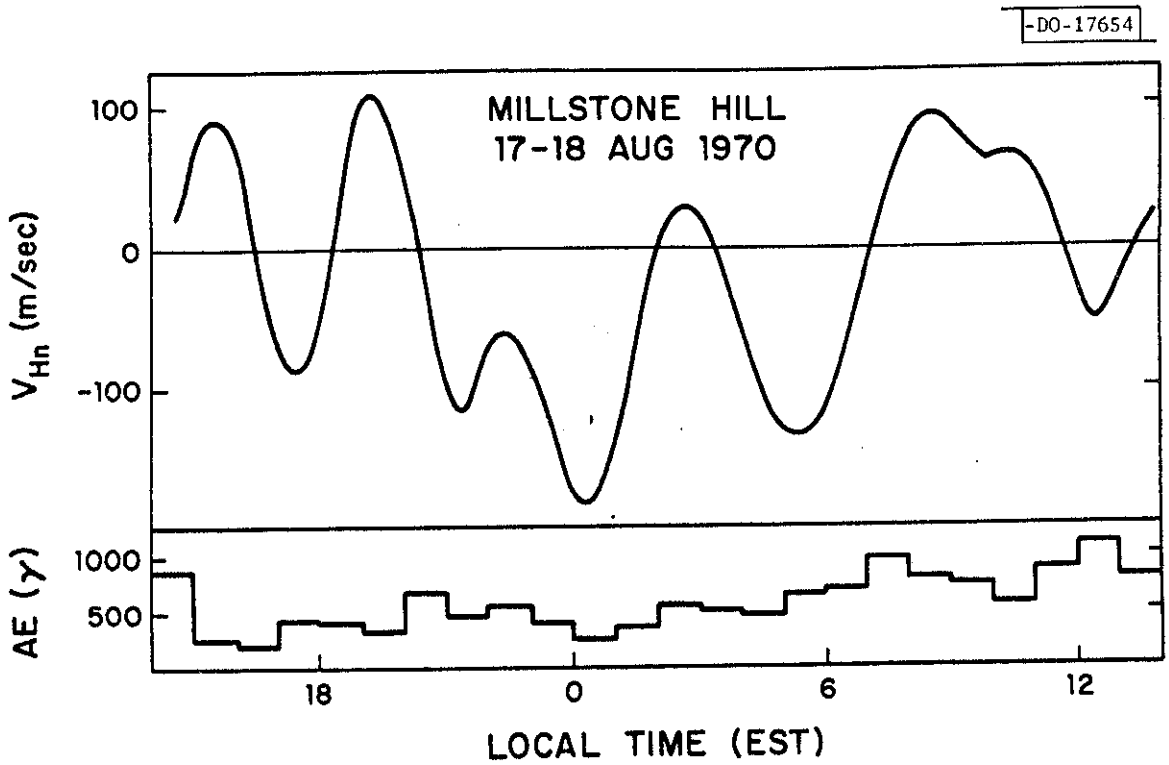

Fig. 22. The wind component along the magnetic meridian, V_{Hn}, derived from the experimental data for 17-18 August 1970 is here compared to the hourly average of the auroral index, AE. Most of the equatorward pulses (negative V_{Hn}) correlate with auroral activity except that occurring near midnight which probably is an extension of the midnight surge seen at high latitudes.

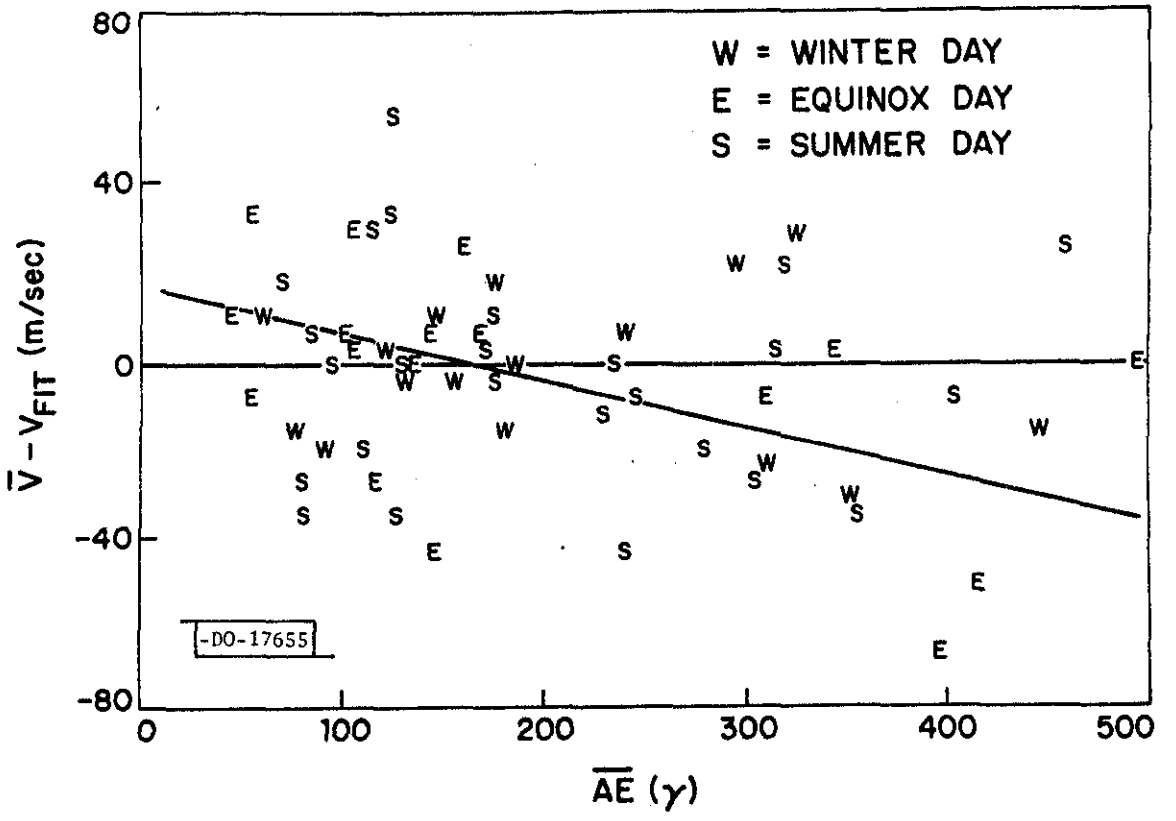

Fig. 23. The difference between average meridional velocity (V) and that predicted (V_{FIT}) from a model fitted to the 64 quiet days plotted against the daily average auroral index AE. The straight line is the least mean square fit. While the trend is for the winds to be more equatorwards on disturbed days, the scatter is so large that the result is not significant statistically.

IBLIOGRAPHIC DATA HEET	1. Report No	3. Recipient's Accession No.
Title and Subtitle Millstone Hill Thomson Scatter Results for 1973		5. Report Date 22 October 1979 6.
Author(s) John V. Evans, R.R. Babcock, Jr., and John M,. Holt		8. Performing Organization Rept. No. Technical Report 537
Performing Organization Name and Address Lincoln Laboratory, M. I. T. P.O. Box 73 Lexington, MA 02173		10. Project/Task/Work Unit No. 11. Contract/Grant No. ATM 75-22193 and ATM 79-09189
!. Sponsoring Organization Name and Address National Science Foundation Atmospheric Science Section Washington, DC 20550		13. Type of Report & Period Covered Technical Report 14.

5. Supplementary Notes

i. Abstracts

During 1973, the vertically-directed incoherent scatter radar at Millstone Hill (42.6°N, 71.5°W) was employed to measure electron density, electron and ion temperature and vertical ion velocity in the F-region over periods of 24 hours one or two times per month. The observations spanned the height interval 200-900 km approximately, and achieved a time resolution of about 30 minutes. This report presents the results of these measurements in a set of contour diagrams.

For a number of the days, the results have been used to derive the diurnal variation of the temperature of the neutral atmosphere above 300 km (the exospheric temperature) as well as the speed of the neutral wind in the magnetic meridian plane at this altitude. These results were used to define a model for the pressure variation in the thermosphere over Millstone whose E-W variation is set by the observed temperature variation, and whose N-S variation was adjusted to reproduce the observed winds calculated by solving momentum equations for the neutral air. These results, together with similar results obtained using data gathered over the six-year period 1970-1975 have been used in a study of the seasonal and sunspot cycle variation of the mean meridional and zonal winds. Also reported are the results of a study of the effect of magnetic storms on the thermospheric winds observed over Millstone Hill.

'. Key Words and Document Analysis. 17a. Descriptors

Millstone radar
F-region
diurnal variations
electron density
ionospheric scatter
seasonal variations
temperature effects
magnetosphere
proton flux

b. Identifiers/Open-Ended Terms

'c. COSATI Field/Group

18. Availability Statement	19.. Security Class (This Report) UNCLASSIFIED	21. No. of Pages 104
	20. Security Class (This Page UNCLASSIFIED	22. Price